Master Thesis

Master's Degree in Energy Engineering

Generalised AC/DC Power Flow

September 16, 2024

Author: Lee Raiyan bin Zulkifli

Supervisors: Eduardo Prieto Araujo

Josep Fanals i Batllori

Escola Tècnica Superior
d'Enginyeria Industrial de Barcelona

Abstract

In modern grids, there exist many devices that are able to control bus and branch magnitudes both locally and remotely: Voltage Source Controllers (VSCs) can control the active and reactive powerflows, offering high flexibility in controlling power transmission and bus voltages. Additionally, modern grids are not pure AC systems: HVDC links are important features that interconnect two or more AC subsystems between countries. These advances in grid technology mean that the traditional powerflow method is no longer sufficient. The traditional Newton-Raphson powerflow method relies on classifying AC buses into one of three categories: PV (known active power and voltage), PQ (known active power and reactive power) and slack buses (known voltage and phase angle). This method is well-known and widely used, but it severely limits how bus and branch magnitudes can be set within the Newton-Raphson formulation. Rather, we require a power flow method that can properly model the grid of the present and the future. This work presents a new generalized power flow method that does not require any pre-selection of bus types. This novel method also allows for the solving of hybrid AC/DC systems in a unified manner, that is, without the use of separate iteration loops for AC and DC subsystems. Using its implementation in GridCal, an open-source power system analysis software, the method is tested on a number of systems, including a 6-bus grid, a modified IEEE 14-bus system, and the IEEE 118-bus system. The results show that the method is able to solve the power flow problem in a reasonable amount of time.

Contents

1 Introduction **15**
1.1 Background . . . 15
1.2 State of the Art . . . 16
1.3 Objectives and Motivation . . . 18
1.4 Outline . . . 18

2 Grid Elements and Model **19**
2.1 Buses . . . 19
2.2 Branches . . . 19
2.3 Bus Analysis and Admittance Matrices . . . 21
2.4 Kirchhoff's Voltage Law (KVL) . . . 21
2.5 Kirchhoff's Current Law (KCL) . . . 21
2.6 Per Unit System . . . 22
2.7 Loads . . . 22
2.8 Synchronous Generators . . . 23
2.9 Voltage Source Converters (VSCs) . . . 24
2.9.1 IGBT Structure and Operation . . . 24
2.9.2 VSC Loss Model . . . 25
2.10 Transformers . . . 29
2.10.1 Phase-Shifting Transformers . . . 29
2.11 Controls . . . 32
2.11.1 Synchronous Generators . . . 33
2.11.2 Voltage Source Converters (VSCs) . . . 33
2.11.3 Phase Shifting Transformers (PSTs) . . . 34
2.12 Conclusion . . . 35

3 Power Flow Equations and Newton-Raphson Method **37**
3.1 Power Flow Equations (Matrix Form) . . . 37
3.2 Newton-Raphson Method . . . 39
3.2.1 Jacobian Matrix . . . 40
3.3 Classical Power Flow with Newton Raphson . . . 41
3.4 Flexible Universal Branch Model (FUBM) and Power Flow Algorithm . . . 42
3.4.1 Branch Admittance Matrix in FUBM . . . 42
3.4.2 Flexible Power Flow Algorithm (FPFA) . . . 43
3.5 Limitations and Challenges . . . 44

4 Generalised Power Flow **45**
4.1 Fundamental rules . . . 46

4.2 Generalised Branch Model . . . 46
4.2.1 Voltage Source Converter (VSC) . . . 48
4.2.2 Transformer . . . 49
4.3 Generalised Bus Model . . . 51
4.4 Solving Generalised power flow with Newton-Raphson . . . 52
4.5 Indices . . . 54
4.5.1 Buses and Lines . . . 54
4.5.2 ZIP Elements . . . 55
4.5.3 AC/DC Link - VSCs . . . 56
4.5.4 Controllable Transformer . . . 56
4.5.5 Bus and Branch Setpoints . . . 57
4.5.6 Cardinality of Unknown Sets . . . 58
4.5.7 Reference Node Identification . . . 60
4.6 Derivatives . . . 62
4.6.1 Nodal Power Balance . . . 64
4.6.2 Controllable Transformer . . . 65
4.6.3 VSC Loss Derivatives . . . 67
4.6.4 Passive Branch Derivatives . . . 68

5 Results **69**
5.1 Error Evaluation and Convergence . . . 69
5.2 6-bus Grid . . . 72
5.3 Modified IEEE 14-Bus . . . 75
5.4 Modified IEEE 118-bus . . . 79
5.5 Runtime Comparison . . . 81

Conclusions **85**

Future Work **87**

Acknowledgements **89**

A Environmental, Social, and Gender Impact **93**
A.1 Environmental Impact . . . 93
A.2 Social Impact . . . 93
A.3 Gender Impact . . . 93

B Time Planning **95**

C Budget **97**

D Test Case Convergence **99**

E Graph Theory and Depth-First Search (DFS) 103
E.1 Graph Theory Basics . . . 103
E.2 Depth-First Search (DFS) . . . 103
E.2.1 DFS Pseudocode . . . 103
E.3 Applications in Power Systems . . . 104
E.4 DFS Example on a Power Grid . . . 104

List of Figures

1 Grid map of Europe and North Africa, with HVDC links in purple [1]. 15
2 Representation of a load with its ZIP model. 23
3 Representation of a generator. 24
4 Example of the switching energy E_{on} and E_{off}. 27
5 Reverse recovery energy characteristics for the anti-parallel diode. 27
6 Energy profiles for a manufacturer's test IGBT [2]. 27
7 Model of a VSC in steady state [3]. 27
8 Representation of a converter. 28
9 Model of a Controllable Transformer (PST). 30
10 Representation of a transformer. 31
11 Newton-Raphson for a well-conditioned scalar function [4]. 40
12 Standard model of a FUBM branch [5]. 42
13 Scheme of the IEEE 14-bus system to illustrate the concept of remote controls. . . 47
14 Representation of a VSC. 48
15 Representation of a transformer. 49
16 Representation of a generic bus with a ZIP shunt model, passive branch connections κ, and active branch connections Γ. 51
17 Evolution of the error of 82 test cases. 70
18 6-bus system including two VSCs. 72
19 VSC 1 Control 73
20 VSC 2 Control 73
21 Control settings for VSCs in 6-Bus grid. 73
22 Convergence for 6-bus system. 73
23 Voltage magnitudes for 6-bus system. 74
24 Modified IEEE 14-bus System [6]. 75
25 Modified IEEE 14-bus system in GridCal. 76
26 Control Mode for Controllable Transformer Trafo 2. 77
27 Convergence for IEEE 14-bus system. 78
28 Voltage magnitudes comparison 78
29 IEEE 118-bus system in GridCal. 80
30 Control scheme of VSCs in IEEE 118-bus system. 80
31 Error evolution for IEEE 118-bus system in GridCal. 81
32 Runtime comparison for three test cases. 82
33 Iterations before convergence for three test cases. 83
34 Gantt Chart for the project. 95

List of Tables

1 Comparison between Classic power flow and Generalised power flow. 45
2 Sets to identify known and unknown magnitudes. 53
3 Sets to identify known and unknown magnitudes. 55
4 Sets to identify bus and branch assertions. 57
5 Voltage angle in degrees. 74
6 Comparison of VSC 1 branch powers. 74
7 Comparison of VSC 2 branch powers. 75
8 Voltage angle in degrees. 79
9 Runtime breakdown for three test cases run on generalised power flow (in milliseconds). 82
10 Costs of the project. 97
11 Test Cases (Converged) 100
12 Test Cases (Did Not Converge) 101
13 Grid Files with Exceptions 101

Glossary

B_{eq} Equivalent susceptance.

J Jacobian matrix.

P Active power.

$P^{\mathbf{zip}}$ Active power in the ZIP model, used for representing loads.

P_f Active power flow on the sending side of a branch.

P_t Active power flow on the receiving side of a branch.

Q Reactive power.

$Q^{\mathbf{zip}}$ Reactive power in the ZIP model.

Q_f Reactive power flow on the sending side of a branch.

Q_t Reactive power flow on the receiving side of a branch.

V_f Voltage on the "from" side of a power system element.

X Vector of state variables.

Y Admittance.

$\mathbf{Y_{bus}}$ Bus admittance matrix.

θ Voltage angle.

θ_{sh} Phase-shift angle.

$\underline{I}$ Complex current.

$\underline{S}$ Complex power.

$\underline{V}$ Complex voltage.

$\underline{V_t}$ Voltage on the "to" side of a power system element.

$\underline{Y}$ Complex admittance of a branch.

$\underline{Z}$ Complex impedance of a branch.

m Modulation amplitude.

$m\angle\tau$ Complex ratio used for modeling transformers.

G' Subgraph representing the electrical grid excluding AC/DC connections.

G Graph representing the electrical grid with nodes I and branches K.

I_V Known bus voltage magnitudes.

I_δ Known bus voltage phase angles.

I_p Known bus ZIP active powers.

I_q Known bus ZIP reactive powers.

K' Modified set of branches after removing AC/DC links.

K Set of branches (edges) in the electrical grid.

K_τ Known branch tap phase shift angles.

K_m Known branch tap ratios.

K_{p_f} Known branch from active powers.

K_{p_t} Known branch to active powers.

K_{q_f} Known branch from reactive powers.

K_{q_t} Known branch to reactive powers.

V Voltage magnitude at bus i.

δ Voltage phase angle at bus i.

$\mathcal{B}_\tau$ Set of asserted branch phase shift angles.

$\mathcal{B}_m$ Set of asserted branch tap ratios.

$\mathcal{B}_{p_f}$ Set of asserted branch from active power flows.

$\mathcal{B}_{q_f}$ Set of asserted branch from reactive power flows.

$\mathcal{N}_V$ Set of asserted nodal voltage magnitudes.

$\mathcal{N}_\delta$ Set of asserted nodal voltage phase angles.

$\mathcal{N}_p$ Set of asserted nodal active power injections.

$\mathcal{N}_q$ Set of asserted nodal reactive power injections.

$\overline{I}_V$ Unknown bus voltage magnitudes.

$\overline{I}_\delta$ Unknown bus voltage phase angles.

$\overline{I}_p$ Unknown bus ZIP active powers.

$\overline{I}_q$ Unknown bus ZIP reactive powers.

$\overline{K}_\tau$ Unknown branch tap phase shift angles.

$\overline{K}_m$ Unknown branch tap ratios.

$\overline{K}_{p_f}$ Unknown branch from active powers.

$\overline{K}_{p_t}$ Unknown branch to active powers.

$\overline{K}_{q_f}$ Unknown branch from reactive powers.

$\overline{K}_{q_t}$ Unknown branch to reactive powers.

AC Alternating Current.

DC Direct Current.

FPFA Flexible Power Flow Algorithm.

FUBM Flexible Universal Branch Model.

HVDC High Voltage Direct Current.

IGBT Insulated Gate Bipolar Transistor.

KCL Kirchhoff's Current Law.

KVL Kirchhoff's Voltage Law.

MTDC Multi Terminal HVDC.

NR Newton-Raphson.

p.u. Per unit system.

PST Phase-Shifting Transformer.

VSC Voltage Source Converter.

ZIP Model constant impedance (Z), constant current (I), and constant power (P).

1 Introduction

1.1 Background

The world's power systems is rapidly evolving, driven by the increasing penetration of advanced power electronics and the need to integrate diverse energy sources into the grid. For a long time, the management of electrical grids was dominated by alternating current (AC) systems, with synchronous generators as the primary active elements controlling the flow of electricity. As we move deeper into the 21st century, however, the power grid is no longer a domain exclusive to synchronous generators. Power flow-controlling devices such as Flexible AC Transmission Systems (FACTS) devices, and converter-interfaced HVDC links are some examples of how the landscape of the energy system has been evolving over time [7]. As seen in Figure 1, HVSC links have become widespread. This is a particularly exciting development over the last few decades, and one that is of interest in this work.

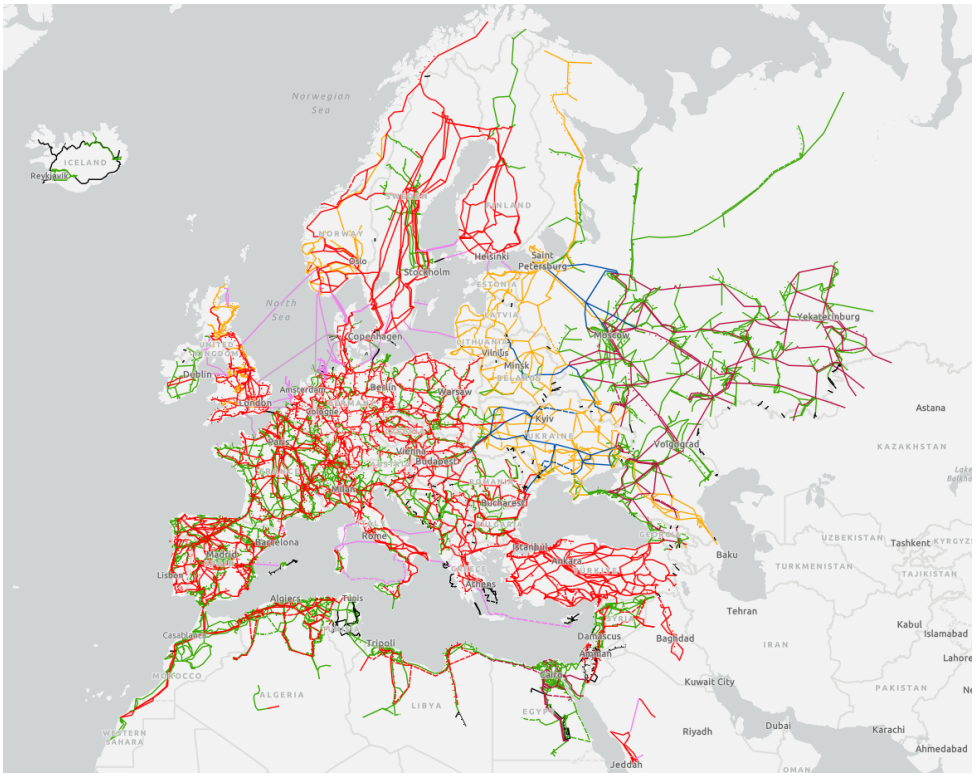

Figure 1: Grid map of Europe and North Africa, with HVDC links in purple [1].

By the beginning of the decade, over 200 HVDC links have been installed globally, with the most advanced systems operating at voltages of $\pm$800 kV and currents exceeding 4500 A [2]. The reasons for these are numerous, not least of which is the ability to transfer bulk power over long distances, the ability to connect asynchronous grids, and the ability to provide dynamic control of power flows. At the core of these capabilities are the power electronics that enable the conversion

of AC to DC and vice versa: line-commutated converters (LCC) and voltage-source converters (VSC). Classic HVDC relied on LCC topologies, powered by thyristors, before VSC-based HVDC systems (HVDC Light) became more widely-used due to their ability to provide reactive power support and black start capabilities, as well as their ability to operate in weak AC systems [8]. While classic HVDC is still favoured in some cases due to lower losses, the flexbility of HVDC Light provides to the overall grid is undeniable. It is with that in mind that this work is focused on VSC-based HVDC systems.

The transformation in how power flows are controlled then also means that there is also a need to evolve the way how power flows are calculated. The traditional approach to power flows designated three types of AC buses: load buses, generator buses, and slack buses. This method was useful to grid operators of the time for managing the flow of power from a few large plants to the rest of the grid in a kind of unidirectional way. With the presence of power flow-controlling devices and distrbuted energy resources, however, the rigidity of the traditional power flow methods quickly becomes a challenge. Most glaringly is the absence of the method to be able to handle the interaction between AC and DC systems in a single framework. Then, there is also the issue of the increasing complexity of the grid, with the need to model more complex controls and the need to be able to handle the grid in a more decentralized manner.

1.2 State of the Art

Relatively soon after the proposal of HVDC as a means to transfer bulk energy, there has been a consistent interest in addressing the limitations of traditional power flow methods and to extend it to the AC/DC problem. In the mid 1970s, Braunagel et al. proposed a method to include equations for DC converters [9]. Their model extended the traditional Newtown Raphson Jacobians to include DC equations in several distinct cases depending on whether the converter was fixing power on the AC side, or values on the DC. It also necessarily included the relationship between the firing angle of the thyristor and the commutation angle of the converter, as well as the power balance in the AC and DC buses. It was however a method exclusive to LCC-based HVDC systems. VSC-focused power flows can be divided into two methods: sequential models and unified models.

In sequential power flow models, the AC and DC grids are decoupled and solved separately, with their interactions linked iteratively through the active power exchange at the interface converter (IC) that controls the DC voltage. In this setup, most of the ICs operate in either PV or PQ mode, meaning the traditional power flow (PF) methods, which are well-established for AC systems, can still be applied to model the AC side of the network. The challenge, however, arises with the converter that is responsible for maintaining the DC voltage. As a "slack" converter, its active power injection is not predetermined and must be calculated dynamically to satisfy the active power balance between the AC and DC networks. This results in the need for multiple internal

loops to solve the power flow. For example, Beerten et al. proposed a method for solving multi-terminal VSC HVDC systems in a sequential manner with MATPOWER [10]. The work, while shown to be able to include an arbitrary DC system into the power flow, required more iterative calculations in order to accurately define the power setpoints with respect to the system bus. In total, three internal and one external loop was used to achieve the power flow solution. Multiple iterative loops are a common theme in sequential models, and can become computationally expensive for large-scale systems, or unstable when internal loops do not converge in reasonable time [11].

Unlike sequential methods, a unified model is one where the AC and DC subsystems, as well as the converter powers, are solved in the same set of nonlinear equations. In Nguyen et al. [12], the authors simultaneously solve nonlinear power balance equations for large-scale, multi-frequency HVAC and HVDC grids while accounting for accounting for generator and converter limits, but the method is limited to only the specific case of voltage-power droop control on the DC side. The authors also model the VSC as a transformer, where the VSCs are treated as compound transformer devices linked to pulse width modulation (PWM) inverter controls, accounting for phase-shifting, scaling, reactive power limits, and associated losses, rather than controllable voltage sources. While useful, this work relies on seeing the VSC as something it is not.

More recently, several authors proposed the Flexible Universal Branch Model (FUBM) [13], wherein all types of branches are modeled generically, but require different parts of the model depending on the device. For example, a VSC is treated as a branch (similar to a line), in which the reactive power on the DC side is made to be zero by a shunt element. The novelty of this method also means that AC and DC nodes are not treated differently, but merely maintain the angle differences on the DC side to account for the absence of the voltage angle difference in real DC systems. This method is made available on MATPOWER and GridCal, and is useful to a high degree. However, in certain cases, it has been found that the initialisation of this shunt impedance or capacitance on the DC side of the VSC model is crucial to the convergence of the algorithm. In other words, the algorithm is sensitive to changes in the initilisation value of the parameters.

Finally, a "general" and unified power flow is presented in [14], where the authors address the issue of only a single VSC regulating the voltage on the DC side. While useful, this method involves defining four new node types for the DC buses as well as the VSCs.

Previous work has shown that there exists methods can effectively model hybrid AC/DC grids and provide accurate power flow solutions. However, these methods often require complex pre-selection of bus types or suffer from convergence issues. Lastly, and most importantly, none of the methods above can be said to be sufficiently "generalised".

1.3 Objectives and Motivation

The previous section shows the urgent need to develop a power flow method that is robust, scalable, and adaptable to the future energy grid. As a result, we require a method that is fully unified, does not require pre-selection of bus types, and also is able to model VSCs power losses accurately.

This work therefore, aims to demonstrate the development of a generalized power flow method that can seamlessly incorporate both AC and DC systems into a unified framework. At the same time, we need not only limit ourselves to the AC/DC problem. The inclusion of more complex controls in the grid also lends itself nicely to the idea of remotely defining setpoints in the grid, be them bus or branch values. Lastly, to further generalise the power flow, this work looks to include controllable transformers as another type of active branch in the model, not just VSCs.

1.4 Outline

This work is organized as follows:

- **Chapter 2: Basic Electrical Engineering Concepts** – This chapter reviews the fundamental concepts of electrical engineering necessary for understanding power flow methods, including AC and DC circuit analysis.
- **Chapter 3: Newton-Raphson Method** – This chapter provides an in-depth analysis of the traditional Newton-Raphson method, its applications, and its limitations in modern power systems.
- **Chapter 4: Proposed Generalized Model** – The novel generalised power flow method is presented, detailing its formulation and implementation in the GridCal software.
- **Chapter 5: Results** – This chapter showcases the results obtained from testing the proposed method on various systems, including a comparative analysis with existing methods.

2 Grid Elements and Model

This section will act as a primer for all following sections, that is, to introduce the concepts needed for our work. We begin with basic concepts related three-phase systems, the per-unit normalisation technique, and admittance matrices. Next, we recall Kirchhoff's Voltage Law (KVL) and Kirchhoff's Current Law (KCL) that will help us to derive power flow equations. Lastly, we present each type of grid element that is used in power flows and the rest of this work.

For the purposes of this work, we assume that all three-phase systems are balanced. A balanced system is one where the magnitude of the voltage and the phase difference between the phases are equal. This assumption allows us to simplify the analysis by considering only one phase, typically referred to as the positive sequence component. The analysis of three-phase systems is often performed using a single line diagram, which represents the system with one line per phase.

2.1 Buses

In power systems, buses are the fundamental nodes where various components such as generators, loads, and branches connect. A bus serves as a common point for power injection or extraction and can represent a physical substation or a conceptual node in a model.

Each bus in the network operates at a certain point depending on the state of the system. This operating point is its voltage. In polar form, a voltage $\underline{V}$ is expressed as:

$$\underline{V} = |V| \angle \theta \tag{1}$$

where $|V|$ is the magnitude of the voltage (measured in volts), and θ is the reference angle of the voltage (measured in degrees or radians). It is important to note, however, that we always refer to voltages, as well as other magnitudes using the per-unit system as explained in Section 2.6. This angle is useful only in relation to other buses in the system. The reference bus, which is often called the slack bus, is the bus at which we set the reference angle to be zero in the power flow. This allows all other buses to take their voltages against this reference. This slack bus is also usually assigned the purpose of compensating for losses in the system by injecting active or reactive power into the grid. Bus voltages and their deviations from one another also serve to show how much power is flowing from one bus to another, through elements called branches.

2.2 Branches

Branches in power systems represent the devices in the grid that connect any two buses. At the most fundamental level, a branch is a conductor that allows current to flow between two points.

The behavior of these branches is determined by their electrical characteristics:

$$\underline{Z} = R + jX \tag{2}$$

$$\underline{Y} = G + jB \tag{3}$$

The resistance R of a branch causes power loss in the form of heat, while the conductance G represents the leakage current flowing through the dielectric material surrounding the conductor. The reactance X of a branch causes voltage drops due to the inductive reactance, while the susceptance B accounts for the capacitance between the conductors and the ground. Together, these parameters define the impedance of the branch.

The relationship between the impedance $\underline{Z}$ and admittance $\underline{Y}$ is given by the following equation:

$$\underline{Y} = \frac{1}{\underline{Z}} \tag{4}$$

where $\underline{Z}$ is the complex impedance of the branch, and $\underline{Y}$ is the complex admittance. The admittance represents how easily current flows through a branch, while impedance represents the opposition to current flow.

For a branch connecting two buses, the voltage $\underline{V}$ and current $\underline{I}$ are related by Ohm's Law:

$$\underline{V} = \underline{Z}\,\underline{I} \tag{5}$$

or equivalently in terms of admittance:

$$\underline{I} = \underline{Y}\,\underline{V} \tag{6}$$

The concept of complex power is integral to understanding power flow in these systems. Complex power $\underline{S}$ is defined as:

$$\underline{S} = P + jQ \tag{7}$$

where P is the active power (measured in watts) and Q is the reactive power (measured in volt-amperes reactive, or var). Complex power encompasses both the active power that does useful work and the reactive power that oscillates between the source and load.

The relationship between voltage, current, and complex power can be expressed as:

$$\underline{S} = \underline{V}\,\underline{I}^{*} \tag{8}$$

where $\underline{V}$ is the voltage across the branch, $\underline{I}^*$ is the complex conjugate of the current, and $\underline{S}$ is the complex power. This equation shows that the complex power $\underline{S}$ flowing into a branch is a function of the voltage and the conjugate of the current. It also links active power (P) and reactive power (Q) to the voltage and current in the system.

2.3 Bus Analysis and Admittance Matrices

Buses represent the nodes where different elements like generators, loads, and branches are connected. The admittance matrix $\mathbf{Y}_{\text{bus}}$, or bus admittance matrix relates the current injection at a bus to the bus voltage via the equation:

$$\mathbf{I} = \mathbf{Y}_{\text{bus}}\mathbf{V} \tag{9}$$

where $\mathbf{I}$ is a column vector of bus current injections, $\mathbf{Y}_{\text{bus}}$ is the bus admittance matrix, and $\mathbf{V}$ is the column vector of bus voltages. The entries of the admittance matrix are derived from the system's topology and the impedances of the network elements.

2.4 Kirchhoff's Voltage Law (KVL)

Kirchhoff's Voltage Law (KVL) states that the algebraic sum of all voltages around any closed loop in a circuit must be equal to zero. This is a direct consequence of the conservation of energy, as the total energy gained per unit charge in traversing a loop must equal the total energy lost.

Mathematically, for any closed loop in a circuit consisting of n elements, we have:

$$\sum_{i=1}^{n} \underline{V}_i = 0 \tag{10}$$

where $\underline{V}_i$ represents the voltage across the i-th element in the loop. KVL is applied in power systems to analyze and determine the voltages at different points in the network, ensuring that the voltage drops and gains around any loop sum to zero.

2.5 Kirchhoff's Current Law (KCL)

Kirchhoff's Current Law (KCL) states that the algebraic sum of currents entering a node (or junction) in an electrical circuit must be zero. This is a result of the conservation of charge, as charge cannot accumulate at a node; hence, the total current flowing into the node must be equal to the total current flowing out.

Mathematically, for any node with n branches connected to it, KCL can be expressed as:

$$\sum_{i=1}^{n} \underline{I}_i = 0 \tag{11}$$

where $\underline{I}_i$ represents the current in the i-th branch connected to the node. Positive currents are typically defined as flowing into the node, and negative currents as flowing out of the node.

KCL is used in the derivation of the VSC power loss equation as well as the power flow equations of the transformer later in this section.

2.6 Per Unit System

The per unit system is a normalization technique widely used in power system analysis to simplify calculations and comparisons. By expressing quantities such as voltage, current, and impedance in per unit (p.u.), we do not need to deal with conversions when we deal with power flows later on. The per unit value of a quantity $\underline{\chi}$ is given by:

$$\underline{\chi}_{p.u.} = \frac{\underline{\chi}_{\text{actual}}}{\underline{\chi}_{\text{base}}} \tag{12}$$

where $\underline{\chi}_{\text{actual}}$ is the actual value of the quantity and $\underline{\chi}_{\text{base}}$ is a chosen base value. This value $\underline{\chi}_{\text{p.u.}}$, is typically used for voltage, current, power, and impedance. We refer you to further reading on the per-unit system as it relates to the equations connecting the per-uni values of impedance, current, voltage and power in [15].

2.7 Loads

Loads in a power system represent the consumption of electrical power. They are typically modeled as constant power, constant current, or constant impedance loads, depending on the nature of the consumption. The modeling of loads is crucial as they directly affect the power flow and stability of the system.

Most commonly, the load characteristics are provided for the active and reactive powers, which are functions of the bus voltage $\underline{V_k}$:

$$P_k^{\text{load}} = \mathcal{P}_k^{\text{load}}(\underline{V_k}) \tag{13}$$

$$Q_k^{\text{load}} = \mathcal{Q}_k^{\text{load}}(\underline{V_k}) \tag{14}$$

However, in the general case, the complex load current can be expressed as a function of the bus voltage:

$$I_k^{\text{load}} = \mathcal{I}_k^{\text{load}}(\underline{V_k}) \tag{15}$$

where the function $\mathcal{I}_k^{\text{load}}(\cdot)$ describes the load characteristics.

This is because when developing load flow equations for high voltage systems, a load is typically the power supplied to a network at a lower voltage level, such as a distribution network. Often,

the voltage in these distribution systems is kept stable by adjusting the tap settings of distribution transformers. As a result, the active and reactive power in such systems is frequently treated as independent of the voltage on the high voltage side.

Therefore, a load is sometimes generally represented as a combination of an impedance, current, or as power. Loads are generally represented using their equivalent ZIP model, which includes constant impedance, constant current, and constant power components. Figure 2 shows the circuit representation of a typical load with a ZIP model. The control of the load is typically passive, meaning it consumes power according to the demand without active regulation.

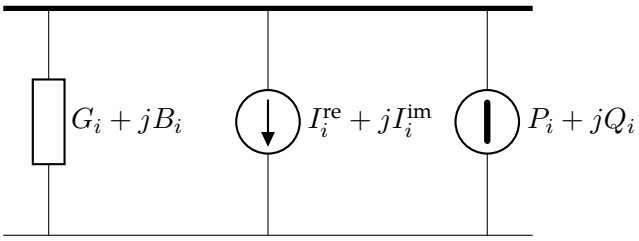

Figure 2: Representation of a load with its ZIP model.

2.8 Synchronous Generators

Generators are the sources of power in a system, converting mechanical energy into electrical energy. Classically, they are typically synchronous generators characterized by their voltage, frequency, and power output. Of course, this can more generally apply to any device that is connected to a single subsystem that is injecting power into the grid. For example, they could be a converter-interfaced renewable energy resource.

In steady-state operation, generators are generally controlled so that the active power they inject into the bus and the voltage at their terminals remain constant. The active power delivered by the generator is regulated by the turbine control system, which must operate within the capabilities of the turbine-generator system.

Voltage regulation is primarily managed by the reactive power injected into the bus. Since the generator must function within its reactive capability curve, it cannot maintain voltage outside certain limits. In this work, the limits of the generator are not considered as yet.

Generators inject active and reactive power P_i and Q_i separately into the grid. Figure 3 shows the generic model of a generator. We see that while attached to a bus with voltage magnitude V and angle δ, the generator's injected power can be defined as in a static generator, or it can be free to control other magnitudes in the grid as a controlled generator.

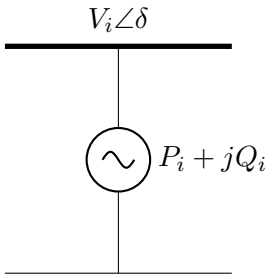

Figure 3: Representation of a generator.

With the information from In Fig. 16, we can observe that the ZIP model is used to represent shunt elements. These components can be combined to form the ZIP power equation as follows:

$$\begin{aligned} P_i^{\text{zip}} + jQ_i^{\text{zip}} = V_i^2(G_i - jB_i) \\ + V_i\angle\delta_i(I_i^{\text{re}} - jI_i^{\text{im}}) \\ + P_i + jQ_i. \end{aligned} \tag{16}$$

2.9 Voltage Source Converters (VSCs)

Voltage Source Converters (VSCs) enable the conversion of AC to DC and vice versa using self-commutating switches. These switches are Insulated Gate Bipolar Transistors (IGBTs), arranged in a bridge configuration. This is different from Line-Commutated Converters (LCCs) in several ways, including allowing independent control of active and reactive power, enabling the generation of leading or lagging reactive power regardless of active power levels. VSCs also provide faster response times than LCCs, making them more suitable for multiterminal HVDC systems and providing superior frequency and voltage support to the AC network.

In exchange, VSCs often have larger losses due to the application of high-frequency switching, which increases switching losses, and the higher on-state voltage drop of IGBT devices compared to thyristors of similar voltage ratings, leading to increased conduction losses at a given power level [16]. It is therefore important for us to take a close look at the losses at the switch-level.

2.9.1 IGBT Structure and Operation

An IGBT is a three-terminal power semiconductor device that combines the advantages of both metal-oxide semiconductor field-effect transistors (MOSFETs) and Bipolar Junction Transistors (BJTs). It is able to have the lower conduction losses of BJTs even for devices with high blocking voltage, and the high frequency switching capacbilities of MOSFETS [17].

The IGBT operates in two states:

- **Blocking State**: In this state, when the gate-source voltage (the voltage applied to the gate

terminal of the IGBT) is below the threshold, there is no inversion layer formed to connect the drain to the source, hence the device is off, and only a very small leakage current flows. The blocking capability is largely determined by the drift region and the depletion region within the device. The IGBT can block reverse voltages, making it suitable for certain AC circuit applications.

- **On-State Operation**: When the gate-source voltage exceeds the threshold, an inversion layer forms in the IGBT, allowing current to flow. This state is also referred to as the saturation state of the IGBT.

The switching between these states is controlled by the gate signal, bty adjusting the gate voltage to be positive to turn it on and to apply zero voltage (or even a small negative voltage in practice to reduce noise) in order to turn it off.

2.9.2 VSC Loss Model

Here, we attempt to define the loss model for the VSC by first defining the conduction and switching losses of the device. Then, by some simplifications of the model, we finally define the total power losses of the VSC at a level that will be useful at the grid level.

Conduction Loss Modelling Conduction losses occur due to the voltage drop across switching devices during conduction. The device voltage V_{FT} is a function of the current and can be expressed as:

$$V_{FT} = V_{T0} + r_{FT} i_{CE} \tag{17}$$

where V_{T0} is the forward voltage drop, r_{FT} is the on-state resistance of the switch, and i_{CE} is the collector-emitter current.

The values of V_{T0} and r_{FT} can be obtained from the IGBT's output characteristic:

$$r_{FT} = \frac{\Delta V_{CE}}{\Delta i_{CE}} = \frac{V_{CE2} - V_{CE1}}{i_{CE2} - i_{CE1}} \tag{18}$$

From here, conduction loss P_{cT} for the IGBT can be calculated as:

$$P_{cT} = \frac{1}{T} \int_0^T V_{FT} i_{CE} dt = \frac{1}{T} \int_0^T (V_{T0} + r_{FT} i_{CE}) i_{CE} dt \tag{19}$$

which simplifies to:

$$P_{cT} = V_{T0} I_{aT} + r_{FT} I_{rT}^2 \tag{20}$$

where T is the fundamental period, I_{aT} and I_{rT} are the average and RMS currents, respectively.

The conduction loss for the anti-parallel diode is modeled similarly:

$$P_{cD} = \frac{1}{T}\int_0^T V_{FD} i_D dt = V_{D0} I_{aD} + r_{FD} I_{rD}^2 \tag{21}$$

Switching Loss Modelling Switching losses in semiconductor devices like IGBTs can be divided into two parts:

- **Turn-on switching loss** E_{on}: Energy lost when the collector-emitter voltage transitions to zero during turn-on.
- **Turn-off switching loss** E_{off}: Energy lost when the voltage begins to rise from zero during turn-off.

The total switching loss in one cycle is the sum of E_{on} and E_{off}. The average switching losses are computed as:

$$P_{swT} = f_s(E_{on} + E_{off}) \tag{22}$$

where f_s is the switching frequency, and E_{on} and E_{off} are the switching energies for a single event at voltage V_{CE} and current I_C.

These energies are given by:

$$E_{on} = E_{on,\text{test}} \frac{V_{CE}}{V_{CE,\text{test}}} \frac{I_C}{I_{C,\text{test}}} \tag{23}$$

$$E_{off} = E_{off,\text{test}} \frac{V_{CE}}{V_{CE,\text{test}}} \frac{I_C}{I_{C,\text{test}}} \tag{24}$$

For the anti-parallel diode, the switching loss primarily arises from the reverse recovery process:

$$P_{swD} = f_s E_{rec} \tag{25}$$

where E_{rec} is the reverse recovery energy, calculated as:

$$E_{rec} = E_{rec,\text{test}} \frac{V_{DC}}{V_{DC,\text{test}}} \frac{I_C}{I_{C,\text{test}}} \tag{26}$$

In practise, we obtain test values from the manufacturer as in Figure 6. From there, we can perform an approximation of the losses as a function of the converter current I_c.

In steady state, the model of a VSC can be seen a interfacing the AC and DC subsystems as in Figure 7. On the AC side, which denote as the *from* side, we have the complex powers coming into the converter from the adjacent bus, with the AC line-to-line voltage denoted by V_f. Similarly, on the DC side, we have the incoming power to the DC bus as P_t and the DC voltage at that bus

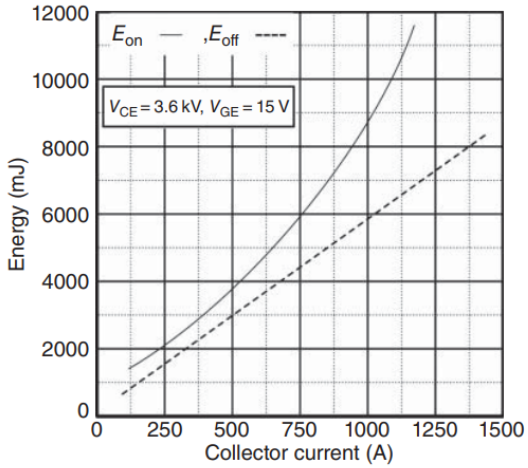

Figure 4: Example of the switching energy E_{on} and E_{off}.

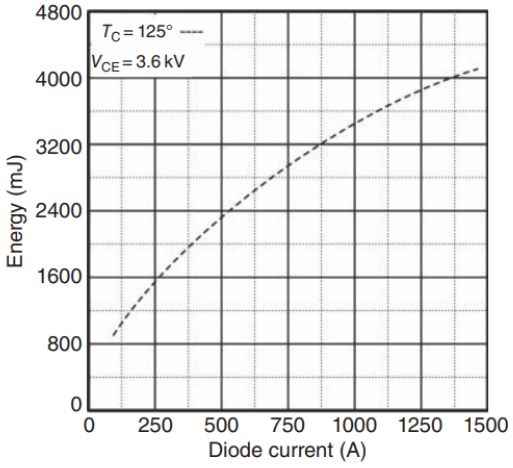

Figure 5: Reverse recovery energy characteristics for the anti-parallel diode.

Figure 6: Energy profiles for a manufacturer's test IGBT [2].

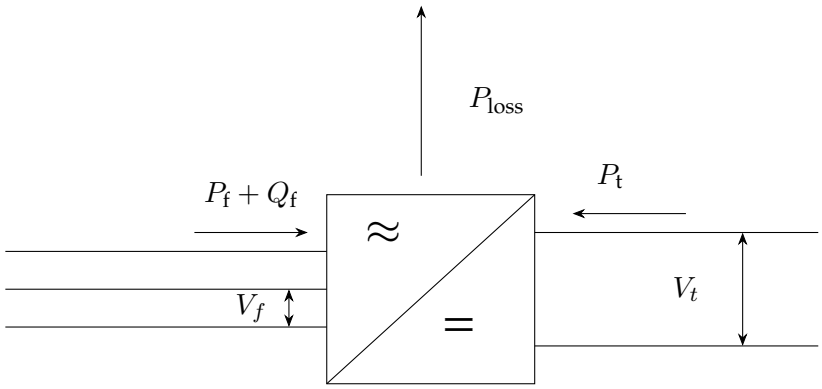

Figure 7: Model of a VSC in steady state [3].

denoted by V_t. Using this, we can calculate the current through the converter as:

$$I_c = \frac{\sqrt{P_f^2 + Q_f^2}}{V_f} \tag{27}$$

Thus, we can begin to form the equation for power loss P_{loss} using a quadratic function described in the IEC 62751-2 standard [18]. This expression is also typically used in literature [19–21]:

$$P_{\text{loss}} = a_i + b_i I_c + (c_i) I_c^2 \tag{28}$$

With coefficients a_i, b_i, c_i, and r_i accounting for different components of converter losses:

- **No-Load Loss Factor** a_i: Includes no-load losses in transformers, and averaged auxiliary equipment losses such as lightning, heating, and control systems.
- **Linear Current Factor** b_i: Accounts for switching losses in valves, especially those related to turn-off losses of IGBTs and free-wheeling diodes.
- **Square Current Factor** c_i: Includes conduction losses in the switches.

Extending KCL, we can form the following equation for the power balance at the converter for the active power, including the loss function that we derived in 28:

$$\begin{aligned} P_f + P_t - P_{\text{loss}} &= 0, \\ P_f + P_t &= P_{\text{loss}}, \\ P_f + P_t &= a + b\frac{\sqrt{(P_f)^2 + (Q_f)^2}}{V_f} + c\frac{(P_f)^2 + (Q_f)^2}{V_f^2}. \end{aligned} \tag{29}$$

In the end, what we have is a model that takes into account the power balance of the converter using the loss function that we have described, and relating the active powers coming in from the AC and the DC side attached to the terminals of the VSC. Finally we obtain the model in the Figure 8 below.

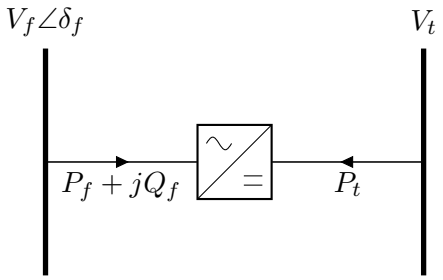

Figure 8: Representation of a converter.

Here, we would like to make a distinction that the model we describe is a particularisation of how a VSC is connected to a grid. VSCs that are connected to a DC source and then to ground (such as when connected a renewable generation source) should be considered to be interfacing between the AC side and a virtual DC node, which is then connected to a grounded generator.

2.10 Transformers

Transformers are used to step up or step down voltage levels for efficient power transmission and distribution. While the fundamental operating principle of a transformer is the same for both single-phase and three-phase transformers, the three-phase transformer is predominantly used at higher voltage levels in transmission and distribution networks due to its efficiency and practicality.

A single-phase transformer consists of primary and secondary windings, which are magnetically coupled through a core, as described by the equations for voltage, current, and flux linkage. However, for the purposes of this work, we focus on three-phase transformers because modern power systems are primarily three-phase in nature. The same principles that govern single-phase transformers can be extended to three-phase transformers, which are essentially three single-phase transformers connected together. These connections can be arranged in different configurations such as Y-Y, Delta-Delta, or Y-Delta, depending on the application and voltage level requirements.

At higher voltage levels, using three-phase transformers offers significant advantages in terms of power handling capability and efficiency, which makes them the preferred choice for large-scale power transmission and distribution systems. Despite the different configurations and complexities of three-phase transformers, their underlying principles remain consistent with those of single-phase transformers, which we will now discuss in more detail. We also use the per-unit model that greatly simplifies the analysis of the system.

2.10.1 Phase-Shifting Transformers

The most general way to model a transformer is by considering it as a Phase-Shifting Transformers (PSTs). This is because a PSTs is able to control power flows using two control variables: its tap module, as well as the phase shift between the primary and secondary side. This forms the complex ratio which we define as $m\angle\tau$.

In the Figure 9, we see an asymmetrical model of a PST, where the lossless transformer is closer to the *from* side and is series with the common π model of a line with series impedance $\underline{z}_s$ is on the *to* end. In between, we have the shunt element $\underline{y}_{sh}$. This model[1] is also used in the widely-available MATPOWER library [22]. We would like to build the admittance matrix of this transformer so that we may express the power flows as a relationship between the two bus voltages $\underline{V}_f\angle\underline{\delta}_f$ and $\underline{V}_t\angle\underline{\delta}_t$, as well as the complex ratio $m\angle\tau$. To do that, we express first the relationships between the voltages of the node *from*, *to*, P, and Q, as well as the currents flowing from node to node:

[1] It is important to note that PSTs are often asymmetrically modelled without the shunt element. This is easily addressed by setting the value of $\underline{y}_{sh}$ to be zero. We include $\underline{y}_{sh}$ simply for generalisability.

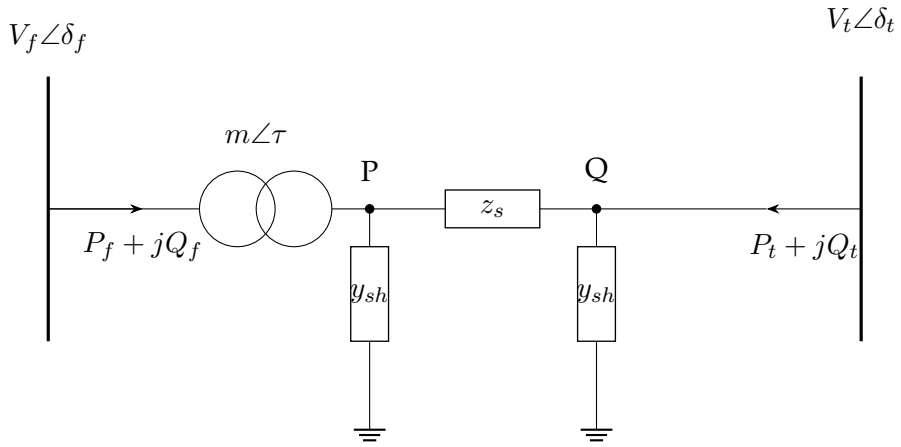

Figure 9: Model of a Controllable Transformer (PST).

$$\begin{aligned} \frac{\underline{V}_P}{\underline{V}_f} &= \frac{1}{me^{j\tau}}, \\ \underline{V}_f &= \underline{V}_P m e^{j\tau}, \\ \underline{V}_P &= \frac{\underline{V}_f}{me^{j\tau}}, \end{aligned} \tag{30}$$

Considering that the transformer model is lossless, we have the following:

$$\begin{aligned} \underline{I}_f^* \underline{V}_f &= \underline{I}_{\text{Tr}\to P}^* \underline{V}_P, \\ \frac{\underline{V}_P}{\underline{V}_f} &= \left[\frac{\underline{I}_f}{\underline{I}_{\text{Tr}\to P}}\right]^*, \\ \frac{\underline{I}_f}{\underline{I}_{\text{Tr}\to P}} &= \left[\frac{1}{me^{j\tau}}\right]^*, \\ \frac{\underline{I}_f}{\underline{I}_{\text{Tr}\to P}} &= \frac{1}{me^{-j\tau}}, \\ \underline{I}_{\text{Tr}\to P} &= \underline{I}_f m e^{-j\tau}. \end{aligned} \tag{31}$$

We perform KCL around the point P in the figure, to obtain:

$$\begin{aligned} \underline{I}_a + \underline{I}_b + \underline{I}_c &= 0, \\ \underline{I}_{\text{Tr}\to P} - \underline{I}_{P\to\text{ground}} - \underline{I}_{P\to t} &= 0, \\ \underline{I}_{\text{Tr}\to P} &= \underline{I}_{P\to\text{ground}} + \underline{I}_{P\to t}, \\ \underline{I}_f \cdot me^{-j\tau} &= \underline{V}_P \underline{y}_{\text{sh}} + (\underline{V}_P - \underline{V}_t)\underline{y}_s, \\ \underline{I}_f \cdot me^{-j\tau} &= \underline{V}_P(\underline{y}_s + \underline{y}_{\text{sh}}) + \underline{V}_t \underline{y}_s, \\ \underline{I}_f &= \underline{V}_f \frac{(\underline{y}_s + \underline{y}_{\text{sh}})}{m^2} - \underline{V}_t \frac{\underline{y}_s}{me^{-j\tau}}. \end{aligned} \tag{32}$$

Similarly, we once again perform KCL around point Q:

$$\begin{aligned} \underline{I}_a + \underline{I}_b + \underline{I}_c &= 0, \\ \underline{I}_{P\to Q} - \underline{I}_{Q\to\text{ground}} + \underline{I}_t &= 0, \\ \underline{I}_t &= \underline{I}_{Q\to\text{ground}} - \underline{I}_{P\to Q}, \\ \underline{I}_t &= \underline{V}_t \underline{y}_{\text{sh}} - \underline{y}_s(\underline{V}_P - \underline{V}_t), \\ \underline{I}_t &= -\underline{y}_s \underline{V}_P + (\underline{y}_{\text{sh}} + \underline{y}_s)\underline{V}_t, \\ \underline{I}_t &= -\underline{V}_f \frac{\underline{y}_s}{m e^{j\tau}} + (\underline{y}_{\text{sh}} + \underline{y}_s)\underline{V}_t. \end{aligned} \tag{33}$$

Arranging the results from 32 and 33 into a $\underline{\text{Y}}$-bus matrix gets us the following:

$$\begin{bmatrix} \underline{I}_f \\ \underline{I}_t \end{bmatrix} = \begin{bmatrix} \dfrac{\underline{y}_s + \underline{y}_{\text{sh}}}{m^2} & -\dfrac{\underline{y}_s}{m e^{-j\tau}} \\ -\dfrac{\underline{y}_s}{m e^{j\tau}} & \underline{y}_s + \underline{y}_{\text{sh}} \end{bmatrix} \begin{bmatrix} \underline{V}_f \\ \underline{V}_t \end{bmatrix}, \tag{34}$$

$$\underline{Y}_{tr} = \begin{bmatrix} \dfrac{\underline{y}_s + \underline{y}_{sh}}{m^2} & -\dfrac{\underline{y}_s}{m e^{-j\tau}} \\ -\dfrac{\underline{y}_s}{m e^{j\tau}} & \underline{y}_s + \underline{y}_{sh} \end{bmatrix}, \tag{35}$$

Using the results from Equation 34, we can start to think of our controllable transformer (the PST), as being an "active" branch, wherein we only need to deal with the power flows between the branches. As seen in Figure 10, we replace the ideal PST and π model with an inductor symbol, with the final power flows on the *from* and *to* sides derived below.

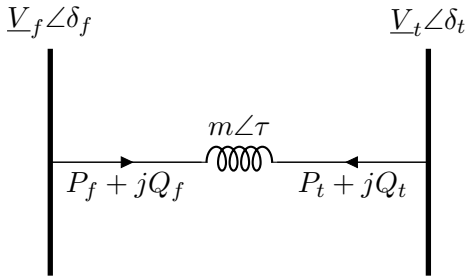

Figure 10: Representation of a transformer.

First, we start from the current equations from Equation 34:

$$\begin{bmatrix} \underline{I}_f \\ \underline{I}_t \end{bmatrix} = \begin{bmatrix} \dfrac{\underline{y}_s + \underline{y}_{\text{sh}}}{m^2} & -\dfrac{\underline{y}_s}{m e^{-j\tau}} \\ -\dfrac{\underline{y}_s}{m e^{j\tau}} & \underline{y}_s + \underline{y}_{\text{sh}} \end{bmatrix} \begin{bmatrix} \underline{V}_f \\ \underline{V}_t \end{bmatrix}. \tag{36}$$

Now, to compute the power flows, we use the formula $\underline{S} = \underline{V} \cdot \underline{I}^*$, where $\underline{I}^*$ is the complex conjugate of the current.

For the sending side f, the power equation is:

$$\underline{S}_f = \underline{V}_f \underline{I}^*_{ft} \tag{37}$$

For the receiving side t, the power equation is:

$$\underline{S}_t = \underline{V}_t \underline{I}^*_t \tag{38}$$

Now substitute the expressions for $\underline{I}_{f\to t}$ and $\underline{I}_{t\to f}$ and compute the complex conjugates of the current terms:

$$\begin{aligned} P^{\text{tr}}_f + jQ^{\text{tr}}_f &= \underline{V}_f \left(\frac{\underline{y}^*_s + \underline{y}^*_{\text{sh}}}{m^2} \underline{V}^*_f - \frac{\underline{y}^*_s}{m e^{j\tau}} \underline{V}^*_t \right), \\ P^{\text{tr}}_t + jQ^{\text{tr}}_t &= \underline{V}_t \left(\frac{\underline{y}^*_s + \underline{y}^*_{\text{sh}}}{m^2} \underline{V}^*_t - \frac{\underline{y}^*_s}{m e^{-j\tau}} \underline{V}^*_f \right). \end{aligned} \tag{39}$$

Next, we distribute the terms to separate the voltage magnitudes:

$$\begin{aligned} P^{\text{tr}}_f + jQ^{\text{tr}}_f &= \underline{V}^2_f \frac{\underline{y}^*_s + \underline{y}^*_{\text{sh}}}{m^2} - \underline{V}_f \underline{V}^*_t \frac{\underline{y}^*_s}{m e^{j\tau}}, \\ P^{\text{tr}}_t + jQ^{\text{tr}}_t &= \underline{V}^2_t \frac{\underline{y}^*_s + \underline{y}^*_{\text{sh}}}{m^2} - \underline{V}_t \underline{V}^*_f \frac{\underline{y}^*_s}{m e^{-j\tau}}. \end{aligned} \tag{40}$$

Resulting in the complex power at both ends of the transformer:

$$\begin{aligned} P^{\text{tr}}_f + jQ^{\text{tr}}_f &= \underline{V}^2_f \frac{\underline{Y}^*_s + \underline{Y}^*_{sh}}{m^2} - \underline{V}_f \underline{V}^*_t \frac{\underline{Y}^*_s}{m e^{j\tau}}, \\ P^{\text{tr}}_t + jQ^{\text{tr}}_t &= \underline{V}^2_t (\underline{Y}^*_s + \underline{Y}^*_{sh}) - \underline{V}_t \underline{V}^*_f \frac{\underline{Y}^*_s}{m e^{-j\tau}}. \end{aligned} \tag{41}$$

2.11 Controls

Generators, VSCs, and controllable transformers can independently control active and reactive power separately, either through *dq* current injections or through phase shifting in the case of transformers. This allows very precise control of bus or branch magnitudes, with various control modes available depending on the type of device.

2.11.1 Synchronous Generators

In synchronous generators, the primary control modes include:

- **Constant Active Power (P)**: The generator produces a constant amount of active power and is not responsible for frequency regulation.
- **Droop Control (P-f Control)**: The generator adjusts its active power output in response to deviations in system frequency, increasing output if the frequency drops.
- **Automatic Generation Control (AGC)**: In this mode, the generator adjusts its power output according to central dispatch signals to maintain nominal frequency.
- **Constant Voltage (V)**: The generator adjusts its reactive power output to maintain a constant voltage at its terminals or a specified bus.
- **Constant Reactive Power (Q)**: The generator provides a fixed amount of reactive power, regardless of voltage fluctuations.
- **Voltage Droop Control (Q-U Control)**: Similar to active power droop, this mode adjusts reactive power output based on voltage deviations from the nominal setpoint.
- **Constant Power Factor**: The generator maintains a fixed power factor by adjusting the reactive power to maintain the ratio between active and reactive power.

2.11.2 Voltage Source Converters (VSCs)

A VSC HVDC converter can independently control the active and reactive power injection with respect to the AC system. The active power injection is modeled in different ways:

- **Constant P**: The converter has a constant active power injection P_s into the AC grid.
- **Constant V_{DC}**: The algorithm adapts the active power injection P_s to maintain a constant DC bus voltage V_{DC}.
- **P–V_{DC} Droop**: The actual active power injection depends on the DC bus voltage V_{DC} according to the droop characteristic.

The ability of the converter to independently control the reactive power results in two different representations in the power flow algorithm:

- **Constant Q**: The converter injects a constant amount of reactive power Q_s into the AC grid.
- **Constant V**: The converter adapts the reactive power injection to maintain a constant AC

bus voltage magnitude V_s.

2.11.3 Phase Shifting Transformers (PSTs)

In phase shifting transformers, the active and reactive power can be controlled by changing the phase angle between the primary and secondary windings. The control modes for PSTs include:

- **Phase Angle Control**: The PST adjusts the phase angle α, which modifies the power flow across the transformer.
- **Constant Power Flow**: The PST maintains a constant power transfer between the connected buses by adjusting the phase angle dynamically.
- **Reactive Power Compensation**: By adjusting the phase angle, the PST can compensate for reactive power flows in the system, helping regulate voltage levels.

In view of the many combinations of control modes that each of these active elements in the grids have, there presents an opportunity to generalise the control modes such that we separate the setpoints in the grids from the devices that control them. We observe that in certain control modes, it is the bus magnitudes that are maintained by the elements in the grid, and in others, branch magnitudes such as active and reactive power are controlled. Therein lies the way in which we will generalise controls; each element will be able to define two values in any arbitrary bus or branch:

- **Bus magnitudes:**
  - Voltage magnitude: $|V|$
  - Voltage angle: θ
  - Active power injected at the bus: P_{zip}
  - Reactive power injected at the bus: Q_{zip}
- **Branch magnitudes:**
  - Active power from the sending side of the branch: P_f
  - Reactive power from the sending side of the branch: Q_f
  - Active power to the receiving side of the branch: P_t
  - Reactive power to the receiving side of the branch: Q_t

2.12 Conclusion

This section has laid the foundation for understanding the key concepts and components that will be used in the subsequent sections. Without any loss of generalibility, from this point on, this work will refer to all complex values simply as for all values such as impedance Z, admittance Y, current I, voltage V and complex power S.

In the next section, we begin to formulate the power flow equations and the method with which we will solve it: the Newton-Raphson method.

3 Power Flow Equations and Newton-Raphson Method

This section introduces the formulation of the power flow equations and describes the application of the Newton-Raphson method to solve these equations. Power flow analysis is critical for determining the steady-state operation of power systems. It provides information about bus voltages, phase angles, active and reactive power flows, and power losses in the network. We first derive the power flow equations based on the relationships between complex power, voltage, and current as explained in the previous section. Then, we describe how the Newton-Raphson method is applied to solve them.

3.1 Power Flow Equations (Matrix Form)

The power flow equations are derived from the fundamental relationship between complex power, voltage, and current. For each bus in a power system, we are interested in calculating the active and reactive power injected into the bus. Complex power S is given by:

$$S = P + jQ \tag{42}$$

where P is the active power (real power), and Q is the reactive power. Recall from Equation 43 that the relationship between complex power, voltage, and current is expressed as:

$$S = VI^* \tag{43}$$

The current injection at each bus can be described as a linear combination of the bus voltages and the admittances between the injected bus and other connected buses. We can express the current at each bus as:

$$\begin{bmatrix} \bar{I}_1 \\ \bar{I}_2 \\ \bar{I}_3 \\ \vdots \\ \bar{I}_n \end{bmatrix} = \begin{bmatrix} \bar{Y}_{11} & \bar{Y}_{12} & \bar{Y}_{13} & \cdots & \bar{Y}_{1n} \\ \bar{Y}_{21} & \bar{Y}_{22} & \bar{Y}_{23} & \cdots & \bar{Y}_{2n} \\ \bar{Y}_{31} & \bar{Y}_{32} & \bar{Y}_{33} & \cdots & \bar{Y}_{3n} \\ \vdots & \vdots & \vdots & \ddots & \vdots \\ \bar{Y}_{n1} & \bar{Y}_{n2} & \bar{Y}_{n3} & \cdots & \bar{Y}_{nn} \end{bmatrix} \begin{bmatrix} \bar{V}_1 \\ \bar{V}_2 \\ \bar{V}_3 \\ \vdots \\ \bar{V}_n \end{bmatrix} \tag{44}$$

$$\mathbf{I} = \mathbf{Y}_{\text{bus}}\mathbf{V} \tag{45}$$

Using the relationship for complex power S, we substitute $\mathbf{I} = \mathbf{Y}_{\text{bus}}\mathbf{V}$ into the complex power equation $S = VI^*$:

$$S_i = V_i I_i^* = V_i \left(\sum_{j=1}^{n} Y_{ij} V_j \right)^* \tag{46}$$

Next, we separate the complex power into real and imaginary components to obtain the active power P and reactive power Q:

$$\mathbf{S} = \mathbf{P} + j\mathbf{Q} \tag{47}$$

$$P_i = \Re \left(V_i \sum_{j=1}^{n} Y_{ij}^* V_j^* \right) \tag{48}$$

$$Q_i = \Im \left(V_i \sum_{j=1}^{n} Y_{ij}^* V_j^* \right) \tag{49}$$

Slack Bus (Reference Bus) The slack bus serves as the reference bus in the power flow problem. Both the voltage magnitude V_{slack} and angle θ_{slack} at the slack bus are known and fixed. This bus compensates for the losses in the network to ensure that the total generated power equals the total consumed power. As both the voltage magnitude and angle are pre-set at the slack bus, no power flow equations are solved for this bus.

PQ Bus (Load Bus) At a PQ bus, both the active power P and reactive power Q are specified. The goal at PQ buses is to solve for the unknown voltage magnitude V and voltage angle θ. For each PQ bus, two non-linear equations are added to the power flow problem:

- The active power equation P_i, which relates to the active power injected at bus i.
- The reactive power equation Q_i, which relates to the reactive power injected at bus i.

PV Bus (Generator Bus) At a PV bus, the active power P and voltage magnitude V are specified, but the reactive power Q is allowed to vary. The goal at a PV bus is to solve for the unknown voltage angle θ while the voltage magnitude remains fixed. For PV buses, only the active power equation P_i is added to the Jacobian matrix, as the voltage magnitude V_i is already specified. The reactive power Q_i is not controlled directly, but it can be monitored as part of the power flow solution.

These are the real and reactive power equations for the network, where P_i represents the active power injected into bus i, and Q_i represents the reactive power. These equations can also be

expressed using the traditional trigonometric form with cosine and sine, but the form above is the more general and compact representation using the admittance matrix.

3.2 Newton-Raphson Method

The Newton-Raphson method is an iterative technique used to solve systems of nonlinear equations. The method is based on linearizing the set of nonlinear power flow equations and solving them iteratively.

For a system of nonlinear equations $f(x) = 0$, where x is a vector of unknowns, the Newton-Raphson method approximates the solution by iteratively solving:

$$x^{(k+1)} = x^{(k)} - [J(x^{(k)})]^{-1} f(x^{(k)}) \tag{50}$$

The general form of the Jacobian matrix $J(x^{(k)})$ is given by:

$$J(x^{(k)}) = \begin{bmatrix} \frac{\partial f_1}{\partial x_1} & \frac{\partial f_1}{\partial x_2} & \cdots & \frac{\partial f_1}{\partial x_n} \\ \frac{\partial f_2}{\partial x_1} & \frac{\partial f_2}{\partial x_2} & \cdots & \frac{\partial f_2}{\partial x_n} \\ \vdots & \vdots & \ddots & \vdots \\ \frac{\partial f_n}{\partial x_1} & \frac{\partial f_n}{\partial x_2} & \cdots & \frac{\partial f_n}{\partial x_n} \end{bmatrix} \tag{51}$$

where $J(x^{(k)})$ is the Jacobian matrix of the system of equations evaluated at the current iteration $x^{(k)}$. Figure 11 illustrates the iterations of Newton-Raphson and how it reaches convergence.

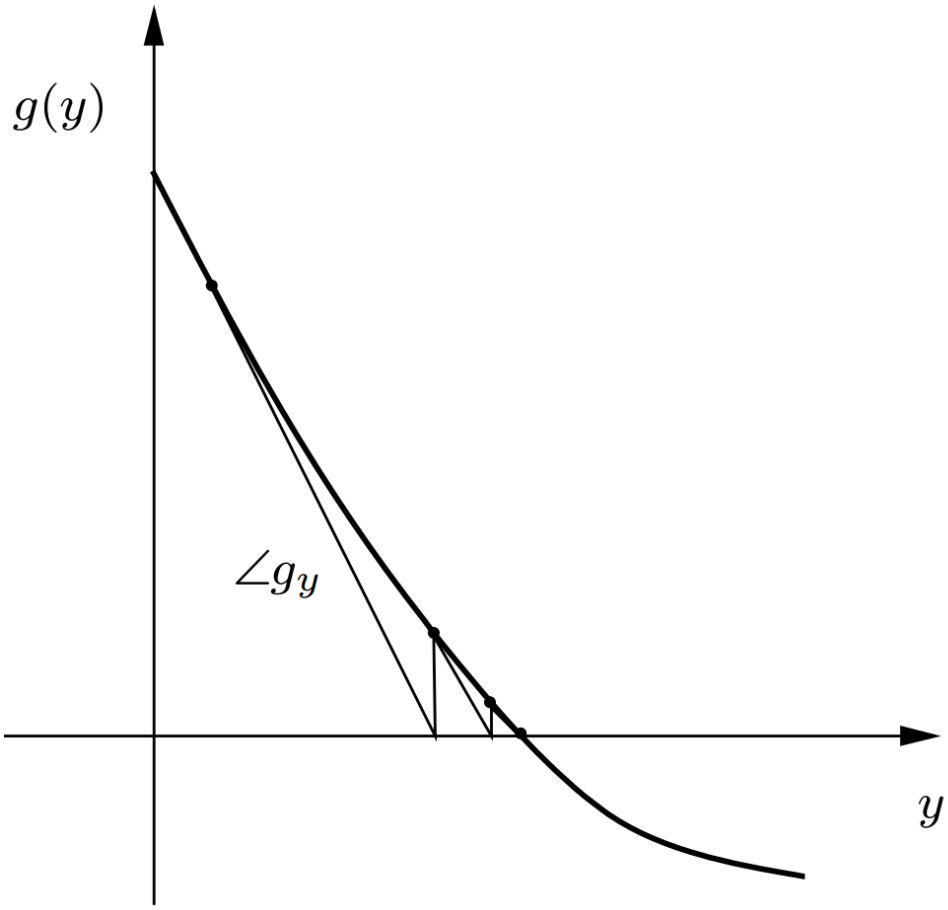

Figure 11: Newton-Raphson for a well-conditioned scalar function [4].

3.2.1 Jacobian Matrix

In power flow analysis, the unknowns are the voltage magnitudes and angles at the buses. The real and reactive power mismatches at each bus are expressed as:

$$\Delta P_i = P_i^{\text{specified}} - P_i^{\text{calculated}} \tag{52}$$

$$\Delta Q_i = Q_i^{\text{specified}} - Q_i^{\text{calculated}} \tag{53}$$

The Jacobian matrix consists of the partial derivatives of the active and reactive power equations with respect to the voltage magnitudes and angles:

$$J = \begin{bmatrix} \frac{\partial P}{\partial \theta} & \frac{\partial P}{\partial |V|} \\ \frac{\partial Q}{\partial \theta} & \frac{\partial Q}{\partial |V|} \end{bmatrix} \tag{54}$$

The entries of the Jacobian depend on the type of bus:

- For *PQ buses*, both active (P) and reactive (Q) power equations are included, so all four blocks ($\frac{\partial P}{\partial \theta}$, $\frac{\partial P}{\partial V}$, $\frac{\partial Q}{\partial \theta}$, and $\frac{\partial Q}{\partial V}$) are relevant.
- For *PV buses*, only the active power equation (P) is included, so only the blocks $\frac{\partial P}{\partial \theta}$ and $\frac{\partial P}{\partial V}$ are used.
- For the *slack bus*, no equations are added to the Jacobian matrix.

These derivatives allow us to build the Jacobian matrix at each iteration. Solving the linearized system for ΔP and ΔQ provides updates for the voltage magnitudes and angles:

$$\Delta\theta = -J^{-1}\Delta P \tag{55}$$

$$\Delta|V| = -J^{-1}\Delta Q \tag{56}$$

3.3 Classical Power Flow with Newton Raphson

The Newton-Raphson method is applied to the power flow equations as follows:

1. **Initialization**: Start with an initial guess for the bus voltage magnitudes and angles. Typically, the voltage magnitude is assumed to be 1 p.u., and the voltage angle is set to zero for all buses except the slack bus.
2. **Power Mismatch Calculation**: Compute the power mismatches ΔP and ΔQ at each bus based on the initial voltage guesses and the specified power injections.
3. **Jacobian Matrix Calculation**: Calculate the Jacobian matrix by evaluating the partial derivatives of the power flow equations with respect to the voltage magnitudes and angles.
4. **Voltage Update**: Solve the linearized system of equations to update the voltage magnitudes and angles using:
$$\Delta\theta = -J^{-1}\Delta P \tag{57}$$
$$\Delta|V| = -J^{-1}\Delta Q \tag{58}$$
5. **Convergence Check**: Check if the power mismatches ΔP and ΔQ are within a predefined tolerance. If the mismatches are below the tolerance, the solution has converged; otherwise, repeat the process from Step 2.

The Newton-Raphson method typically converges quickly due to its quadratic convergence properties, making it highly efficient for large-scale power systems. An important note to make

is that in Equations 57 and 58, we have to deal with the inverse of the Jacobian matrix. This is very expensive computationally, and typically increases by a factor of n^3, where n is the number of variables in large systems. In order to avoid performing inversions at every iteration, methods we instead rely on column pre-ordering, taking advantage of the structure of sparse matrices for matrix decomposition and multiplication [23].

3.4 Flexible Universal Branch Model (FUBM) and Power Flow Algorithm

An important development in unified AC/DC power flow is the FUBM. The idea of the FUBM is to represent various components in power systems (transmission lines, transformers, and VSCs) in a standardised manner as seen in Figure 12.

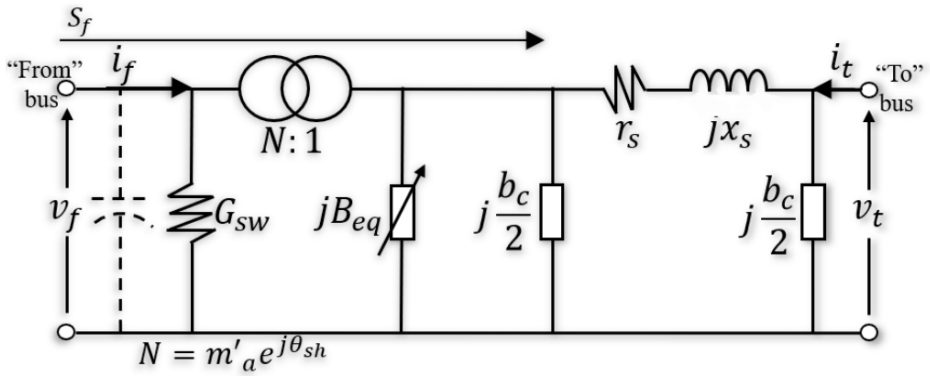

Figure 12: Standard model of a FUBM branch [5].

3.4.1 Branch Admittance Matrix in FUBM

The branch admittance matrix in FUBM can be expressed in terms of current injections at both ends of the branch (i_f and i_t) and terminal voltages (v_f and v_t):

$$\begin{bmatrix} i_f \\ i_t \end{bmatrix} = \begin{bmatrix} y_{ff} & y_{ft} \\ y_{tf} & y_{tt} \end{bmatrix} \begin{bmatrix} v_f \\ v_t \end{bmatrix} \tag{59}$$

Where the admittance matrix for the FUBM can be written as:

$$Y_{br} = \begin{bmatrix} G_{sw} + (y_s + \frac{jB_c}{2} + jB_{eq}) & -\frac{y_s}{me^{j\theta_{sh}}} \\ -\frac{y_s}{me^{-j\theta_{sh}}} & y_s + \frac{jB_c}{2} \end{bmatrix} \tag{60}$$

The parameters involved are:

- G_{sw} represents the shunt conductance for switching losses.

- B_{eq} compensates reactive power in VSCs.
- θ_{sh} is the phase-shift angle.
- m is the modulation amplitude coefficient of the VSC.

3.4.2 Flexible Power Flow Algorithm (FPFA)

The Flexible Power Flow Algorithm (FPFA) integrates the FUBM into power flow calculations for both AC and DC networks. The FPFA introduces new state variables and control equations to handle elements such as VSCs and phase-shifting transformers.

The FPFA modifies the traditional mismatch equations to include new variables such as the modulation index (m) and phase-shifting angle (θ_{sh}):

$$g(X) = \begin{bmatrix} g_P \\ g_Q \\ g_{\theta_{sh}} \\ g_{Qz} \\ g_{V_f} \\ g_{V_t} \\ g_{Q_t} \end{bmatrix} = \begin{bmatrix} P_{\text{specified}} - P_{\text{calculated}} \\ Q_{\text{specified}} - Q_{\text{calculated}} \\ \text{Real Power Control Mismatch} \\ \text{Zero Constraint for Reactive Power} \\ \text{Voltage Control at Bus f} \\ \text{Voltage Control at Bus t} \\ \text{Reactive Power at Bus t} \end{bmatrix} \tag{61}$$

To Jacobian matrix is expanded to account for the additional state variables, and involves the variables in the **X** column vector in Equation 63. We see that instead of the typical set of voltage angle and magnitude, there is also the control variables $\theta_{sh}^{(i)}$ and $m_a^{(i)}$, as well as the reactive power zero-ing susceptance $B_{eq}^{(i)}$.

$$\mathbf{J} = \begin{bmatrix} \frac{\partial g_P}{\partial V_a} & \frac{\partial g_P}{\partial V_m} & \frac{\partial g_P}{\partial \theta_{sh}} & \frac{\partial g_P}{\partial B_{eq}} & \frac{\partial g_P}{\partial m_a} & \frac{\partial g_P}{\partial m_a} & \frac{\partial g_P}{\partial B_{eq}} \\ \frac{\partial g_Q}{\partial V_a} & \frac{\partial g_Q}{\partial V_m} & \frac{\partial g_Q}{\partial \theta_{sh}} & \frac{\partial g_Q}{\partial B_{eq}} & \frac{\partial g_Q}{\partial m_a} & \frac{\partial g_Q}{\partial m_a} & \frac{\partial g_Q}{\partial B_{eq}} \\ \frac{\partial g_{sh}}{\partial V_a} & \frac{\partial g_{sh}}{\partial V_m} & \frac{\partial g_{sh}}{\partial \theta_{sh}} & \frac{\partial g_{sh}}{\partial B_{eq}} & \frac{\partial g_{sh}}{\partial m_a} & \frac{\partial g_{sh}}{\partial m_a} & \frac{\partial g_{sh}}{\partial B_{eq}} \\ \frac{\partial g_{Qz}}{\partial V_a} & \frac{\partial g_{Qz}}{\partial V_m} & \frac{\partial g_{Qz}}{\partial \theta_{sh}} & \frac{\partial g_{Qz}}{\partial B_{eq}} & \frac{\partial g_{Qz}}{\partial m_a} & \frac{\partial g_{Qz}}{\partial m_a} & \frac{\partial g_{Qz}}{\partial B_{eq}} \\ \frac{\partial g_{V_f}}{\partial V_a} & \frac{\partial g_{V_f}}{\partial V_m} & \frac{\partial g_{V_f}}{\partial \theta_{sh}} & \frac{\partial g_{V_f}}{\partial B_{eq}} & \frac{\partial g_{V_f}}{\partial m_a} & \frac{\partial g_{V_f}}{\partial m_a} & \frac{\partial g_{V_f}}{\partial B_{eq}} \\ \frac{\partial g_{V_t}}{\partial V_a} & \frac{\partial g_{V_t}}{\partial V_m} & \frac{\partial g_{V_t}}{\partial \theta_{sh}} & \frac{\partial g_{V_t}}{\partial B_{eq}} & \frac{\partial g_{V_t}}{\partial m_a} & \frac{\partial g_{V_t}}{\partial m_a} & \frac{\partial g_{V_t}}{\partial B_{eq}} \\ \frac{\partial g_{Q_t}}{\partial V_a} & \frac{\partial g_{Q_t}}{\partial V_m} & \frac{\partial g_{Q_t}}{\partial \theta_{sh}} & \frac{\partial g_{Q_t}}{\partial B_{eq}} & \frac{\partial g_{Q_t}}{\partial m_a} & \frac{\partial g_{Q_t}}{\partial m_a} & \frac{\partial g_{Q_t}}{\partial B_{eq}} \end{bmatrix} \tag{62}$$

$$\mathbf{X} = \begin{bmatrix} V_a^{(i)} \\ V_m^{(i)} \\ \theta_{sh}^{(i)} \\ B_{eq}^{(i)} \\ m_a^{(i)} \\ m_a^{(i)} \\ B_{eq}^{(i)} \end{bmatrix} \tag{63}$$

3.5 Limitations and Challenges

The use of B_{eq} in order to absorb or produce reactive power on the DC side of a VSC terminal is seen as a practical way of ensuring that there is not reactive power exchange on the DC interface. The FUBM therefore, can be shown to be very useful in AC/DC hybrid systems. At the same time, implentations of this method in GridCal and MATPOWER have seen that at times, there are cases when the FUBM fails to converge because of some sentivity towards the initialisation of the value B_{eq}. This means that, for a given system, the initial setpoint of B_{eq} may affect the gradients so much so as to push the solver in the wrong direction of the root in the solution space.

Additionally, by modelling the VSC as a transmission line in series with an ideal phase shifting transformer, we may lose some nuance in the operation of the converter. For example, a VSC does not perhaps set its tap module and angle in the same way that a transformer does, even if it does so virtually in the power flow. We then lose some direct applicability to real systems in this way.

It is here that we see a potential to change the VSC model - to represent the VSC by relating the power in and out of its terminals with the voltages and the current through the converter. We can also the extend the branch concept. Instead of a unified model in the FUBM, we split our branches into two distinct sets: "active" branches like VSCs and controllable transformers, and passive ones like conventional transmission lines. This is the idea that we wish to expand on in the next section.

4 Generalised Power Flow

In previous sections, we introduced the Flexible Universal Branch Model (FUBM) as a step forward from the traditional power flow methodologies. The FUBM improves upon traditional power flow analysis by incorporating modern control capabilities, such as flexible switching between control modes, and the ability to handle both AC and DC grids. While FUBM is a powerful tool in modeling contemporary grids with various active elements like Voltage Source Converters (VSCs) and phase-shifting transformers (PSTs), it still has its own limitations when dealing with more complex, flexible control strategies present in modern energy systems.

The limitations of the FUBM are primarily related to how it handles power flow control and system complexity:

- **Absence of remote controls**: The FUBM cannot handle remote controls, that is to say, controlling elements that are not directly connected to the terminals of the device. In modern systems, Voltage and Current Transformers can be put at any part of the system to measure quantities, and so control need not be local anymore.

- **Pre-selected bus types**: The FUBM requires pre-selection of bus types such as PV, PQ, PVQ, and VD, which restricts its flexibility. The bus type must be determined in advance, and defining all the combinations of bus types is not so feasible when dealing with the many control options.

- **Use of B_{eq} for reactive power control**: The use of B_{eq} in the FUBM can significantly influence convergence. Poor initialisation of B_{eq} may result in non-convergence.

The generalised power flow is an attempt to resolve these problems. This new formulation would be capable of handling various control modes, flexible switching between bus types, remote and multiple control strategies, and the inclusion of both AC and DC grids, providing a more comprehensive approach to solving modern power system challenges. The Table 1 below summarises the features that we aim to contribute in the new formulation. From here on, we refer to the FUBM as the "classical" model.

Feature	Classic Power Flow	Generalised Power Flow
Handles AC systems	✓	✓
Remote controls	×	✓
Control more than two magnitudes at a bus	✓	✓
Controlled branch magnitudes	✓	✓
Interconnected AC/DC grids	✓	✓
Flexible bus type definition	×	✓

Table 1: Comparison between Classic power flow and Generalised power flow.

4.1 Fundamental rules

In the absence of the typical rules of classic power flows such as pre-defined bus types, it is important to define several other more general guidelines in order to maintain solvability while staying coherent to real systems.

- Each subgrid has to have only 1 slack bus [2]. This applies to both AC and DC grids. In AC grids the magnitude V and angle δ have to be specified, whereas in DC grids only the magnitude V.
- Control of a remote bus is possible, as seen from Figure 13. The generator at Bus 6 is defining the voltage magnitude at Bus 13 using its injected active power P_6. This means that the variable P_zip at Bus 6 is left as an unknown in the system. Similarly, the transformer between Buses 4 and Bus 9 controls the active power $P_{t,52}$ flowing from Bus 2 to Bus 5, by adjusting its tap module m_{49} [3].
- It is not possible to have two devices controlling the same nodal voltage. There is an important reason for this which will be explained in later sections, relating to the size of the Jacobian matrix of the system. (Droop has yet to be implemented)
- Buses can have from 0 to 4 controlled magnitudes (V, δ, P_{zip}, Q_{zip}) in AC subsystems and a maximum of 2 in DC subsystems (V, P_{zip}).

4.2 Generalised Branch Model

In our formulation we define two sets of branches:

- κ: the set of passive branches (e.g., power lines, non-controllable transformers).
- Γ: the set of active branches that cannot be modeled purely with admittances (e.g., AC/DC interfacing converters (VSCs), controllable transformers).

This separation of passive and active sets is due to the fact that branches in the passive set κ are reduced only to their admittances, and included in the Y_{bus} matrix of the system. On the

[2] The only exception being distributed slacks, which are simply slack buses with coordination rules. While only one slack node is defined for each subgrid, it is possible to define a distributed slack. If N distributed slacks are connected to a given subgrid, there will be one slack and N-1 power relations defining the relationship of power sharing between all the involved distributed slacks. The same idea can be applied to distributed reactive power sharing for voltage control in one node, where only one element will be in charge of controlling the voltage, but other elements can be sharing this control by defining reactive power relationships between them

[3] Although these associations between the controlled magnitudes and the corresponding unknowns may not directly reflect practical scenarios, they must be permitted within the framework of generalized power flow. This flexibility is essential to maintain the generalizability of the model, allowing it to accommodate a wide range of potential configurations and control strategies.

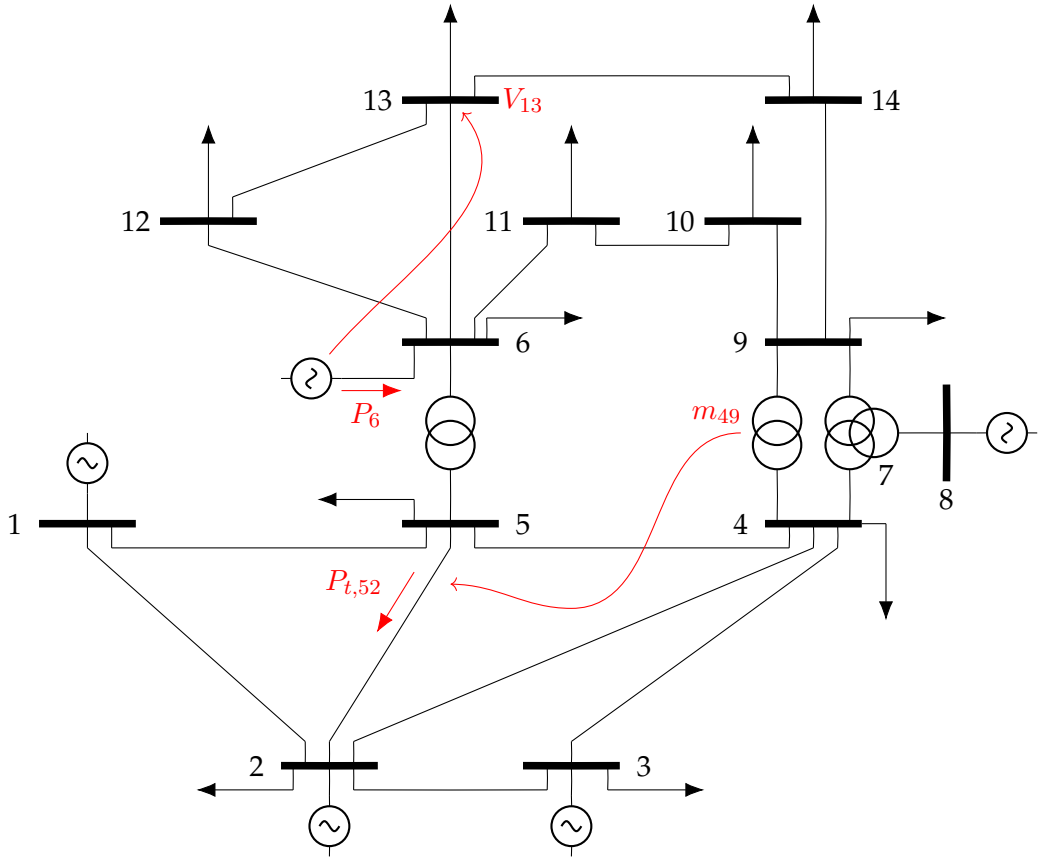

Figure 13: Scheme of the IEEE 14-bus system to illustrate the concept of remote controls.

other hand, VSCs and controllable transformers are modelled using the power flows through the terminals of the devices, and thus need to be treated specifically.

To build the Y_{bus} that represents the passive bus admittance matrix, it is important to discuss the models applied for all branches in the system. For any branch b that belongs to the set κ, that is to say, the passive set, it can be represented using a two-by-two admittance matrix, given by:

$$Y_{b\in\kappa} = \begin{bmatrix} Y_{ff} & Y_{ft} \\ Y_{tf} & Y_{tt} \end{bmatrix},$$

where the terms Y_{ff}, Y_{ft}, Y_{tf}, and Y_{tt} represent the admittance values of the branch, observed from the perspective of the buses at the *from* (f) and *to* (t) sides, which is arbitrary and left at the initialisation step of the model by the user.

Branches connecting the bus to active elements that cannot be accurately modeled using passive admittance models are categorized within the set Γ. These active devices, such as AC/DC converters and controllable transformers, interface with the bus through power injections at the branches, denoted by P_f^Γ, Q_f^Γ, P_t^Γ, and Q_t^Γ. We think of these connections between active branches

and buses as being described by adjacency matrices, which we call connectivity matrices C_f^Γ and C_t^Γ. C_f^Γ and C_t^Γ correspond to the from and to connectivity matrices for the active elements in the set Γ.

For example, consider an active branch indexed as 2 that connects bus 1 to the system (one-indexed). The connectivity matrix C_f^Γ will have a value of 1 at row 1, column 2, indicating that the branch is connected from bus 1. The matrix C_t^Γ would similarly indicate the connection of the branch to another bus. The matrix format could look like this:

$$C_f^\Gamma = \begin{bmatrix} 0 & 0 & 1 \\ 0 & 0 & 0 \\ 0 & 0 & 0 \end{bmatrix}, \quad C_t^\Gamma = \begin{bmatrix} 0 & 0 & 0 \\ 0 & 0 & 1 \\ 0 & 0 & 0 \end{bmatrix}.$$

In this example, Branch 2 is an active branch such as a VSC or a controllable converter that is connected from Bus 1 and to Bus 2, as represented in the first row of the matrix C_f^Γ and the second row of C_t^Γ.

4.2.1 Voltage Source Converter (VSC)

A VSC is used in interlinking subsystems, such as HVDC lines, connecting two buses without grounding either of them. These converters can control power flow between subgrids by adjusting voltage and power parameters at both ends of the link.

Figure 14 illustrates the model of a VSC.

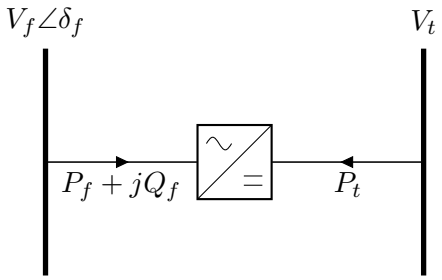

Figure 14: Representation of a VSC.

As seen from Figure 14, we see that the active and reactive powers on the AC side (defined as the *from* side), and the active power on the DC side (the *to* side), are related according to the

equations in the active powers on the f and t sides are related through the power loss equation:

$$\begin{aligned} P_f + P_t - P_{\text{loss}} &= 0, \\ P_f + P_t &= P_{\text{loss}}, \\ P_f + P_t &= a + b\frac{\sqrt{(P_f)^2 + (Q_f)^2}}{V_f} + c\frac{(P_f)^2 + (Q_f)^2}{V_f^2}, \\ P_f^{\text{acdc}} + P_t^{\text{acdc}} &= a + b\frac{\sqrt{P_f^{2,\text{acdc}} + Q_f^{2,\text{acdc}}}}{V_f} + c\frac{P_f^{2,\text{acdc}} + Q_f^{2,\text{acdc}}}{V_f^2}, \\ g_{p,acdc} &\coloneqq P_{fk}^{\text{acdc}} + P_{tk}^{\text{acdc}} - P_{\text{loss},k}^{\text{acdc}} = 0 \quad \forall k \in ACDC, \\ &. \end{aligned} \tag{64}$$

where ACDC is the set of all VSCs interfacing AC and DC subsystems. ACDC is itself a subset of the set Γ. The parameters a, b, and c are the coefficients of the power loss equation, and P_f and Q_f are the active and reactive powers on the AC side. We simply extend the notation from previous sections to mark the power flows as ACDC for our purposes in this chapter.

4.2.2 Transformer

Transformers regulate power flow by changing the voltage magnitude or phase angle between the primary and secondary windings. Figure 15 shows the representation of a controllable transformer.

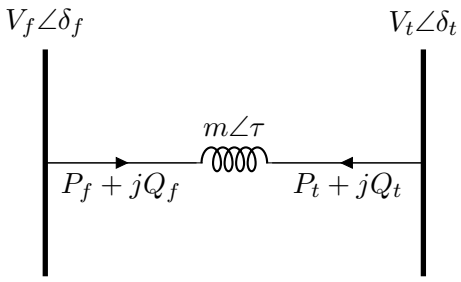

Figure 15: Representation of a transformer.

Transformers that are not dynamically changing their tap module or angle are in the κ set, while controllable transformers are part of the Γ set. This is because we model controllable transformers as PSTs, relating the power flows at the *from* and *to* sides to the tap ratio and the

phase shift angle. The equations for a controllable transformer are:

$$
\begin{aligned}
P_f^{\text{tr}} + jQ_f^{\text{tr}} &= V_f \left(\frac{y_s^* + y_{\text{sh}}^*}{m^2} V_f^* - \frac{y_s^*}{me^{j\tau}} V_t^* \right) = V_f^2 \frac{Y_s^* + Y_{sh}^*}{m^2} - V_f V_t^* \frac{Y_s^*}{me^{j\tau}}, \\
P_t^{\text{tr}} + jQ_t^{\text{tr}} &= V_t \left(\frac{y_s^* + y_{\text{sh}}^*}{m^2} V_t^* - \frac{y_s^*}{me^{-j\tau}} V_f^* \right) = V_t^2 (Y_s^* + Y_{sh}^*) - V_t V_f^* \frac{Y_s^*}{me^{-j\tau}}, \\
g_{p_f,tr} &:= P_{fk}^{\text{tr}} = f(\delta, V, \tau, m) \quad \forall k \in TR, \\
g_{p_t,tr} &:= P_{tk}^{\text{tr}} = f(\delta, V, \tau, m) \quad \forall k \in TR, \\
g_{q_f,tr} &:= Q_{fk}^{\text{tr}} = f(\delta, V, \tau, m) \quad \forall k \in TR, \\
g_{q_t,tr} &:= Q_{tk}^{\text{tr}} = f(\delta, V, \tau, m) \quad \forall k \in TR.
\end{aligned}
\tag{65}
$$

where TR is the set of all controllable transformers. TR is itself a subset of the set Γ.

4.3 Generalised Bus Model

We denote a bus using the index r, that connects several elements including loads, generators, and branches. Buses may connect to both passive and active branches. Passive branches are represented through admittances and consist of typical power lines or non-controllable transformers. In contrast, active branches such as AC/DC converters or controllable transformers require more complex models. Using this, and the notation for the branch sets in the previous section, we get the representation of a general bus as in Figure 16.

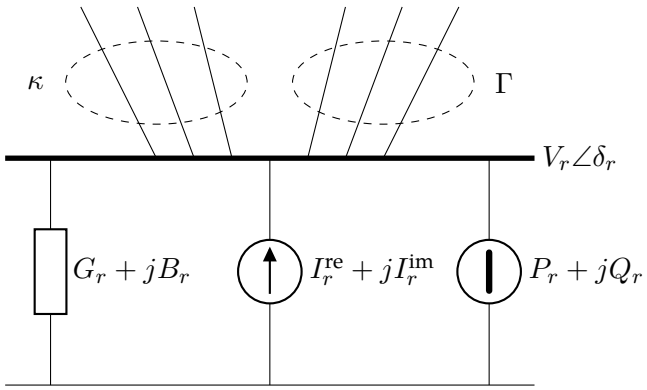

Figure 16: Representation of a generic bus with a ZIP shunt model, passive branch connections κ, and active branch connections Γ.

From here, we can apply Kirchhoff's laws to express the nodal balance equation as:

$$
\begin{aligned}
0 &= VY_{\text{bus}}^{*}V^{*} + C_f^{\Gamma}(P_f^{\Gamma} + jQ_f^{\Gamma}) + C_t^{\Gamma}(P_t^{\Gamma} + jQ_t^{\Gamma}) \\
&\quad - P^{\text{zip}} - jQ^{\text{zip}}, \\
0 &= \text{Re}\left\{VY_{\text{bus}}^{*}V^{*} + C_f^{\Gamma}(P_f^{\Gamma} + jQ_f^{\Gamma}) + C_t^{\Gamma}(P_t^{\Gamma} + jQ_t^{\Gamma})\right\} \\
&\quad - P^{\text{zip}}, \\
0 &= \text{Im}\left\{VY_{\text{bus}}^{*}V^{*} + C_f^{\Gamma}(P_f^{\Gamma} + jQ_f^{\Gamma}) + C_t^{\Gamma}(P_t^{\Gamma} + jQ_t^{\Gamma})\right\} \\
&\quad - Q^{\text{zip}}, \\
g_{p,ac} &:= \sum P_i = 0 \quad \forall i \in \text{AC}, \\
g_{q,ac} &:= \sum Q_i = 0 \quad \forall i \in \text{AC}, \\
g_{p,dc} &:= \sum P_i = 0 \quad \forall i \in \text{DC}.
\end{aligned}
\tag{66}
$$

where AC is the set of all AC buses and DC is the set of all DC buses.

4.4 Solving Generalised power flow with Newton-Raphson

From this, we can deduce that a set of known and unknown magnitudes must be defined. The known magnitudes are those that are actively controlled, while the unknowns correspond to quantities that are not controlled by the system. The unknown set, denoted as x, includes:

$$x = [\delta, V, \tau, m, P^{\text{zip}}, Q^{\text{zip}}, P_f, P_t, Q_f, Q_t]. \tag{67}$$

In contrast to conventional power flow, which only considers the first two terms (voltage angles δ and voltage magnitudes V), this generalized formulation incorporates more unknowns, accounting for elements such as regulated transformers, AC/DC links, and controlled ZIP loads, thereby extending the scope of the traditional model.

To solve the system, we must balance the number of unknowns with the number of equations. The total number of equations required should be independent of the control modes or bus types. The nodal balance equations for active and reactive power at AC buses and the active power balance in DC buses Equation 66, power loss equations for AC/DC links in Equation 64), and four power equations for controlled transformers Equation 65 must all be included in the system. In a compact form, these equations are represented as:

$$\begin{aligned}
g_{p,ac} &:= \sum P_i = 0 \quad \forall i \in AC, \\
g_{q,ac} &:= \sum Q_i = 0 \quad \forall i \in AC, \\
g_{p,dc} &:= \sum P_i = 0 \quad \forall i \in DC, \\
g_{p,acdc} &:= P^{\text{acdc}}_{fk} + P^{\text{acdc}}_{tk} - P^{\text{acdc}}_{\text{loss},k} = 0 \quad \forall k \in ACDC, \\
g_{p_f,tr} &:= P^{\text{tr}}_{fk} = f(\delta, V, \tau, m) \quad \forall k \in TR, \\
g_{p_t,tr} &:= P^{\text{tr}}_{tk} = f(\delta, V, \tau, m) \quad \forall k \in TR, \\
g_{q_f,tr} &:= Q^{\text{tr}}_{fk} = f(\delta, V, \tau, m) \quad \forall k \in TR, \\
g_{q_t,tr} &:= Q^{\text{tr}}_{tk} = f(\delta, V, \tau, m) \quad \forall k \in TR,
\end{aligned} \tag{68}$$

where AC refers to the set of AC buses, DC to DC buses, $ACDC$ to AC/DC interfaces, and TR to controlled transformers. The indices i are used for buses, and k is used for branches. In some cases, it becomes necessary to include additional equations in the case of controlling the power through a passive branch in the set κ. This will be explained in the later sections.

Next, we construct sets to track whether bus and branch magnitudes are set as known or unknown. This is done through sets: i identifies known bus magnitudes, $\bar{i}$ identifies unknown bus magnitudes, k for known branch magnitudes, and $\bar{k}$ for unknown branch magnitudes. These sets are summarized in Table 3.

Table 2: Sets to identify known and unknown magnitudes.

Set	Description
I_δ	Known bus voltage phase
I_V	Known bus voltage magnitudes
I_p	Known bus ZIP active powers
I_q	Known bus ZIP reactive powers
K_τ	Known branch tap phase shift angles
K_m	Known branch tap ratios
K_{p_f}	Known branch from active powers
K_{p_t}	Known branch to active powers
K_{q_f}	Known branch from reactive powers
K_{q_t}	Known branch to reactive powers
$\overline{I}_\delta$	Unknown bus voltage phase
$\overline{I}_V$	Unknown bus voltage magnitudes
$\overline{I}_p$	Unknown bus ZIP active powers
$\overline{I}_q$	Unknown bus ZIP reactive powers
$\overline{K}_\tau$	Unknown branch tap phase shift angles
$\overline{K}_m$	Unknown branch tap ratios
$\overline{K}_{p_f}$	Unknown branch from active powers
$\overline{K}_{p_t}$	Unknown branch to active powers
$\overline{K}_{q_f}$	Unknown branch from reactive powers
$\overline{K}_{q_t}$	Unknown branch to reactive powers

To solve the generalized power flow using the Newton-Raphson method, the Jacobian matrix in Equation 75 is constructed based on the partial derivatives of the above equations with respect to the unknown variables. At each iteration, we need to solve the linear system formed by these equations.

$$\mathbf{J}\Delta\mathbf{x} = -\mathbf{g} \tag{69}$$

$$\mathbf{J} = \begin{bmatrix}
\frac{\partial g_{p,ac}}{\partial \delta} & \frac{\partial g_{p,ac}}{\partial V} & \frac{\partial g_{p,ac}}{\partial \tau} & \frac{\partial g_{p,ac}}{\partial m} & \frac{\partial g_{p,ac}}{\partial P^{\text{zip}}} & \frac{\partial g_{p,ac}}{\partial Q^{\text{zip}}} & \frac{\partial g_{p,ac}}{\partial P_f} & \frac{\partial g_{p,ac}}{\partial P_t} & \frac{\partial g_{p,ac}}{\partial Q_f} & \frac{\partial g_{p,ac}}{\partial Q_t} \\
\frac{\partial g_{q,ac}}{\partial \delta} & \frac{\partial g_{q,ac}}{\partial V} & \frac{\partial g_{q,ac}}{\partial \tau} & \frac{\partial g_{q,ac}}{\partial m} & \frac{\partial g_{q,ac}}{\partial P^{\text{zip}}} & \frac{\partial g_{q,ac}}{\partial Q^{\text{zip}}} & \frac{\partial g_{q,ac}}{\partial P_f} & \frac{\partial g_{q,ac}}{\partial P_t} & \frac{\partial g_{q,ac}}{\partial Q_f} & \frac{\partial g_{q,ac}}{\partial Q_t} \\
\frac{\partial g_{p,dc}}{\partial \delta} & \frac{\partial g_{p,dc}}{\partial V} & \frac{\partial g_{p,dc}}{\partial \tau} & \frac{\partial g_{p,dc}}{\partial m} & \frac{\partial g_{p,dc}}{\partial P^{\text{zip}}} & \frac{\partial g_{p,dc}}{\partial Q^{\text{zip}}} & \frac{\partial g_{p,dc}}{\partial P_f} & \frac{\partial g_{p,dc}}{\partial P_t} & \frac{\partial g_{p,dc}}{\partial Q_f} & \frac{\partial g_{p,dc}}{\partial Q_t} \\
\frac{\partial g_{p,acdc}}{\partial \delta} & \frac{\partial g_{p,acdc}}{\partial V} & \frac{\partial g_{p,acdc}}{\partial \tau} & \frac{\partial g_{p,acdc}}{\partial m} & \frac{\partial g_{p,acdc}}{\partial P^{\text{zip}}} & \frac{\partial g_{p,acdc}}{\partial Q^{\text{zip}}} & \frac{\partial g_{p,acdc}}{\partial P_f} & \frac{\partial g_{p,acdc}}{\partial P_t} & \frac{\partial g_{p,acdc}}{\partial Q_f} & \frac{\partial g_{p,acdc}}{\partial Q_t} \\
\frac{\partial g_{p_f,tr}}{\partial \delta} & \frac{\partial g_{p_f,tr}}{\partial V} & \frac{\partial g_{p_f,tr}}{\partial \tau} & \frac{\partial g_{p_f,tr}}{\partial m} & \frac{\partial g_{p_f,tr}}{\partial P^{\text{zip}}} & \frac{\partial g_{p_f,tr}}{\partial Q^{\text{zip}}} & \frac{\partial g_{p_f,tr}}{\partial P_f} & \frac{\partial g_{p_f,tr}}{\partial P_t} & \frac{\partial g_{p_f,tr}}{\partial Q_f} & \frac{\partial g_{p_f,tr}}{\partial Q_t} \\
\frac{\partial g_{p_t,tr}}{\partial \delta} & \frac{\partial g_{p_t,tr}}{\partial V} & \frac{\partial g_{p_t,tr}}{\partial \tau} & \frac{\partial g_{p_t,tr}}{\partial m} & \frac{\partial g_{p_t,tr}}{\partial P^{\text{zip}}} & \frac{\partial g_{p_t,tr}}{\partial Q^{\text{zip}}} & \frac{\partial g_{p_t,tr}}{\partial P_f} & \frac{\partial g_{p_t,tr}}{\partial P_t} & \frac{\partial g_{p_t,tr}}{\partial Q_f} & \frac{\partial g_{p_t,tr}}{\partial Q_t} \\
\frac{\partial g_{q_f,tr}}{\partial \delta} & \frac{\partial g_{q_f,tr}}{\partial V} & \frac{\partial g_{q_f,tr}}{\partial \tau} & \frac{\partial g_{q_f,tr}}{\partial m} & \frac{\partial g_{q_f,tr}}{\partial P^{\text{zip}}} & \frac{\partial g_{q_f,tr}}{\partial Q^{\text{zip}}} & \frac{\partial g_{q_f,tr}}{\partial P_f} & \frac{\partial g_{q_f,tr}}{\partial P_t} & \frac{\partial g_{q_f,tr}}{\partial Q_f} & \frac{\partial g_{q_f,tr}}{\partial Q_t} \\
\frac{\partial g_{q_t,tr}}{\partial \delta} & \frac{\partial g_{q_t,tr}}{\partial V} & \frac{\partial g_{q_t,tr}}{\partial \tau} & \frac{\partial g_{q_t,tr}}{\partial m} & \frac{\partial g_{q_t,tr}}{\partial P^{\text{zip}}} & \frac{\partial g_{q_t,tr}}{\partial Q^{\text{zip}}} & \frac{\partial g_{q_t,tr}}{\partial P_f} & \frac{\partial g_{q_t,tr}}{\partial P_t} & \frac{\partial g_{q_t,tr}}{\partial Q_f} & \frac{\partial g_{q_t,tr}}{\partial Q_t}
\end{bmatrix} \tag{70}$$

$$\Delta \mathbf{x} = \begin{bmatrix} \Delta\delta \\ \Delta V \\ \Delta\tau \\ \Delta m \\ \Delta P^{\text{zip}} \\ \Delta Q^{\text{zip}} \\ \Delta P_f \\ \Delta P_t \\ \Delta Q_f \\ \Delta Q_t \end{bmatrix} \tag{71}$$

$$\mathbf{g} = \begin{bmatrix} g_{p,ac} \\ g_{q,ac} \\ g_{p,dc} \\ g_{p,acdc} \\ g_{p_f,tr} \\ g_{p_t,tr} \\ g_{q_f,tr} \\ g_{q_t,tr} \end{bmatrix} \tag{72}$$

4.5 Indices

This subsection outlines a systematic way of creating the sets of indices given in Table 3 below. First, we understand the system as a set of buses I connected by a set of branches K. The table below is also found in previous subsections, and is identical except that the sets are slightly differently defined using capital letters:

The following subsubsections should be seen as a particular order of logic that fills the sets by starting from the most basic elements in a grid - buses & lines, and then subsequently processing the more active elements in the grid.

4.5.1 Buses and Lines

Recall that we use the set $\mathcal{AC}$ and $\mathcal{DC}$ to refer to the set of bus indices that are AC buses and DC buses respectively. Now, we fill the following sets:

Table 3: Sets to identify known and unknown magnitudes.

Set	Description
I_δ	Known bus voltage phase
I_V	Known bus voltage magnitudes
I_p	Known bus ZIP active powers
I_q	Known bus ZIP reactive powers
K_τ	Known branch tap phase shift angles
K_m	Known branch tap ratios
K_{p_f}	Known branch from active powers
K_{p_t}	Known branch to active powers
K_{q_f}	Known branch from reactive powers
K_{q_t}	Known branch to reactive powers
$\overline{I}_\delta$	Unknown bus voltage phase
$\overline{I}_V$	Unknown bus voltage magnitudes
$\overline{I}_p$	Unknown bus ZIP active powers
$\overline{I}_q$	Unknown bus ZIP reactive powers
$\overline{K}_\tau$	Unknown branch tap phase shift angles
$\overline{K}_m$	Unknown branch tap ratios
$\overline{K}_{p_f}$	Unknown branch from active powers
$\overline{K}_{p_t}$	Unknown branch to active powers
$\overline{K}_{q_f}$	Unknown branch from reactive powers
$\overline{K}_{q_t}$	Unknown branch to reactive powers

$$\overline{I}_V = \{\forall i \in \mathcal{AC} \cup \mathcal{DC}\}$$
$$\overline{I}_\delta = \{\forall i \in \mathcal{AC}\}$$
$$I_\mathrm{p} = \{\forall i \in \mathcal{AC} \cup \mathcal{DC}\}$$
$$I_\mathrm{q} = \{\forall i \in \mathcal{AC}\}$$

Above, we see that the voltages and phase angles of all buses are unknown initially, and all real and active ZIP power are known, that is, equal to 0. At this point, one can see that in a hybrid AC/DC system, the reactive power and phase angle are not relevant for DC buses, and thus, their indices are not included in the appropriate sets.

4.5.2 ZIP Elements

Next, we begin to look at ZIP elements. It is trivial to note that only controllable (and therefore variable) ZIP elements will change the sets created above. Some examples may include generators, SVCs, STATCOMs, and VFDs. For now, however, we will deal with the specific case of generators as in traditional power flow. Let us define a set of indices that contains the bus indices that have a controllable generator attached. We call this GEN. We also keep a set GEN_{AC} as a subset of GEN for only the AC indices. We then move the indices in GEN and GEN_{AC} from the known

to the unknown sets:

$$
\begin{aligned}
GEN &= \{\forall i \mid \text{bus i has a generator}\} \\
GEN_{AC} &= \{i \in GEN \mid i \text{ is an AC bus}\} \\
I_p &= I_p \setminus GEN \\
I_q &= I_q \setminus GEN_{AC} \\
\overline{I}_p &= \overline{I}_p \cup GEN \\
\overline{I}_q &= \overline{I}_q \cup GEN_{AC}
\end{aligned}
$$

4.5.3 AC/DC Link - VSCs

Recall from an earlier subsection that branches belong to two sets: κ, the set of passive branches that can be represented through admittances, and Γ, the set of branches interfaced to elements that cannot be inherently modelled through admittances.

Recall also that we keep a set ACDC, which is a subset of Γ, and holds the branches that represent interfaces between AC and DC subsystems. The structure in which we keep the directed edges in a graph will simply be an index that represents the branch index. [4]

Doing this, we simply add the indices of the branches to the unknown set of powers:

$$
\begin{aligned}
\overline{K}_{pf} &= \overline{K}_{pf} \cup \{k \mid k \in ACDC\} \\
\overline{K}_{pt} &= \overline{K}_{pt} \cup \{k \mid k \in ACDC\} \\
\overline{K}_{qt} &= \overline{K}_{qt} \cup \{k \mid k \in ACDC\}
\end{aligned}
$$

4.5.4 Controllable Transformer

Here, we use the set TR, which we have defined to be the set of controllable transformers and is also a subset of Γ. Once again, TR is a set of integers that represent the branch indices. The introduction of the controllable transformer similarly introduces unknowns in the form of active and reactive powers at both its terminals. Additionally, it introduces unknowns related to its modulation and phase shift. Therefore, we assign the following sets:

[4] This branch index will contain a mapping to a tuple $(from, to)$, which represents the indices of the bus *from* and the bus *to*. While we would like to give flexibility to the user in defining the orientation of the *from* and *to* buses, we should enforce that in AC/DC links, the *from* bus is the DC side and the *to* bus is the AC side.

$$\overline{K}_{pf} = \overline{K}_{pf} \cup \{k \,|\, k \in TR\}$$
$$\overline{K}_{qf} = \overline{K}_{qf} \cup \{k \,|\, k \in TR\}$$
$$\overline{K}_{pt} = \overline{K}_{pt} \cup \{k \,|\, k \in TR\}$$
$$\overline{K}_{qt} = \overline{K}_{qt} \cup \{k \,|\, k \in TR\}$$
$$\overline{K}_{\tau} = \overline{K}_{\tau} \cup \{k \,|\, k \in TR\}$$
$$\overline{K}_{m} = \overline{K}_{m} \cup \{k \,|\, k \in TR\}$$

4.5.5 Bus and Branch Setpoints

We have seen how the above elements have introduces new elements into the set of unknowns denoted by the $\overline{overlined}$ sets. Now that that is done, we can start to look at what these elements are attempting to assert in the network. That is to say, we can begin moving indices from the unknown sets to the known sets if there is a specific attempt by an active element in the grid to assert its value.

In order for us to ensure that we only shift from unknown to known sets, we must first ensure that there is overall uniqueness[5] in what these active elements want to assert: a nodal voltage, phase angle, a branch active power, etc. This is inherently guaranteed in our use of sets as opposed to lists or multi-sets.

More formally, we must define two new sets of "assertions", nodal assertions $\mathcal{N}$ and branch assertions $\mathcal{B}$. Within those sets exist several subsets, enumerated in the Table 4.

Table 4: Sets to identify bus and branch assertions.

Set	Description
$\mathcal{N}_{\delta}$	Asserted nodal voltage phase angles
$\mathcal{N}_{V}$	Asserted nodal voltage magnitudes
$\mathcal{N}_{p}$	Asserted nodal ZIP active power injections
$\mathcal{N}_{q}$	Asserted nodal ZIP reactive power injections
$\mathcal{B}_{\tau}$	Asserted branch phase shift angles
$\mathcal{B}_{m}$	Asserted branch tap ratios
$\mathcal{B}_{p_f}$	Asserted branch from active power flows
$\mathcal{B}_{p_t}$	Asserted branch to active power flows
$\mathcal{B}_{q_f}$	Asserted branch from reactive power flows
$\mathcal{B}_{q_t}$	Asserted branch to reactive power flows

The superset $\mathcal{N}$ encompasses subsets of nodal parameters, where each element is a tuple in the form $(i, value)$, with i representing the index of a bus, and $value$ signifying the asserted voltage

[5] In grid operation, multiple elements may be trying to reference and control the same magnitude in the same location in the grid. For now, we want to ensure uniqueness so as to not have to deal with the "hierarchy of control" of multiple active elements.

magnitude, angle, ZIP active power and ZIP reactive power that is associated with that bus. Similarly, the set $\mathcal{B}$ includes subsets related to branch parameters, with each element structured as a tuple $(k, value)$, where k denotes the branch index, and $value$ stands for the asserted value pertinent to that branch, such as tap ratios, phase shift angles, or power flows.

For each nodal assertion in $\mathcal{N}$, perform:

If $(i, \text{value}) \in \mathcal{N}_V$, then:

$$I_V = I_V \cup \{i\}, \qquad \overline{I}_V = \overline{I}_V \setminus \{i\}$$

If $(i, \text{value}) \in \mathcal{N}_\delta$, then:

$$I_\delta = I_\delta \cup \{i\}, \qquad \overline{I}_\delta = \overline{I}_\delta \setminus \{i\}$$

If $(i, \text{value}) \in \mathcal{N}_p$, then:

$$I_p = I_p \cup \{i\}, \qquad \overline{I}_p = \overline{I}_p \setminus \{i\}$$

If $(i, \text{value}) \in \mathcal{N}_q$, then:

$$I_q = I_q \cup \{i\}, \qquad \overline{I}_q = \overline{I}_q \setminus \{i\}$$

For each branch assertion in $\mathcal{B}$, perform:

If $(k, \text{value}) \in \mathcal{B}_\tau$, then:

$$K_\tau = K_\tau \cup \{k\}, \qquad \overline{K}_\tau = \overline{K}_\tau \setminus \{k\}$$

If $(k, \text{value}) \in \mathcal{B}_m$, then:

$$K_m = K_m \cup \{k\}, \qquad \overline{K}_m = \overline{K}_m \setminus \{k\}$$

If $(k, \text{value}) \in \mathcal{B}_{p_f}$, then:

$$K_{p_f} = K_{p_f} \cup \{k\}, \qquad \overline{K}_{p_f} = \overline{K}_{p_f} \setminus \{k\}$$

If $(k, \text{value}) \in \mathcal{B}_{p_t}$, then:

$$K_{p_t} = K_{p_t} \cup \{k\}, \qquad \overline{K}_{p_t} = \overline{K}_{p_t} \setminus \{k\}$$

If $(k, \text{value}) \in \mathcal{B}_{q_f}$, then:

$$K_{q_f} = K_{q_f} \cup \{k\}, \qquad \overline{K}_{q_f} = \overline{K}_{q_f} \setminus \{k\}$$

If $(k, \text{value}) \in \mathcal{B}_{q_t}$, then:

$$K_{q_t} = K_{q_t} \cup \{k\}, \qquad \overline{K}_{q_t} = \overline{K}_{q_t} \setminus \{k\}$$

At this point, we have processed all the elements in the sets $\mathcal{N}$ and $\mathcal{B}$, and moved the bus or branch indices from the unknowns to the known sets.

4.5.6 Cardinality of Unknown Sets

In order to form the Jacobian matrix, we must ensure that the number of unknowns is equal to the number of mismatch equations. In a given grid, we can calculate the number of equations

that each element in the grid provides:

$$
\begin{aligned}
g_{p,ac} &:= \sum P_i = 0 && \forall i \in AC, \\
g_{q,ac} &:= \sum Q_i = 0 && \forall i \in AC, \\
g_{p,dc} &:= \sum P_i = 0 && \forall i \in DC, \\
g_{p,acdc} &:= P_{fk}^{\text{acdc}} + P_{tk}^{\text{acdc}} - P_{\text{loss},k}^{\text{acdc}} = 0 && \forall k \in ACDC, \\
g_{p_f,tr} &:= P_{fk}^{\text{tr}} = f(\delta, V, \tau, m) && \forall k \in TR, \\
g_{p_t,tr} &:= P_{tk}^{\text{tr}} = f(\delta, V, \tau, m) && \forall k \in TR, \\
g_{q_f,tr} &:= Q_{fk}^{\text{tr}} = f(\delta, V, \tau, m) && \forall k \in TR, \\
g_{q_t,tr} &:= Q_{tk}^{\text{tr}} = f(\delta, V, \tau, m) && \forall k \in TR,
\end{aligned}
\tag{73}
$$

We see that each AC node gives 2 equations, each DC nodes gives 1 equation, each AC/DC link gives 1 equation and each controllable transformer gives 4 equations. This helps in understanding why there is a natural parity between the number of equations in the grid (independent of controls) and the number of unknowns:

- **Generator:**
  - Each generator introduces 2 unknowns at the attached bus, p_{zip} and q_{zip}
  - It is associated with 2 assertions, removing 2 unknowns from the system.
  - Also, no new equations are added to the system of equations due to a generator.
- **Controllable Transformer:**
  - Each controllable transformer introduces 6 unknowns.
  - It comes with 2 assertions.
  - Contributes 4 new equations to the system.
- **AC/DC Link:**
  - Every AC/DC link introduces 3 new unknowns.
  - It is associated with 2 assertions.
  - Contributes 1 new equation.

There is thus always an equal number of unknowns being added into the system of equations as the number of new equations contributed by each active element in the grid. However, this is

only true when the assertions are directly affecting branches for which we must move a branch k from an unknown set to a known set. That is to say, if a particular element asserts control over a branch for which the system did not have in the unknown set in the first place, then the cardinality of the unknown set will not match the number of equations. It is therefore important to add the following control-dependent equations into the system of equations that we see in Equation 73:

$$
\begin{aligned}
g_{p_{ij},\kappa} &:= P_{ij} = \Re\{V_i \cdot (V_i - V_j)^* \cdot Y_{ij}^*\} && \forall b \in \mathcal{B}_{p_{ij},\kappa} \\
g_{q_{ij},\kappa} &:= Q_{ij} = \Im\{V_i \cdot (V_i - V_j)^* \cdot Y_{ij}^*\} && \forall b \in \mathcal{B}_{q_{ij},\kappa} \\
g_{p_{ji},\kappa} &:= P_{ji} = \Re\{V_j \cdot (V_j - V_i)^* \cdot Y_{ij}^*\} && \forall b \in \mathcal{B}_{p_{ji},\kappa} \\
g_{q_{ji},\kappa} &:= Q_{ji} = \Im\{V_j \cdot (V_j - V_i)^* \cdot Y_{ij}^*\} && \forall b \in \mathcal{B}_{q_{ji},\kappa}
\end{aligned}
$$

Where $\mathcal{B}_{p_{ij},\kappa}, \mathcal{B}_{q_{ij},\kappa}, \mathcal{B}_{p_{ji},\kappa}, \mathcal{B}_{q_{ji},\kappa}$ are the sets of controls asserting active and reactive power in a passive branch (line, transformer, etc.) in both directions, and b denotes individual elements within these sets.

4.5.7 Reference Node Identification

In traditional power flow, it is important that each connected system has exactly one node wherein the voltage magnitude and phase angle are known. In the proposed power flow, there is a slightly different criteria: for every AC subsystem, there must be (at least) one node wherein the phase angle is known and (at least) one known voltage magnitude; and for every DC subsystem, there exists (at least) one node for which the voltage magnitude is known[6].

To identify the candidate references in every subsystem, we first understand a network as a tuple of the set of nodes I (buses) and edges K (branches) in the form (I, K). These two sets are not new to us, they are simply the supersets that contain all the nodes and all the branches respectively in Table 3. Let's give this tuple the shorter variable name G:

$$G = (I, K)$$

We refer readers to Appendix E for a primer on graphs and search algorithms. Now, to separate the AC and DC subsystems, we must create a subgraph where we remove all AC/DC links. We thus define a set of branches K' that contains all elements of K except for those in the subset $ACDC$. We then represent the grid as an undirected graph G' with a set of nodes I and the

[6] whether to use the condition "at least one" or "exactly one", can be discussed

modified set of edges K':

$$K' := K \setminus ACDC,$$
$$G' = (I, K'),$$

where K' contains only the branches that do not represent AC/DC links, ensuring that G reflects the structure of the grid excluding connections between AC and DC subsystems:

$$G = (I, K),$$
$$K' \subseteq K,$$
$$G' = (I, K'),$$
$$G' \subseteq G.$$

Continuing from our definition G', we can start identifying connected components within an AC or DC subsystem, and thus identify the reference nodes in each subsystem.

To ensure each AC and DC subsystem meets its reference conditions, we integrate a check within the Depth-First Search (DFS) traversal to identify if a node can serve as a reference node.

Identifying Connected Components (DFS) Another way of thinking of the problem of finding all nodes in G' that are electrically connected is to see if there exists a path between any two nodes within the system. If there is a path, then they are in the same subsystem.

Given $G' = (I, K')$, where K' excludes AC/DC links, we aim to identify subsets of I where nodes are interconnected by paths formed by edges in K'. To achieve this, we use a Depth-First Search (DFS) algorithm, a standard graph traversal method that is guaranteed to traverse the graph in time that is proportional to the cardinality of the sets I and K' combined.

Incorporating Reference Node Checks into DFS Given the sets of known and unknown magnitudes I_V and I_δ, and $\overline{I}_V$ and $\overline{I}_\delta$ respectively, we can extend the DFS algorithm to include checks for identifying reference nodes:

1. **Initialize** sequences of sets, representing finite families of sets, where n is the number of subsystems identified in the graph. These are $R_\delta = \{R_{\delta j}\}_{j=1}^n$, $R_V = \{R_{Vj}\}_{j=1}^n$, and $R_{DC} = \{R_{DCj}\}_{j=1}^n$, to track nodes with known angle references for AC systems, known voltages for AC systems, and known voltages for DC systems, respectively. Each connected set of buses is represented by B_j within the finite family $B = \{B_j\}_{j=1}^n$. Initially, let each $R_{\delta j} = \emptyset$, $R_{Vj} = \emptyset$, and $R_{DCj} = \emptyset$ for all j, and each $B_j = \emptyset$.

2. **During the DFS traversal**, dynamically populate each B_j with connected nodes to form

the finite family of subsystems. Concurrently, update the corresponding $R_{\delta j}$, R_{Vj}, and R_{DCj} when a new vertex i is visited:

- If $i \in I_\delta$, then the node has a known angle reference, and update $R_{\delta j} = R_{\delta j} \cup \{i\}$ for the corresponding subsystem B_j.
- If $i \in I_V$, then the node has a known voltage magnitude, for AC systems, update $R_{Vj} = R_{Vj} \cup \{i\}$. For DC systems, update $R_{DCj} = R_{DCj} \cup \{i\}$ for the corresponding subsystem B_j.

3. **After completing the DFS traversal** for the entire graph, evaluate each subsystem (connected component) B_j to identify reference nodes by assessing the intersubsections of $R_{\delta j}$, R_{Vj}, and R_{DCj} with B_j:
   - For an AC system represented by B_j, if $|R_{\delta j} \cap B_j| \geq 1$ and $|R_{Vj} \cap B_j| \geq 1$, the conditions for identifying a reference node within the subsystem B_j are met.
   - For a DC system represented by B_j, if $|R_{DCj} \cap B_j| \geq 1$, the necessary condition for identifying a reference node within the subsystem B_j is met.
   - The presence of multiple elements in the intersubsections for any B_j indicates the need for a decision process to select the appropriate reference node(s) for that subsystem.

Complexity Consideration The time complexity of the modified DFS algorithm remains $O(I + K)$, as the additional checks for reference nodes involve only constant-time operations within the traversal process.

4.6 Derivatives

Recall from an earlier subsection that the set of non-linear equations is meant to be solved with the Newton-Raphson method, where the Jacobian matrix is built from the partial derivatives of the equations with respect to the unknowns:

$$\mathbf{J}\Delta\mathbf{x} = -\mathbf{g} \tag{74}$$

$$\mathbf{J} = \begin{bmatrix}
\frac{\partial g_{p,ac}}{\partial \delta} & \frac{\partial g_{p,ac}}{\partial V} & \frac{\partial g_{p,ac}}{\partial \tau} & \frac{\partial g_{p,ac}}{\partial m} & \frac{\partial g_{p,ac}}{\partial P^{\text{zip}}} & \frac{\partial g_{p,ac}}{\partial Q^{\text{zip}}} & \frac{\partial g_{p,ac}}{\partial P_f} & \frac{\partial g_{p,ac}}{\partial P_t} & \frac{\partial g_{p,ac}}{\partial Q_f} & \frac{\partial g_{p,ac}}{\partial Q_t} \\
\frac{\partial g_{q,ac}}{\partial \delta} & \frac{\partial g_{q,ac}}{\partial V} & \frac{\partial g_{q,ac}}{\partial \tau} & \frac{\partial g_{q,ac}}{\partial m} & \frac{\partial g_{q,ac}}{\partial P^{\text{zip}}} & \frac{\partial g_{q,ac}}{\partial Q^{\text{zip}}} & \frac{\partial g_{q,ac}}{\partial P_f} & \frac{\partial g_{q,ac}}{\partial P_t} & \frac{\partial g_{q,ac}}{\partial Q_f} & \frac{\partial g_{q,ac}}{\partial Q_t} \\
\frac{\partial g_{p,dc}}{\partial \delta} & \frac{\partial g_{p,dc}}{\partial V} & \frac{\partial g_{p,dc}}{\partial \tau} & \frac{\partial g_{p,dc}}{\partial m} & \frac{\partial g_{p,dc}}{\partial P^{\text{zip}}} & \frac{\partial g_{p,dc}}{\partial Q^{\text{zip}}} & \frac{\partial g_{p,dc}}{\partial P_f} & \frac{\partial g_{p,dc}}{\partial P_t} & \frac{\partial g_{p,dc}}{\partial Q_f} & \frac{\partial g_{p,dc}}{\partial Q_t} \\
\frac{\partial g_{p,acdc}}{\partial \delta} & \frac{\partial g_{p,acdc}}{\partial V} & \frac{\partial g_{p,acdc}}{\partial \tau} & \frac{\partial g_{p,acdc}}{\partial m} & \frac{\partial g_{p,acdc}}{\partial P^{\text{zip}}} & \frac{\partial g_{p,acdc}}{\partial Q^{\text{zip}}} & \frac{\partial g_{p,acdc}}{\partial P_f} & \frac{\partial g_{p,acdc}}{\partial P_t} & \frac{\partial g_{p,acdc}}{\partial Q_f} & \frac{\partial g_{p,acdc}}{\partial Q_t} \\
\frac{\partial g_{p_f,tr}}{\partial \delta} & \frac{\partial g_{p_f,tr}}{\partial V} & \frac{\partial g_{p_f,tr}}{\partial \tau} & \frac{\partial g_{p_f,tr}}{\partial m} & \frac{\partial g_{p_f,tr}}{\partial P^{\text{zip}}} & \frac{\partial g_{p_f,tr}}{\partial Q^{\text{zip}}} & \frac{\partial g_{p_f,tr}}{\partial P_f} & \frac{\partial g_{p_f,tr}}{\partial P_t} & \frac{\partial g_{p_f,tr}}{\partial Q_f} & \frac{\partial g_{p_f,tr}}{\partial Q_t} \\
\frac{\partial g_{p_t,tr}}{\partial \delta} & \frac{\partial g_{p_t,tr}}{\partial V} & \frac{\partial g_{p_t,tr}}{\partial \tau} & \frac{\partial g_{p_t,tr}}{\partial m} & \frac{\partial g_{p_t,tr}}{\partial P^{\text{zip}}} & \frac{\partial g_{p_t,tr}}{\partial Q^{\text{zip}}} & \frac{\partial g_{p_t,tr}}{\partial P_f} & \frac{\partial g_{p_t,tr}}{\partial P_t} & \frac{\partial g_{p_t,tr}}{\partial Q_f} & \frac{\partial g_{p_t,tr}}{\partial Q_t} \\
\frac{\partial g_{q_f,tr}}{\partial \delta} & \frac{\partial g_{q_f,tr}}{\partial V} & \frac{\partial g_{q_f,tr}}{\partial \tau} & \frac{\partial g_{q_f,tr}}{\partial m} & \frac{\partial g_{q_f,tr}}{\partial P^{\text{zip}}} & \frac{\partial g_{q_f,tr}}{\partial Q^{\text{zip}}} & \frac{\partial g_{q_f,tr}}{\partial P_f} & \frac{\partial g_{q_f,tr}}{\partial P_t} & \frac{\partial g_{q_f,tr}}{\partial Q_f} & \frac{\partial g_{q_f,tr}}{\partial Q_t} \\
\frac{\partial g_{q_t,tr}}{\partial \delta} & \frac{\partial g_{q_t,tr}}{\partial V} & \frac{\partial g_{q_t,tr}}{\partial \tau} & \frac{\partial g_{q_t,tr}}{\partial m} & \frac{\partial g_{q_t,tr}}{\partial P^{\text{zip}}} & \frac{\partial g_{q_t,tr}}{\partial Q^{\text{zip}}} & \frac{\partial g_{q_t,tr}}{\partial P_f} & \frac{\partial g_{q_t,tr}}{\partial P_t} & \frac{\partial g_{q_t,tr}}{\partial Q_f} & \frac{\partial g_{q_t,tr}}{\partial Q_t} \\
\frac{\partial g_{pf,\kappa}}{\partial \delta} & \frac{\partial g_{pf,\kappa}}{\partial V} & \frac{\partial g_{pf,\kappa}}{\partial \tau} & \frac{\partial g_{pf,\kappa}}{\partial m} & \frac{\partial g_{pf,\kappa}}{\partial P^{\text{zip}}} & \frac{\partial g_{pf,\kappa}}{\partial Q^{\text{zip}}} & \frac{\partial g_{pf,\kappa}}{\partial P_f} & \frac{\partial g_{pf,\kappa}}{\partial P_t} & \frac{\partial g_{pf,\kappa}}{\partial Q_f} & \frac{\partial g_{pf,\kappa}}{\partial Q_t} \\
\frac{\partial g_{qf,\kappa}}{\partial \delta} & \frac{\partial g_{qf,\kappa}}{\partial V} & \frac{\partial g_{qf,\kappa}}{\partial \tau} & \frac{\partial g_{qf,\kappa}}{\partial m} & \frac{\partial g_{qf,\kappa}}{\partial P^{\text{zip}}} & \frac{\partial g_{qf,\kappa}}{\partial Q^{\text{zip}}} & \frac{\partial g_{qf,\kappa}}{\partial P_f} & \frac{\partial g_{qf,\kappa}}{\partial P_t} & \frac{\partial g_{qf,\kappa}}{\partial Q_f} & \frac{\partial g_{qf,\kappa}}{\partial Q_t} \\
\frac{\partial g_{pt,\kappa}}{\partial \delta} & \frac{\partial g_{pt,\kappa}}{\partial V} & \frac{\partial g_{pt,\kappa}}{\partial \tau} & \frac{\partial g_{pt,\kappa}}{\partial m} & \frac{\partial g_{pt,\kappa}}{\partial P^{\text{zip}}} & \frac{\partial g_{pt,\kappa}}{\partial Q^{\text{zip}}} & \frac{\partial g_{pt,\kappa}}{\partial P_f} & \frac{\partial g_{pt,\kappa}}{\partial P_t} & \frac{\partial g_{pt,\kappa}}{\partial Q_f} & \frac{\partial g_{pt,\kappa}}{\partial Q_t} \\
\frac{\partial g_{qt,\kappa}}{\partial \delta} & \frac{\partial g_{qt,\kappa}}{\partial V} & \frac{\partial g_{qt,\kappa}}{\partial \tau} & \frac{\partial g_{qt,\kappa}}{\partial m} & \frac{\partial g_{qt,\kappa}}{\partial P^{\text{zip}}} & \frac{\partial g_{qt,\kappa}}{\partial Q^{\text{zip}}} & \frac{\partial g_{qt,\kappa}}{\partial P_f} & \frac{\partial g_{qt,\kappa}}{\partial P_t} & \frac{\partial g_{qt,\kappa}}{\partial Q_f} & \frac{\partial g_{qt,\kappa}}{\partial Q_t}
\end{bmatrix} \tag{75}$$

$$\Delta\mathbf{x} = \begin{bmatrix}
\Delta\delta \\ \Delta V \\ \Delta\tau \\ \Delta m \\ \Delta P^{\text{zip}} \\ \Delta Q^{\text{zip}} \\ \Delta P_f \\ \Delta P_t \\ \Delta Q_f \\ \Delta Q_t
\end{bmatrix} \tag{76}$$

$$\mathbf{g} = \begin{bmatrix}
g_{p,ac} \\ g_{q,ac} \\ g_{p,dc} \\ g_{p,acdc} \\ g_{p_f,tr} \\ g_{p_t,tr} \\ g_{q_f,tr} \\ g_{q_t,tr}
\end{bmatrix} \tag{77}$$

In this subsection, we attempt to define a symbolic representation of each derivative in the Jacobian.

$$
\begin{aligned}
g_{p,ac} &:= \sum P_i = 0 && \forall i \in AC, \\
g_{q,ac} &:= \sum Q_i = 0 && \forall i \in AC, \\
g_{p,dc} &:= \sum P_i = 0 && \forall i \in DC, \\
g_{p,acdc} &:= P_{fk}^{\text{acdc}} + P_{tk}^{\text{acdc}} - P_{\text{loss},k}^{\text{acdc}} = 0 && \forall k \in ACDC, \\
g_{p_f,tr} &:= P_{fk}^{\text{tr}} = f(\delta, V, \tau, m) && \forall k \in TR, \\
g_{p_t,tr} &:= P_{tk}^{\text{tr}} = f(\delta, V, \tau, m) && \forall k \in TR, \\
g_{q_f,tr} &:= Q_{fk}^{\text{tr}} = f(\delta, V, \tau, m) && \forall k \in TR, \\
g_{q_t,tr} &:= Q_{tk}^{\text{tr}} = f(\delta, V, \tau, m) && \forall k \in TR, \\
g_{p_{ij},\kappa} &:= P_{ij} = \Re\{V_i \cdot (V_i - V_j)^* \cdot Y_{ij}^*\} && \forall b \in \mathcal{B}_{p_{ij},\kappa} \\
g_{q_{ij},\kappa} &:= Q_{ij} = \Im\{V_i \cdot (V_i - V_j)^* \cdot Y_{ij}^*\} && \forall b \in \mathcal{B}_{q_{ij},\kappa} \\
g_{p_{ji},\kappa} &:= P_{ji} = \Re\{V_j \cdot (V_j - V_i)^* \cdot Y_{ij}^*\} && \forall b \in \mathcal{B}_{p_{ji},\kappa} \\
g_{q_{ji},\kappa} &:= Q_{ji} = \Im\{V_j \cdot (V_j - V_i)^* \cdot Y_{ij}^*\} && \forall b \in \mathcal{B}_{q_{ji},\kappa}
\end{aligned}
\tag{78}
$$

In a systematic way, we can move through each equation above and find the corresponding derivatives.

4.6.1 Nodal Power Balance

$$
\begin{aligned}
g_{p,ac} &:= \sum P_i = 0 && \forall i \in AC, \\
g_{q,ac} &:= \sum Q_i = 0 && \forall i \in AC,
\end{aligned}
\tag{79}
$$

Recall that the active and reactive power balance equations at each AC bus are given by the nodal balance by applying Kirchhoff laws:

$$
0 = VY_{\text{bus}}^* V^* + C_f^\Gamma (P_f^\Gamma + jQ_f^\Gamma) + C_t^\Gamma (P_t^\Gamma + jQ_t^\Gamma) - C^{zip}(P^{\text{zip}} - jQ^{\text{zip}}), \tag{80}
$$

$$
P_r^{\text{zip}} + jQ_r^{\text{zip}} = V_r^2 (G_r - jB_r) + V_r \angle \delta_r (I_r^{\text{re}} - jI_r^{\text{im}}) + P_r + jQ_r. \tag{81}
$$

From observation of the expressions above, we can see that the non-zero partial derivatives of

these power balances, necessary for forming the Jacobian matrix, are as follows:

$$\frac{\partial g_{p,ac}}{\partial V_i} = \text{derivatives of real parts of } S_{\text{calc}} \text{ and } S_{\text{bus}} \text{ w.r.t. } V_i, \tag{82}$$

$$\frac{\partial g_{q,ac}}{\partial V_i} = \text{derivatives of imaginary parts of } S_{\text{calc}} \text{ and } S_{\text{bus}} \text{ w.r.t. } V_i, \tag{83}$$

$$\frac{\partial g_{p,ac}}{\partial \delta_i} = \text{derivatives of real parts of } S_{\text{calc}} \text{ w.r.t. } \delta_i, \tag{84}$$

$$\frac{\partial g_{q,ac}}{\partial \delta_i} = \text{derivatives of imaginary parts of } S_{\text{calc}} \text{ w.r.t. } \delta_i. \tag{85}$$

Non-zero Derivatives:

$$\begin{aligned}
S_{\text{bus}} &= VY_{\text{bus}}^* V^* + C_f^\Gamma (P_f^\Gamma + jQ_f^\Gamma) + C_t^\Gamma (P_t^\Gamma + jQ_t^\Gamma) - C^{zip}(P^{\text{zip}} + jQ^{\text{zip}}) \\
\frac{\partial S_{\text{bus}}}{\partial V} &= \frac{\partial}{\partial V}(VY_{\text{bus}}^* V^*) \\
\frac{\partial S_{\text{bus}}}{\partial \theta} &= \frac{\partial}{\partial \theta}(VY_{\text{bus}}^* V^*) \\
\frac{\partial S_{\text{bus}}}{\partial P_{zip}} &= -1 \\
\frac{\partial S_{\text{bus}}}{\partial Q_{zip}} &= -1j \\
\frac{\partial S_{\text{bus}}}{\partial P_f^\Gamma} &= 1 \\
\frac{\partial S_{\text{bus}}}{\partial Q_f^\Gamma} &= 1j \\
\frac{\partial S_{\text{bus}}}{\partial P_t^\Gamma} &= 1 \\
\frac{\partial S_{\text{bus}}}{\partial Q_t^\Gamma} &= 1j
\end{aligned} \tag{86}$$

4.6.2 Controllable Transformer

The behavior of a controllable transformer is modeled through its power injection equations at both the *from* and *to* sides, denoted as $P_f^{\text{tr}} + jQ_f^{\text{tr}}$ and $P_t^{\text{tr}} + jQ_t^{\text{tr}}$, respectively.

The transformer from-side power is represented by the equation:

$$P_f^{\text{tr}} + jQ_f^{\text{tr}} = V_f^2 \frac{Y_s^* + Y_{sh}^*}{m^2} - V_f V_t^* \frac{Y_s^*}{m e^{j\tau}}, \tag{87}$$

while the to-side power is represented as:

$$P_t^{\text{tr}} + jQ_t^{\text{tr}} = V_t^2 (Y_s^* + Y_{sh}^*) - V_t V_f^* \frac{Y_s^*}{m e^{-j\tau}}. \tag{88}$$

The power mismatches for the transformer, represented by the complex power S_f^{tr} and S_t^{tr}, can then be written as:

$$\begin{aligned} S_f^{\text{tr}} &= V_f^2 \frac{Y_s e^{j(-\theta_{Y_s})} + Y_{sh} e^{j(-\theta_{Y_{sh}})}}{m^2} - V_f V_t Y_s \frac{1}{m} e^{j(\theta_{V_f} - \theta_{V_t} - \theta_{Y_s} - \tau)} - P_f^{\text{tr}} - jQ_f^{\text{tr}}, \\ S_t^{\text{tr}} &= V_t^2 (Y_s e^{j(-\theta_{Y_s})} + Y_{sh} e^{j(-\theta_{Y_{sh}})}) - V_t V_f Y_s \frac{1}{m} e^{j(\theta_{V_t} - \theta_{V_f} - \theta_{Y_s} + \tau)} - P_t^{\text{tr}} - jQ_t^{\text{tr}}. \end{aligned} \tag{89}$$

From these equations, the partial derivatives of the transformer powers with respect to voltage magnitude, phase angle, tap ratio, and phase shift can be derived. For the to-side power S_t^{tr}, the derivatives are given as:

$$\begin{aligned} \frac{\partial S_t^{\text{tr}}}{\partial V_t} &= 2V_t (Y_s e^{j(-\theta_{Y_s})} + Y_{sh} e^{j(-\theta_{Y_{sh}})}) - V_f Y_s \frac{1}{m} e^{j(\theta_{V_t} - \theta_{V_f} - \theta_{Y_s} + \tau)}, \\ \frac{\partial S_t^{\text{tr}}}{\partial V_f} &= -V_t Y_s \frac{1}{m} e^{j(\theta_{V_t} - \theta_{V_f} - \theta_{Y_s} + \tau)}, \\ \frac{\partial S_t^{\text{tr}}}{\partial \theta_{V_t}} &= 1j \times V_t V_f Y_s \frac{1}{m} e^{j(\theta_{V_t} - \theta_{V_f} - \theta_{Y_s} + \tau)}, \\ \frac{\partial S_t^{\text{tr}}}{\partial \theta_{V_f}} &= -1j \times V_t V_f Y_s \frac{1}{m} e^{j(\theta_{V_t} - \theta_{V_f} - \theta_{Y_s} + \tau)}, \\ \frac{\partial S_t^{\text{tr}}}{\partial \tau} &= 1j \times V_t V_f Y_s \frac{1}{m} e^{j(\theta_{V_t} - \theta_{V_f} - \theta_{Y_s} + \tau)}, \\ \frac{\partial S_t^{\text{tr}}}{\partial m} &= V_t V_f Y_s \frac{1}{m^2} e^{j(\theta_{V_t} - \theta_{V_f} - \theta_{Y_s} + \tau)}. \end{aligned} \tag{90}$$

Similarly, for the from-side power S_f^{tr}, the derivatives are:

$$\begin{aligned} \frac{\partial S_f^{\text{tr}}}{\partial V_f} &= 2V_f (Y_s e^{j(-\theta_{Y_s})} + Y_{sh} e^{j(-\theta_{Y_{sh}})}) \frac{1}{m^2} - V_t Y_s \frac{1}{m} e^{j(\theta_{V_f} - \theta_{V_t} - \theta_{Y_s} - \tau)}, \\ \frac{\partial S_f^{\text{tr}}}{\partial V_t} &= -V_f Y_s \frac{1}{m} e^{j(\theta_{V_f} - \theta_{V_t} - \theta_{Y_s} - \tau)}, \\ \frac{\partial S_f^{\text{tr}}}{\partial \theta_{V_f}} &= -1j \times V_f V_t Y_s \frac{1}{m} e^{j(\theta_{V_f} - \theta_{V_t} - \theta_{Y_s} - \tau)}, \\ \frac{\partial S_f^{\text{tr}}}{\partial \theta_{V_t}} &= 1j \times V_f V_t Y_s \frac{1}{m} e^{j(\theta_{V_f} - \theta_{V_t} - \theta_{Y_s} - \tau)}, \\ \frac{\partial S_f^{\text{tr}}}{\partial \tau} &= 1j \times V_f V_t Y_s \frac{1}{m} e^{j(\theta_{V_f} - \theta_{V_t} - \theta_{Y_s} - \tau)}, \\ \frac{\partial S_f^{\text{tr}}}{\partial m} &= -2V_f^2 (Y_s e^{j(-\theta_{Y_s})} + Y_{sh} e^{j(-\theta_{Y_{sh}})}) \frac{1}{m^3} + V_f V_t Y_s \frac{1}{m^2} e^{j(\theta_{V_f} - \theta_{V_t} - \theta_{Y_s} - \tau)}. \end{aligned} \tag{91}$$

4.6.3 VSC Loss Derivatives

We recall that for VSCs, active power loss across the converter can be expressed in terms of the losses in the *from* and "to" sides, denoted by P_f and P_t, respectively. The total active power balance, including losses, is governed by the equation:

$$P_f + P_t - P_{\text{loss}} = 0, \tag{92}$$

where P_{loss} represents the total power loss in the VSC. These losses are typically modeled as a function of both the active and reactive power components at the terminal buses, which gives:

$$P_f + P_t = a + b\frac{\sqrt{P_f^2 + Q_f^2}}{V_f} + c\frac{P_f^2 + Q_f^2}{V_f^2}, \tag{93}$$

where a, b, and c are constants defining the loss model, P_f and Q_f are the active and reactive powers at the *from* side, and V_f is the voltage at the *from* side bus. The same equation applies to the *to* side of the VSC.

In the context of generalized power flow, we can define the total loss equation for the VSC branch as:

$$g_{p,acdc} := P_f^{\text{acdc}} + P_t^{\text{acdc}} - P_{\text{loss},k}^{\text{acdc}} = 0 \quad \forall k \in ACDC, \tag{94}$$

where P_f^{acdc} and P_t^{acdc} are the active power flows on the AC/DC branch, and $P_{\text{loss},k}^{\text{acdc}}$ represents the power loss across the VSC converter for branch k.

The loss model can be more generally expressed as:

$$L^{vsc} = P_f + P_t - \left(a + b\frac{\sqrt{P_t^2 + Q_t^2}}{V_t} + c\frac{P_t^2 + Q_t^2}{V_t^2}\right), \tag{95}$$

where P_t and Q_t are the active and reactive powers on the *to* side of the VSC, and V_t is the voltage at the *to* bus.

The derivatives of the loss function L^{vsc} with respect to the relevant variables are given by:

$$\begin{aligned}
\frac{\partial L^{vsc}}{\partial V_t} &= b\frac{\sqrt{P_t^2 + Q_t^2}}{V_t^2} + 2c\frac{P_t^2 + Q_t^2}{V_t^3}, \\
\frac{\partial L^{vsc}}{\partial P_t} &= 1 - b\frac{P_t}{V_t\sqrt{P_t^2 + Q_t^2}} - 2c\frac{P_t}{V_t^2}, \\
\frac{\partial L^{vsc}}{\partial Q_t} &= -b\frac{Q_t}{V_t\sqrt{P_t^2 + Q_t^2}} - 2c\frac{Q_t}{V_t^2}, \\
\frac{\partial L^{vsc}}{\partial P_f} &= 1.
\end{aligned} \tag{96}$$

4.6.4 Passive Branch Derivatives

In passive branches, such as lines or transformers, the power flow is determined by the voltage difference across the branch and the admittance of the branch. The apparent power injected into the "from" bus of a passive branch S_f^κ is given by:

$$\begin{aligned} S_f^\kappa &= P_f^{set} + jQ_f^{set} - \bar{V}_f(\bar{V}_t - \bar{V}_f)\bar{Y}_{ft}^*, \\ S_f^\kappa &= P_f^{set} + jQ_f^{set} - (\bar{Y}_{ft}^* V_f V_t e^{j(\theta_{V_f}+\theta_{V_t})} - \bar{Y}_{ft}^* V_f^2 e^{j(2\theta_{V_f})}). \end{aligned} \tag{97}$$

The derivatives of S_f^κ with respect to the relevant variables are as follows:

$$\begin{aligned} \frac{\partial S_f^\kappa}{\partial V_f} &= -\bar{Y}_{ft}^* V_t e^{j(\theta_{V_f}+\theta_{V_t})} + 2\bar{Y}_{ft}^* V_f e^{j(2\theta_{V_f})}, \\ \frac{\partial S_f^\kappa}{\partial V_t} &= -\bar{Y}_{ft}^* V_f e^{j(\theta_{V_f}+\theta_{V_t})}, \\ \frac{\partial S_f^\kappa}{\partial \theta_{V_f}} &= -1j \times \bar{Y}_{ft}^* V_f V_t e^{j(\theta_{V_f}+\theta_{V_t})} + 2j \times \bar{Y}_{ft}^* V_f^2 e^{j(2\theta_{V_f})}, \\ \frac{\partial S_f^\kappa}{\partial \theta_{V_t}} &= -1j \times \bar{Y}_{ft}^* V_f V_t e^{j(\theta_{V_f}+\theta_{V_t})}. \end{aligned} \tag{98}$$

5 Results

The algorithm explained in the previous section was implemented Python 3.10. This code was implemented using the software structure of GridCal, with the final aim of including it as a feature in future releases of the software. GridCal is an open-source power systems planning and simulation software with up-to-date implementations of state of the art methods in power systems [24]. For our purposes, GridCal has an Newtown Raphson solver that is able to solve AC/DC systems using the Flexible Universal Branch Model that we introduced in Section 1.2. The results presented in this section for our formulation will thus be benchmarked against the existing methods used in original GridCal.

The system, machine and environment specifications used for the results are as follows:

- **Processor**: 11th Gen Intel(R) Core(TM) i7-1165G7 @ 2.80GHz
- **Installed RAM**: 16.0 GB (15.7 GB usable)
- **System Type**: 64-bit operating system, x64-based processor
- **Operating System**: Windows 11 Home, Version 23H2
- **Python Version**: 3.10
- **GridCal Version**: 5.1.9
- **IDE**: Visual Studio Code

We first begin with the error evolution of the method for pure AC systems. In this way, we can check if the formulation converges in a reasonable number of iterations of Newton Raphson. Then, we look at the correctness of the algorithm by comparing it to the existing solver in GridCal. Next, we begin with an analysis of multi-terminal DC systems, where VSC converters connect the AC and DC subsystem. For that, we use a modified IEEE 14-bus system with VSC-interfaced wind farms. Finally, we deal with the complexity of the overall algorithm and a comparison of the solving time.

5.1 Error Evaluation and Convergence

Before addressing performance metrics such as computational time, we first evaluate the solver's convergence behavior and accuracy. In order to run the models together with GridCal, the algorithm was altered slightly in order to account for the compilation method of the existing solver. This is because, in original GridCal, the control modes of the transformer are limited, and thus for the purposes of close benchmarking with GridCal, controllable transformers are simply modeled as passive branches using the GridCal compiler.

We ran a total of 110 test cases that are shipped together with the GridCal software. Of those, 78 converged, as seen in Appendix D, four did not converge, and a total of 28 returned some form of compiler error due to the fact that the models were made for more conventional power flows.

The results show that most test cases converged successfully. These systems are mainly pure AC systems, but some test cases converged for the HVDC case, such as the `10_bus_hvdc.gridcal`. Additionally, the generalized power flow solved some of the very large test cases (of bus size around 13,000). However, it is notable that the models provided by the transmission system operator, Réseau de Transport d'Électricité, did not converge regardless of size (`case1888rte.m`, `case2868rte.m`, `case6495rte.m`).

The failures due to compiler errors are most often due to a slack node not being explicitly identified. As we recall from one of our rules, we require an explicit reference node to be chosen. Other reasons for the compiler failing is because one or more active devices in the grid such as VSCs did not select a control mode that controlled two magnitudes in the grid. This is allowed in original GridCal models, but does not align as well with our fundamental rules.

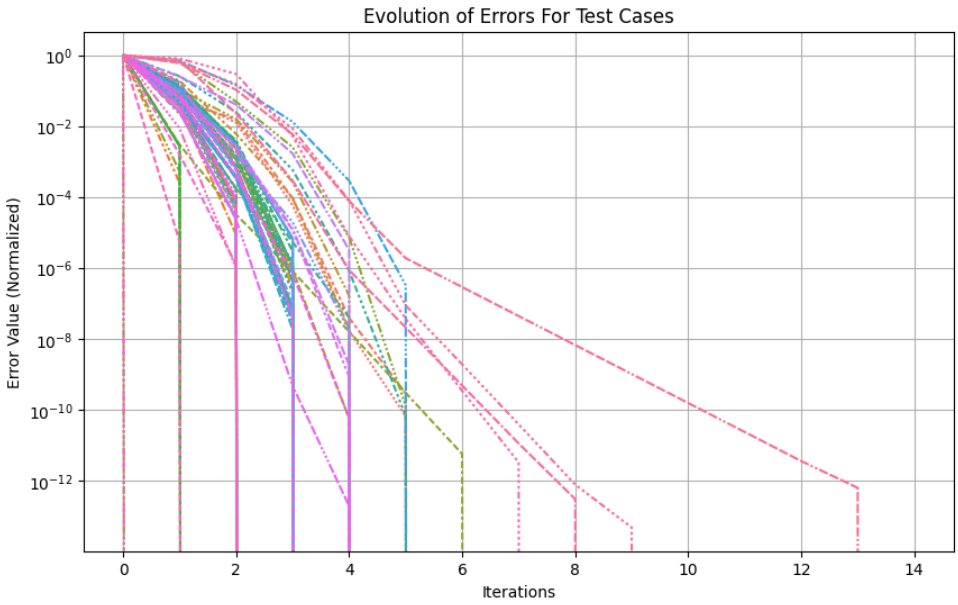

Figure 17: Evolution of the error of 82 test cases.

The plot in Figure 27 illustrates the error evolution for 82 test cases. Each line represents one test case. The raw error values were tracked iteratively until they decreased below a threshold of 1×10^{-10}, at which point the system was considered to have converged. To standardize the comparison across test cases, the error lists were normalized so that all iterations began with a value of 1, enabling a consistent view of error reduction over time. The figure demonstrates how various test cases evolve in terms of error reduction during the iterative process of solving power flow problems.

A few important observations can be made. Most test cases exhibit rapid convergence, with the majority reaching the desired threshold within 3 to 4 iterations. A smaller subset of cases takes longer, extending up to 6 iterations, while very few extend beyond 10 iterations. Notably, the test cases that require more than 10 iterations for convergence include `Texas_7k_2022.gridcal`, `case9241pegase.m`, `case8387pegase.m`, and `case13659pegase.m`. These grids represent very large systems, and it is expected that the size and complexity of these grids would require more time to reach convergence. It is also true that the threshold chosen for convergence is quite fine compared to the default GridCal value of 1×10^{-6}, and so the raw values of the initial errors of these larger systems resulted a greater number of iterations to achieve the desired precision.

5.2 6-bus Grid

The 6-bus system represents a small network that includes two VSCs and a controllable transformer. For ease of analysis, this case is particularly simple, so that we may compare the effect of different control settings on the power flow solutions between the generalised and the classical methods. The grid, as shown in Figure 18, is modeled using GridCal, and has been used extensively to test the FUBM formulation in GridCal. It has two DC nodes interfacing the AC buses via VSC 1 and VSC 2. We see that the grid is meshed such that the HVDC system is interconnected with the same main AC grid.

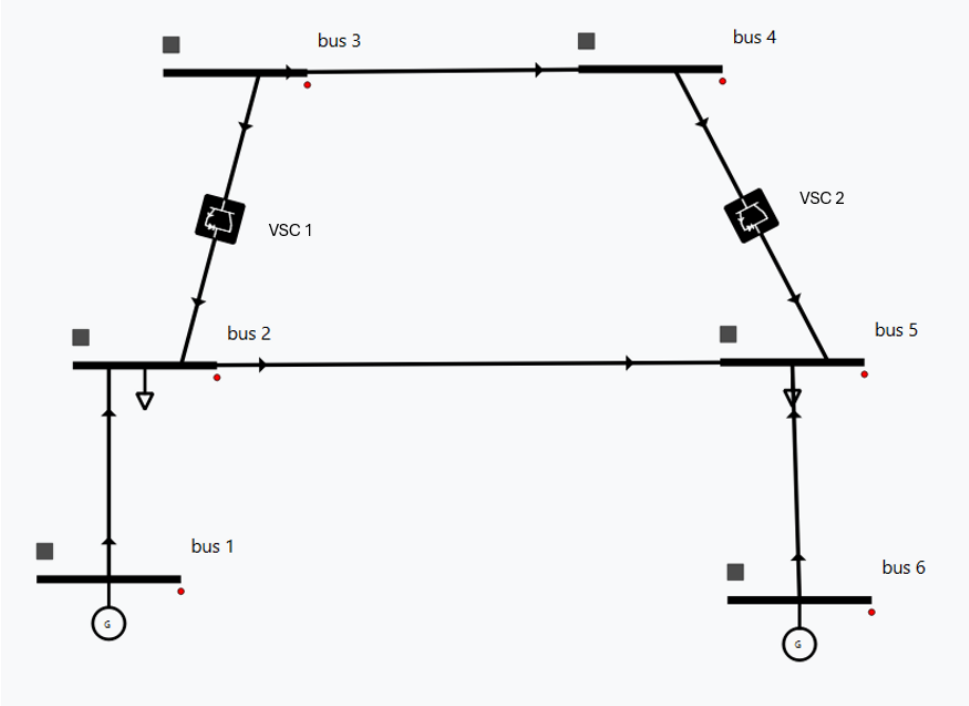

Figure 18: 6-bus system including two VSCs.

Figure 19 shows the VSC control modes that we have set for this problem. VSC 2 sets the voltage on the DC subsystem at bus 4, ensuring there is a reference node. VSC 1, on the other hand, controls the reactive power flow on its AC side. This configuration allows us to compare the effect of the VSC control more closely with the classical method as it is a control scheme that can be achieved in both formulations.

We run the two power flows and observe that the generalised approach converges in 5 iterations while the classical approach converges in 7 iterations. In Figure 22, we see that the raw error shows the convergence of the traditional method as exponentially approaching zero. However, in the case of the classical approach, its convergence starts to waver slightly after the third iteration. On the right side of the same figure, we see the shape more clearly as the values are normalised.

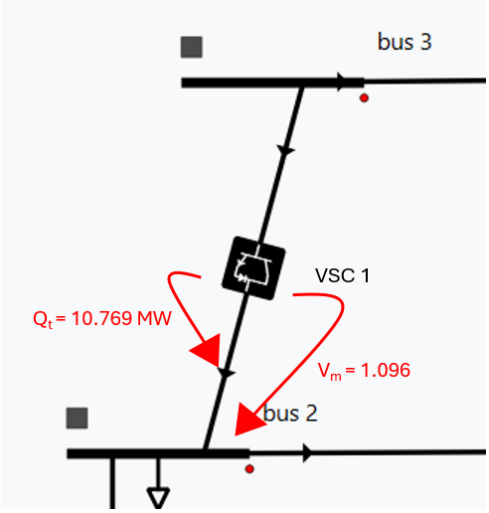

Figure 19: VSC 1 Control

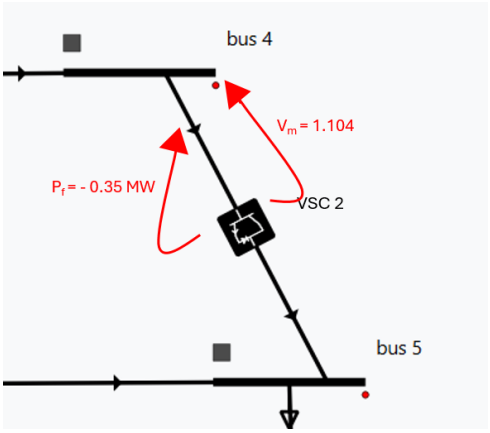

Figure 20: VSC 2 Control

Figure 21: Control settings for VSCs in 6-Bus grid.

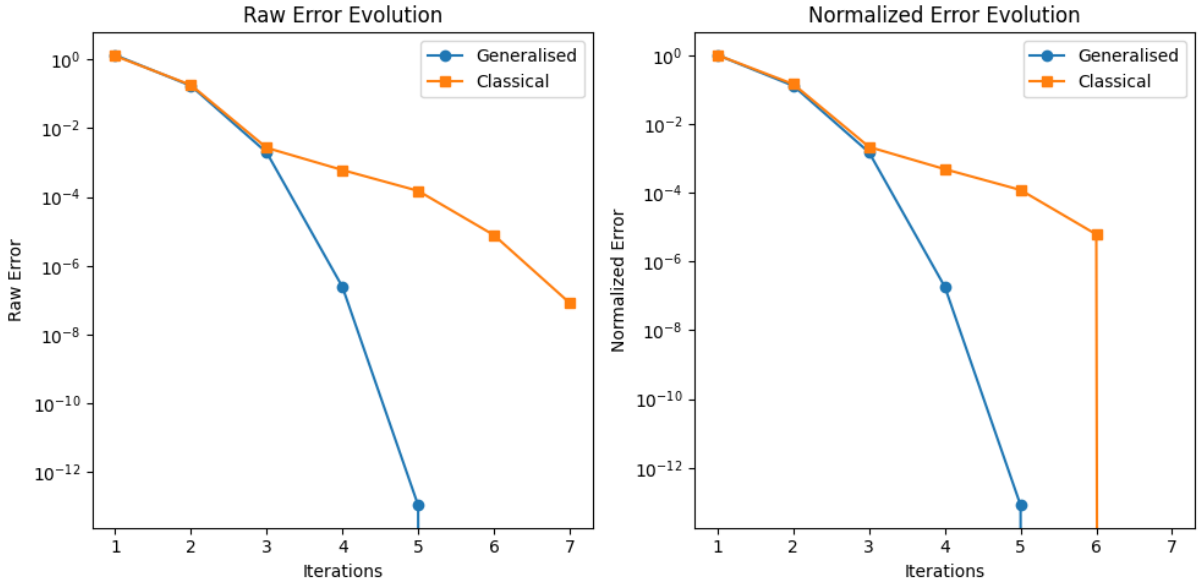

Figure 22: Convergence for 6-bus system.

The voltage magnitudes across the buses are compared in Figure 23. Both formulations achieve similar results in terms of voltage magnitude. Similarly, in Table 5, we observe that the voltage angles for the AC buses are consistent between both methods, but there is a notable difference for the DC buses, especially buses DC 1 and DC 4, where the classical method incorrectly assigns voltage angles to DC buses. This mainly shows a drawback of the classical method: treating AC and DC buses similarly in this formulation means that voltage angles are also present in the DC bus results.

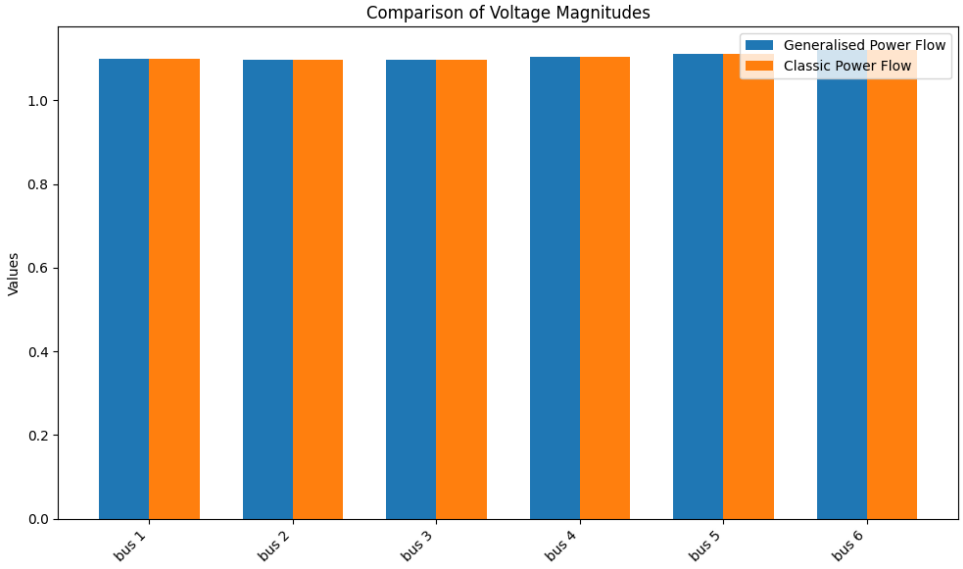

Figure 23: Voltage magnitudes for 6-bus system.

Table 5: Voltage angle in degrees.

Bus	**Generalised (°)**	**Classical (°)**
Bus 1	0	0
Bus 2	-0.2616	-0.2617
Bus 3	0	4.386
Bus 4	0	4.386
Bus 5	-4.023	-4.023
Bus 6	-3.981	-3.981

The power flows through the VSC branches in Figure 6 and 7 reflect the similarity in the solutions between the two formulations. Once again, the only differences come from the reactive power on the DC side that the classical approach returns as an answer, which we should safely ignore. This assures us of the correctness of the generalised approach, which not only improves convergence but also provides more accurate and meaningful results for DC nodes, particularly by correctly reflecting the absence of reactive power on the DC side.

Table 6: Comparison of VSC 1 branch powers.

Power Flow	**Generalised (MW/Mvar)**	**Classical (MW/Mvar)**
Pf (Active Power From)	0.3479	0.3479
Qf (Reactive Power From)	0	6.5041
Pt (Active Power To)	0.7437	0.7437
Qt (Reactive Power To)	10.77	10.77

Table 7: Comparison of VSC 2 branch powers.

Power Flow	Generalised (MW/Mvar)	Classical (MW/Mvar)
Pf (Active Power From)	-0.3500	-0.3500
Qf (Reactive Power From)	0.0	1.2962
Pt (Active Power To)	0.3794	0.3793
Qt (Reactive Power To)	1.550	1.550

5.3 Modified IEEE 14-Bus

We now move on to a slightly more practical test case. This test case comes from a study of a system with high penetration of wind generation [6]. However, we have modified it slightly to include just one HVDC line for better comparison between the two formulations.The grid as shown in Figure 24, is modelled in GridCal, as shown in Figure 25.

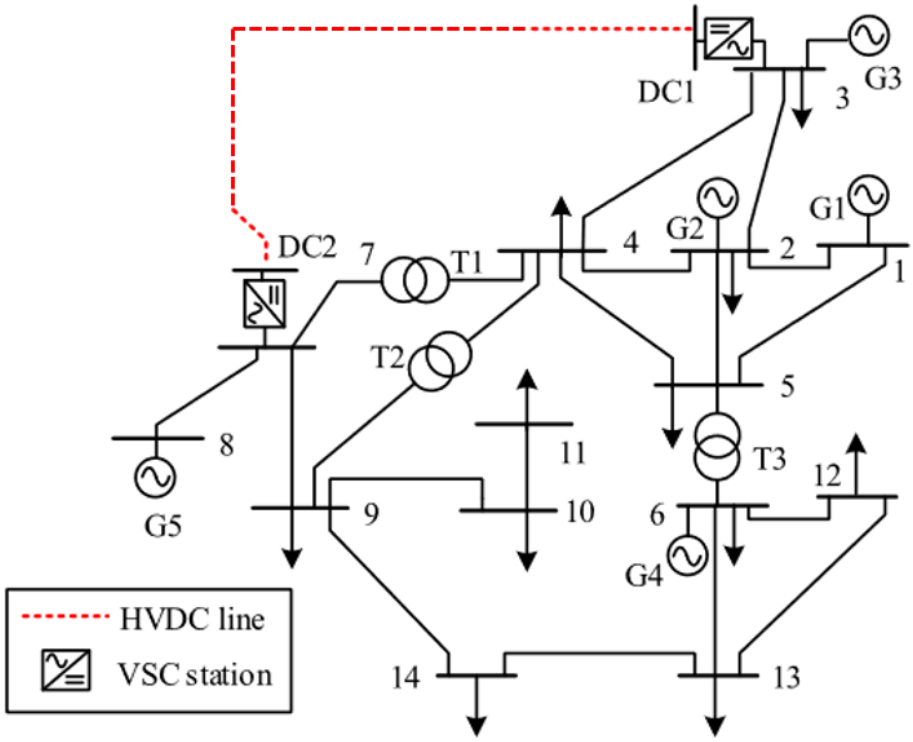

Figure 24: Modified IEEE 14-bus System [6].

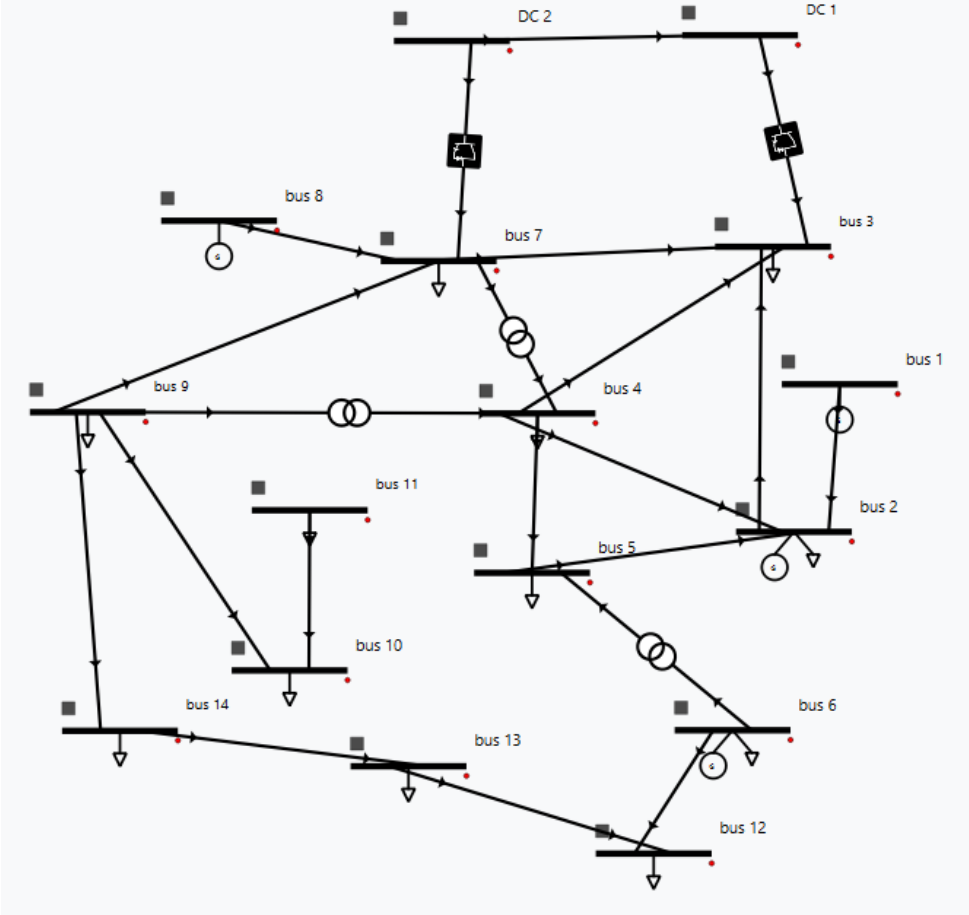

Figure 25: Modified IEEE 14-bus system in GridCal.

The AC system interfaces with HVDC lines that connect to other DC nodes, similar to the system in the previous section. The main AC grid also has a number of transformers (Trafo 1, Trafo 2, Trafo 3). Figure 26 below gives the setpoints defined by the controllable transformer, Trafo 2, which sets its tap module and angle. The other two in the grid, that is, Trafo 1 and Trafo 3, are left as passive elements. This means that the latter two are included in the Y_{bus} matrix, while Trafo 2 is considered an active element in the grid. The converters VSC 1 and VSC 2 maintain the same setpoints as they did in the previous case as shown in Figure 21.

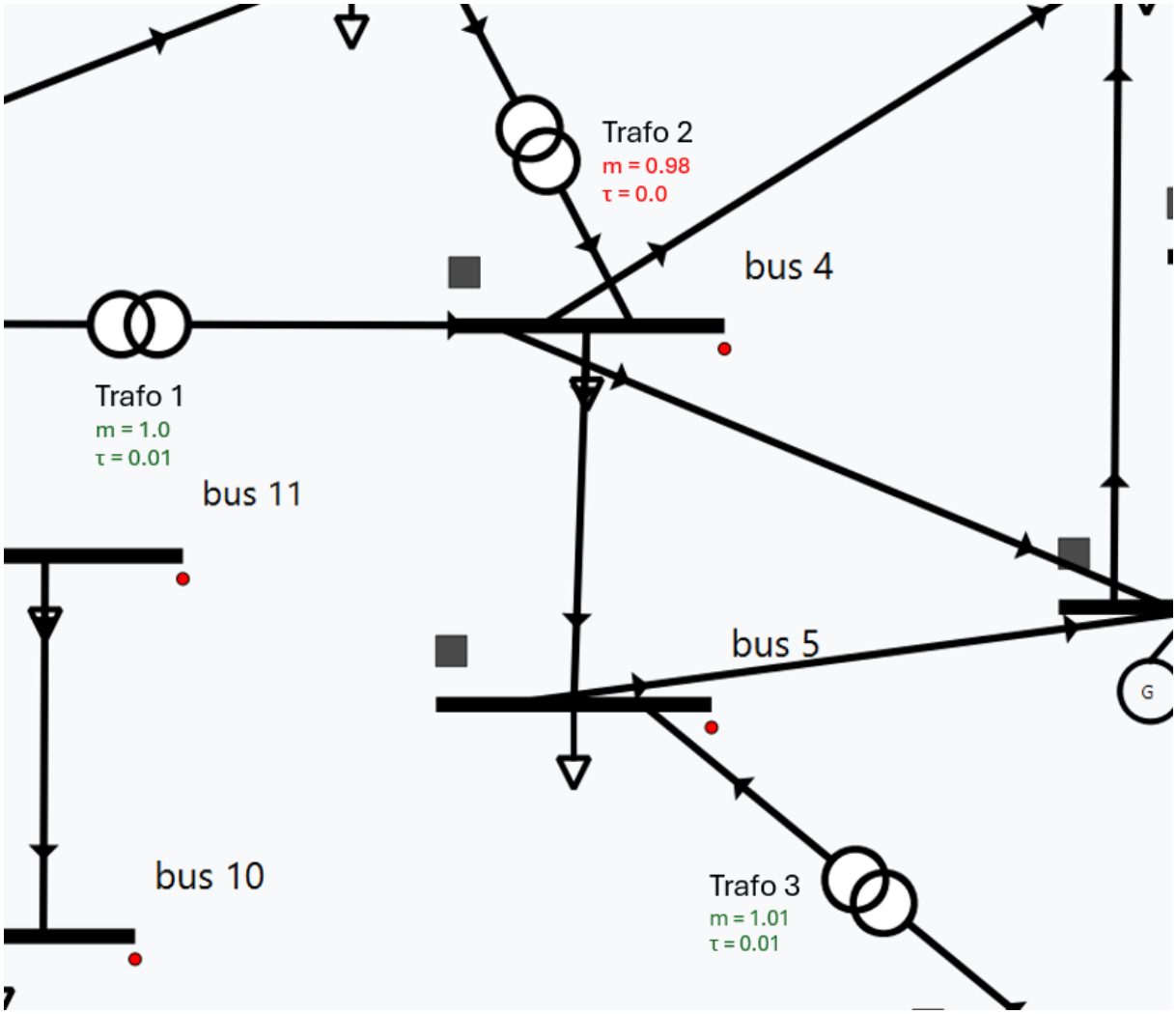

Figure 26: Control Mode for Controllable Transformer Trafo 2.

In both the generalised and classical formulations, the solver converges to a solution. As shown in Figure 27, the raw error values decrease steadily with each iteration. We observe that the generalised case generally maintains a lower error compared to the classical approach, especially in the later stages of convergence. The normalised error plot shows a similar plot, where both methods show exponential reductions in error. However, the generalised formulation reaches convergence in 8 iterations, one sooner than the classical formulation.

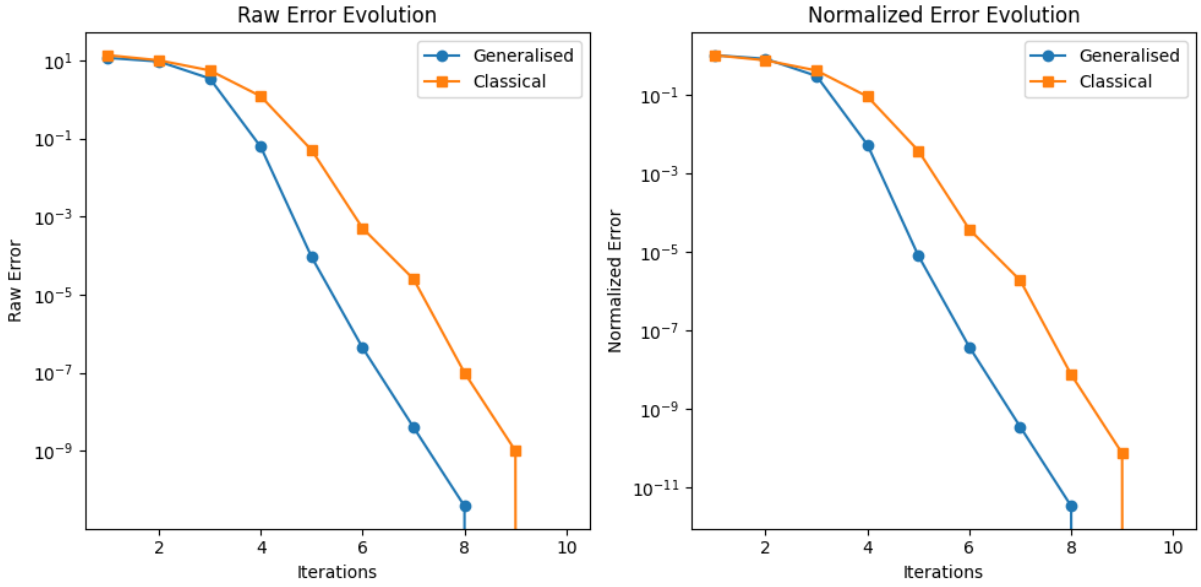

Figure 27: Convergence for IEEE 14-bus system.

The power flow results as shown in Figure 28. We see that all of the buses have very similar results between the two. This seems to also be the case with the voltage angles which we see in Table 8. However, as before, we see the presence of voltage angles for all the DC buses.

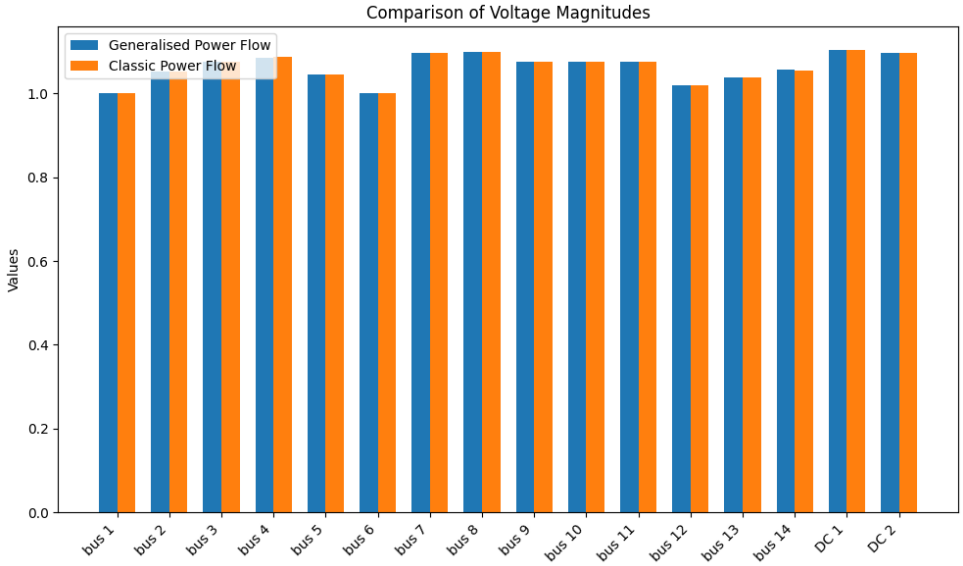

Figure 28: Voltage magnitudes comparison

Table 8: Voltage angle in degrees.

Name	**Generalised (°)**	**Classical (°)**
bus 1	-0.9200	-0.9207
bus 2	-1.0030	-1.0035
bus 3	-1.0293	-1.0313
bus 4	-0.9752	-0.9752
bus 5	-1.0306	-1.0306
bus 6	-1.0600	-1.0646
bus 7	-0.9751	-0.9751
bus 8	-0.0000	0.0000
bus 9	-0.9726	-0.9752
bus 10	-1.0679	-1.0740
bus 11	-1.1244	-1.1235
bus 12	-1.1368	-1.1359
bus 13	-1.1442	-1.1505
bus 14	-1.1124	-1.1124
DC1	0	-9.1727
DC2	0	-9.1727

5.4 Modified IEEE 118-bus

In this section, we look at a slightly larger grid, in which we embed a HVDC system. In Figure 29, we see the IEEE 118-bus test system. We have modified it slightly to include a HVDC element that is connected at the slack bus of the AC system, which is called *Riversde*. The other end of the HVDC line is connected to a single-node AC subsystem, which is itself connected to a generator to represent the energy source. We see the layout of the new DC buses and the AC subsystems more clearly in Figure 30. In this case, we have connected it to the slack node of the AC grid, to try to ensure that we do not force some nodal voltages to be too low so as to not converge.

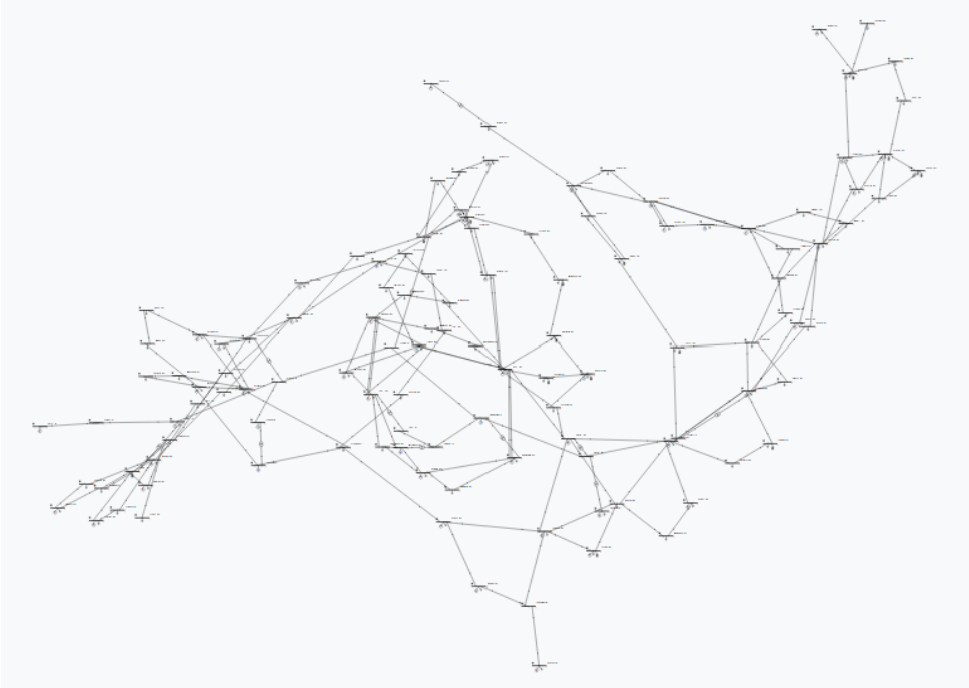

Figure 29: IEEE 118-bus system in GridCal.

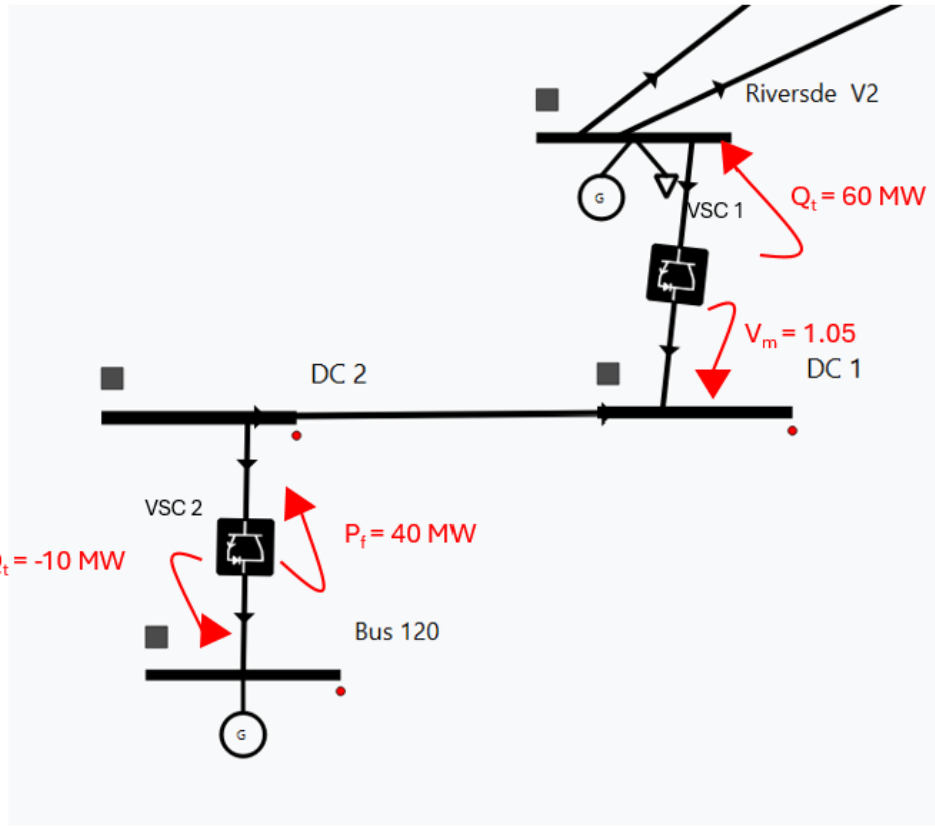

Figure 30: Control scheme of VSCs in IEEE 118-bus system.

The error evolution of this case is plotted in Figure 31. The results from the classical power flow are not included as it did not seem to converge in GridCal. Therefore, we just show the evolution of the error for our method in this case. We see that the plot shows quite a steady convergence rate, with the error exponentially decreasing across the iterations. The threshold for convergence is reached by iteration twelve.

The reason for the lack of convergence of the classical formulation is unclear. But it could once again point to a fundamental difference in dealing with the controls of the VSCs. Leaving the VSC controls to be "free" in the classical approach also does not help with convergence.

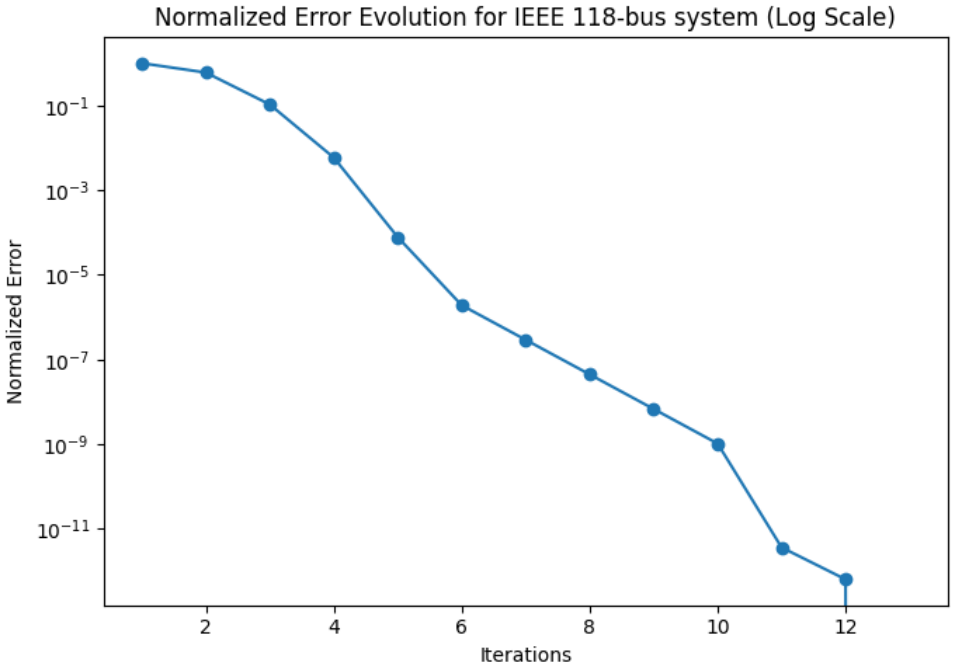

Figure 31: Error evolution for IEEE 118-bus system in GridCal.

5.5 Runtime Comparison

In this section, we compare the runtime of three different test cases— 6-bus grid, IEEE 14-bus, IEEE 118-bus — between the generalised and classical power flow methods. For fairness, we include all the time necessary for the compiler to parse the system, and add that time to the time for the convergence, because that entire process constitutes one entire power flow solution being found. We performed 5 independent runs of the two algorithms to solve these test cases. Their results are summarized in Figure 32. As observed in the figure, the generalised method has comparable runtime to the classical method for the smaller test cases. The classical method failed to produce results for the larger case, the IEEE 118-bus, as indicated by the absence of bars for the classical method in Figure 32.

In the case of the larger system, we see a noticeable increase in the runtime for the generalised method. The IEEE 118-bus shows the greatest runtime for the generalised method, slightly over 700 ms. Much of the increase in runtime can be attributed to the increase in execution time of the mismatch and Jacobian. Referring to Table 9, the execution time for all three critical parts of the algorithm does increase quite significantly when we jump from the 14-bus to the 118-bus system.

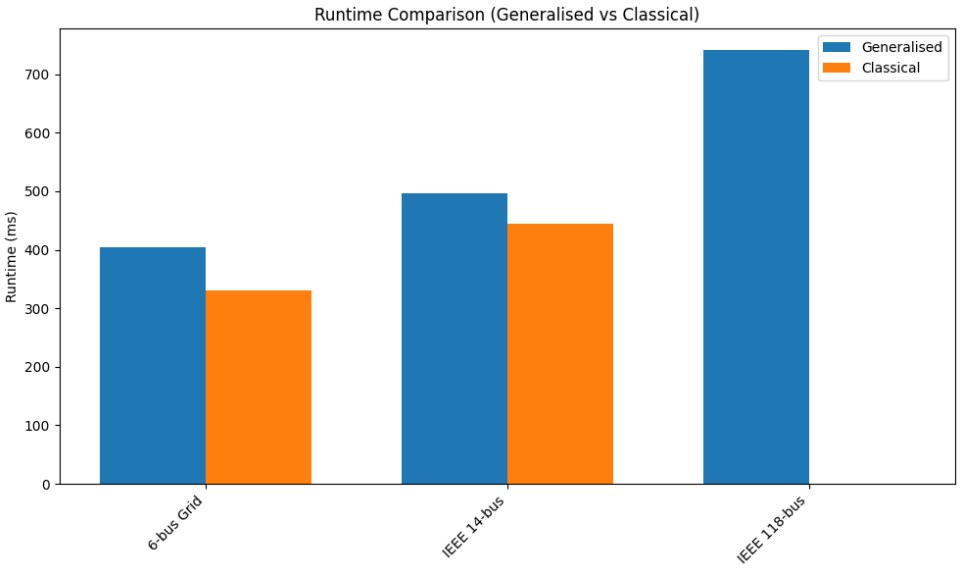

Figure 32: Runtime comparison for three test cases.

Table 9: Runtime breakdown for three test cases run on generalised power flow (in milliseconds).

Test Case	Mismatch (ms)	Jacobian (ms)	Solve (ms)
6-bus Grid	1.7267	1.8666	2.2551
IEEE 14-bus	1.8940	2.2084	2.9206
IEEE 118-bus	3.7404	6.1091	5.5986

Figure 33 shows the relationship between bus size and the number of iterations required for convergence. It is expected that that larger system introduce more complexity, leading to a higher number of iterations needed to achieve convergence. However, it is clear to see that although the relationship is linear, it is less than proportional, which is useful behaviour to encounter especially when dealing with larger systems.

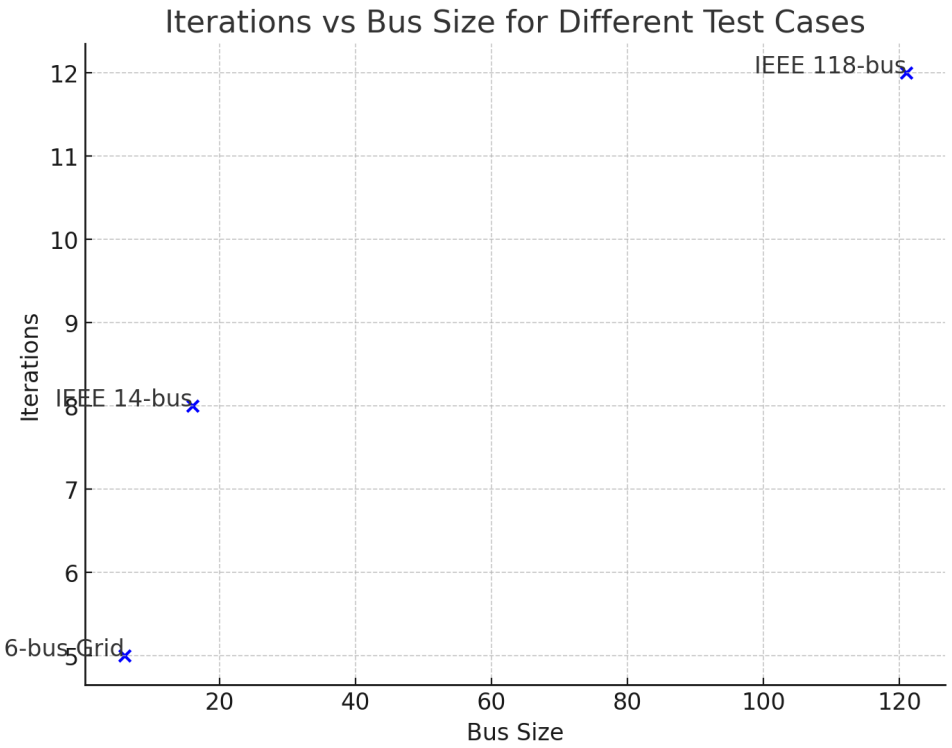

Figure 33: Iterations before convergence for three test cases.

Conclusions

This work has demonstrated a generalised power flow formulation that solves AC and DC systems using a generalised approach, benchmarked against GridCal's classical methods. The results indicate that the proposed solver not only converges reliably in most of the test cases but also exhibits strong accuracy agaisnt the classical method.

However, it is clear from the HVDC test cases that the generalised formulation introduces new possibilities when interfacing AC and DC subsystems, especially given the differences in how controls are handled between our approach and GridCal's conventional methods. The generalised approach also proved to be capable of solving systems where the classical method could not: the modified AC/DC IEEE 118-bus converged with our formulation within a reasonable number of iterations.

On the performance side, runtime comparisons indicate that while the generalised power flow solver converges faster than the classical power flow on the smaller test cases, its computational burden increases significantly as system size grows. This is particularly evident in large networks like the IEEE 118-bus system. The increase in iterations and execution time for calculating mismatches, Jacobians, and solving linear systems reflects the higher complexity of the model. However, despite the runtime increase, the solver scales efficiently, maintaining a linear relationship between system size and the number of iterations required for convergence.

Future Work

To extend this work, there are several key areas to enhance the proposed generalised power flow formulation. These improvements will not only increase the model's applicability to real systems but also address some of the limitations observed in the current implementation:

- **Incorporation of Power Limits for VSCs**: Power limits for VSCs refer to the maximum and minimum levels of active and reactive power that the converters can realistically handle. We may begin to consider the capability curves of the converters by performing checks between every iteration to see if limits have been reached and to adjust setpoints accordingly.

- **Code Optimization**: There is an opportunity to optimize handling of large-scale mismatch matrices and Jacobians. Currently, the implemented version of this generalised approach in GridCal has been optimized for readability and for debugging for the purposes of this work. After validating the approach, more work can be done to reduce computational complexity, especially when it comes to dealing with sparse matrices.

- **Common Compiler**: We observe so far that there is a fundamental difference in compiling the control types from current GridCal grid models and our formulation. Specifically, there is a difference in handling the schemes of control for VSCs and controllable transformers. There can be work done to align the two in order to extend GridCal's capabilities and to ensure that the control schemes that we allow are also logical from a power system's perspective.

Acknowledgements

I extend my thanks to my supervisors, Eduardo Prieto Araujo and Josep Fanals i Batllori, for their guidance and support throughout this project. I would also like to thank my colleagues at eRoots Analytics their assistance and resources. Finally, I am grateful to my family and friends for their encouragement during this time.

Bibliography

[1] entsoe, "Grid map," 2024, accessed: 2024-03-15. [Online]. Available: https://www.entsoe.eu/data/map/

[2] D. Jovcic, *High Voltage Direct Current Transmission: Converters, Systems and DC Grids*. Wiley, 2019.

[3] J. Beerten, S. Cole, and R. Belmans, "A sequential ac/dc power flow algorithm for networks containing multi-terminal vsc hvdc systems," in *IEEE PES General Meeting*, 2010, pp. 1–7.

[4] F. Milano, *Power System Modelling and Scripting*. Springer, 2010.

[5] A. Alvarez Bustos and B. Kazemtabrizi, "Flexible general branch model unified power flow algorithm for future flexible ac/dc networks," in *2018 IEEE International Conference on Environment and Electrical Engineering and 2018 IEEE Industrial and Commercial Power Systems Europe (EEEIC / ICPS Europe)*, 2018, pp. 1–6.

[6] Z. Jiang, Y. Liu, Z. Kang, T. Han, and J. Zhou, "Security-constrained unit commitment for hybrid vsc-mtdc/ac power systems with high penetration of wind generation," *IEEE Access*, vol. 10, pp. 1–1, 01 2022.

[7] S. Borlase, *Smart Grids Infrastructure, Technology, and Solutions*. CRC Press, 2017. [Online]. Available: https://www.taylorfrancis.com/books/edit/10.1201/b13003/smart-grids-stuart-borlase

[8] entsoe, "Hvdc links in system operations," 2019. [Online]. Available: https://eepublicdownloads.entsoe.eu/clean-documents/SOC%20documents/20191203_HVDC%20links%20in%20system%20operations.pdf

[9] D. Braunagel, L. Kraft, and J. Whysong, "Inclusion of dc converter and transmission equations directly in a newton power flow," *IEEE Transactions on Power Apparatus and Systems*, vol. 95, no. 1, pp. 76–88, 1976.

[10] J. Beerten, S. Cole, and R. Belmans, "A sequential ac/dc power flow algorithm for networks containing multi-terminal vsc hvdc systems," in *IEEE PES General Meeting*, 2010, pp. 1–7.

[11] M. Baradar, M. Ghandhari, and D. Van Hertem, "The modeling multi-terminal vsc-hvdc in power flow calculation using unified methodology," in *2011 2nd IEEE PES International Conference and Exhibition on Innovative Smart Grid Technologies*, 2011, pp. 1–6.

[12] Q. Nguyen, G. Todeschini, and S. Santoso, "Power flow in a multi-frequency hvac and hvdc system: Formulation, solution, and validation," *IEEE Transactions on Power Systems*, vol. 34,

no. 4, pp. 2487–2497, 2019.

[13] A. Alvarez-Bustos, B. Kazemtabrizi, M. Shahbazi, and E. Acha-Daza, "Universal branch model for the solution of optimal power flows in hybrid ac/dc grids," *International Journal of Electrical Power Energy Systems*, vol. 126, p. 106543, 2021. [Online]. Available: https://www.sciencedirect.com/science/article/pii/S0142061520319566

[14] W. Lambrichts and M. Paolone, "General and unified model of the power flow problem in multiterminal ac/dc networks," *IEEE Transactions on Power Systems*, pp. 1–11, 2024.

[15] G. Andersson, *Power System Analysis*. ETH Zürich, 2012.

[16] A. Y. R. Iravani, *Voltage-Sourced Converters in Power Systems: Modeling, Control, and Applications*. Wiley-IEEE Press, 2010.

[17] N. M. T. M. U. W. P. Robbins, *Power Electronics: Converters, Applications, and Design, 3rd Edition*. Wiley, 2002.

[18] IEC, "International standard amendement 2: Power losses in voltage sourced converter (vsc) valves for high-voltage direct current (hvdc) systems," https://cdn.standards.iteh.ai/samples/107698/9e5c8f624e2d43d0bfbbae139b8847eb/IEC-62751-2-2014-AMD2-2023.pdf, 2023.

[19] M. G. Hosseini Aghdam and G. B. Gharehpetian, "Modeling of switching and conduction losses in three-phase spwm vsc using switching function concept," in *2005 IEEE Russia Power Tech*, 2005, pp. 1–6.

[20] P. K. O. W. S. Sudhoff, *Analysis of Electric Machinery and Drive Systems*. Wiley-IEEE Press, 2002.

[21] D. V. H. O. G.-B. J. Liang, *HVDC Grids: For Offshore and Supergrid of the Future*. Wiley-IEEE Press, 2016.

[22] MATPOWER, "Matpower user's manual map," 2024, accessed: 2024-09-04. [Online]. Available: https://matpower.org/docs/MATPOWER-manual.pdf

[23] T. A. Davis, "Algorithm 832: Umfpack v4.3—an unsymmetric-pattern multifrontal method," *ACM Trans. Math. Softw.*, vol. 30, no. 2, p. 196–199, jun 2004. [Online]. Available: https://doi.org/10.1145/992200.992206

[24] S. P. Vera, "Gridcal," https://github.com/SanPen/GridCal, 2016–2024.

A Environmental, Social, and Gender Impact

The development and implementation of the new power flow algorithm present significant positive impacts across environmental, social, and gender dimensions.

A.1 Environmental Impact

This power flow algorithm is designed to efficiently handle complex AC/DC systems and networks with numerous control mechanisms, which are essential for integrating renewable energy sources into the grid. By improving the accuracy and speed of power flow calculations, it facilitates the seamless integration of renewable energy, such as wind and solar power, into the existing grid infrastructure. This integration is critical for reducing greenhouse gas emissions and promoting sustainable energy solutions. Moreover, the enhanced capabilities of the power flow algorithm ensure that renewable energy sources can be reliably managed, which helps to stabilize the grid while promoting a cleaner and more sustainable environment.

A.2 Social Impact

The increased efficiency of the power flow algorithm leads to a reduction in the operational costs associated with managing power systems. As these costs decrease, the savings can be passed on to consumers, making electricity more affordable and accessible. This has a direct positive impact on communities, particularly in developing regions where access to reliable and affordable electricity can significantly improve quality of life. By making power systems cheaper and more efficient, this algorithm plays a crucial role in reducing energy poverty, thereby enabling more people around the world to enjoy the benefits of reliable electricity.

A.3 Gender Impact

The development of this power flow algorithm also holds potential in addressing the disproportionate burden that women often face regarding household energy costs. In many households, especially in developing regions, women are typically responsible for managing energy-related expenses, which can be a significant financial strain, particularly when energy prices are high or unreliable. By reducing the operational costs of power systems and making electricity more affordable, may alleviate some of the financial pressures that disproportionately affect women.

Furthermore, in many communities, improved energy access leads to better opportunities for education, healthcare, and economic participation, particularly for women and girls who may otherwise spend significant time on energy-intensive domestic tasks such as cooking or gathering fuel. The improved efficiency of power systems facilitated by this algorithm thus helps create more equitable opportunities for women by reducing the time and financial burdens associated with energy management.

B Time Planning

The time spent on this project is broken down in the chart below. Many tasks were performed in parallel, and at times going back and forth between different processes.

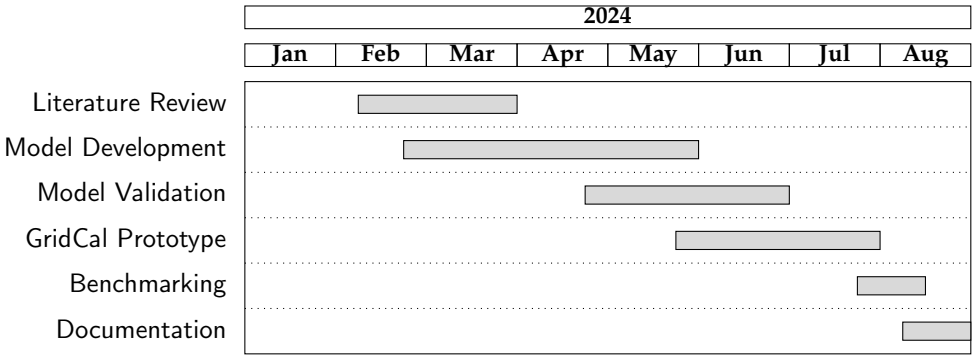

Figure 34: Gantt Chart for the project.

C Budget

In Table 10, we see the costs associated to the project. The project was done in conjunction with eRoots Analytics SL, over a period of 24 weeks. These hours were split between the development engineer and the supervisor, with the development engineer working 520 hours and the supervisor working 260 hours. The hourly rate for the development engineer was €25, while the hourly rate for the supervisor was €30. The total cost of the project was €20.800.

Table 10: Costs of the project.

Role	**Hours**	**Hourly Rate (€)**	**Total Cost (€)**
Development Engineer	520	50	26.000
Supervisor	260	60	15.600
Total	**780**		**41.600**

D Test Case Convergence

We note that a proportion of the systems fail to converge within the accuracy limits. This is primarily attributed to the fact that the generator or converter configurations in these models do not align with the specific control schemes that our formulation assumes. Existing models, particularly those designed in environments like GridCal, frequently utilize different types of controls or rely on simplified representations of HVDC systems, such as aggregating Voltage Source Converter (VSC) components or DC lines into composite models for ease of use. While this simplifies the modeling process, it also introduces discrepancies when compared to the more generalized and detailed approach we apply.

Therefore, we see that we need to tweak the models or even create our own in order to accurately solve AC/DC systems using our generalised approach.

Table 11: Test Cases (Converged)

File Name	File Name
10_bus_hvdc.gridcal	10_bus_hvdc_no_oscillations.gridcal
1354 Pegase.xlsx	2869 Pegase.gridcal
2bus_HVDC.gridcal	3Bus_controlled_transformer.gridcal
4Bus_SalvadorAchaDaza.gridcal	5bus_HVDC.gridcal
8_nodes_2_islands.gridcal	8_nodes_2_islands_hvdc.gridcal
ACTIVSg 500 - South Carolina 500 Bus System.gridcal	Australia.xlsx
Brazil11_loading05.gridcal	case14.m
case300.m	case6ww.m
case89pegase.m	case9.m
case_ACTIVSg500.m	ding0_test_network_2_mvlv.gridcal
example_transformer_tpe.xlsx	GB Network.gridcal
GB reduced network.gridcal	grid.raw
Grid4Bus-OPF.gridcal	hydro_grid2.gridcal
hydro_grid3.gridcal	hydro_IEEE39.gridcal
hydro_simple.gridcal	IEEE 118 Bus - ntc_areas.gridcal
IEEE 118 Bus - ntc_areas.raw	IEEE 118 Bus - ntc_areas_two.gridcal
IEEE 118 Bus v2.raw	IEEE 118.xlsx
IEEE 14 bus.raw	IEEE 14 zip.gridcal
IEEE 14.xlsx	IEEE 145 Bus.xlsx
IEEE 30 Bus with storage.xlsx	IEEE 30 Bus.gridcal
IEEE 30 bus.raw	IEEE 39 dynamic bus types.gridcal
IEEE 39+HVDC line.gridcal	IEEE 5 Bus.xlsx
IEEE 57.xlsx	IEEE 9 Bus.gridcal
IEEE14 - ntc areas.gridcal	IEEE14 - ntc areas_voltages.gridcal
IEEE14 - ntc areas_voltages_hvdc.gridcal	IEEE14 - ntc areas_voltages_hvdc_shifter.gridcal
IEEE14 - ntc areas_voltages_hvdc_shifter_l10free.gridcal	IEEE14_from_raw.gridcal
IEEE25.gridcal	IEEE39.gridcal
IEEE39.xlsx	IEEE39_1W.gridcal
Illinois 200 Bus.gridcal	Illinois200Bus.xlsx
KULeuven_5node.gridcal	Lynn 5 Bus (pq).gridcal
Lynn 5 bus (SVC).gridcal	Lynn 5 Bus pv (opf).gridcal
Lynn 5 Bus pv.gridcal	lynn5buspq.xlsx
lynn5buspv.xlsx	NETS-NYPS 68 Bus System.raw
New England 68 Bus.xlsx	Nord pool model.xlsx
Pegasus 89 Bus.xlsx	PGOC_6bus(from .raw).gridcal
PGOC_6bus.gridcal	PGOC_6bus_modNTC.gridcal
Random grid 1000 buses.gridcal	sc_test.xlsx
Simple_NTC_test_grid.gridcal	test_temp_correction.xlsx
Texas_7k_2022.gridcal	case9241pegase.m
case8387pegase.m	case13659pegase.m

Table 12: Test Cases (Did Not Converge)

File Name
case1888rte.m
case2868rte.m
case_ACTIVSg10k.m
case6495rte.m

Table 13: Grid Files with Exceptions

File Name	Exception
1951 Bus RTE.xlsx	Slack not specified
3 node battery opf.xlsx	Slack not specified
6-node-ACOPF.gridcal	Slack not specified
ACTIVSg500 + VSC.gridcal	Exactly two controls must be chosen but found 1, 8:Vdc
Europe winter 2009 model.xlsx	Slack not specified
fubm_caseHVDC_vt.gridcal	Division by zero
fubm_case_57_14_2MTDC_ctrls.gridcal	Exactly two controls must be chosen but found 0, 0:Free
grid_2_islands.xlsx	Slack not specified
hydro_grid1.gridcal	Slack not specified
hydro_grid4.gridcal	Slack not specified
IEEE 39 (2 islands).gridcal	Slack not specified
IEEE 39 (3 islands).gridcal	Slack not specified
IEEE118_locations.xlsx	The file sheet IEEE118 is not allowed. Did you create this file manually? Use GridCal instead.
IEEE14 - multi-island hvdc.gridcal	Slack not specified
IEEE57+IEEE14 DC grid.gridcal	Exactly two controls must be chosen but found 0, 0:Free
LineHVDCGrid.gridcal	Exactly two controls must be chosen but found 0, 0:Free
Lynn 5 Bus pv (2 islands).gridcal	Slack not specified
simple double hvdc.gridcal	Slack not specified
Some distribution grid (Video).gridcal	Slack not specified
Some distribution grid.gridcal	Slack not specified
Texas 2000 + VSC.gridcal	Exactly two controls must be chosen but found 0, 0:Free
Test_IPA_5_bus_feeder.xlsx	Slack not specified
Test_SRAP_4hours_new_rates 1.gridcal	Slack not specified
Test_SRAP_4hours_new_rates.gridcal	Slack not specified
trafo.gridcal	Slack not specified
trafo2.gridcal	Slack not specified
two_island_grid.xlsx	Slack not specified
ZIP load example.raw	Slack not specified

E Graph Theory and Depth-First Search (DFS)

E.1 Graph Theory Basics

Graph theory provides a mathematical structure to model pairwise relationships between objects. A graph G is represented as a tuple consisting of two sets:

$$G = (I, K) \tag{99}$$

where:

- I is the set of *nodes* (or *vertices*), and
- K is the set of *edges* (or *branches*) connecting pairs of nodes.

Each edge $k \in K$ connects two nodes in I. In an *undirected graph*, the edges do not have a direction, and k represents a symmetric connection between the nodes. In a *directed graph*, each edge has an orientation, indicating a direction from one node to another.

In graph theory, a connected component of a graph is a subgraph in which any two nodes are connected to each other by paths, and which is connected to no additional nodes. For a graph $G = (I, K)$, we can partition the graph into connected components. Each connected component corresponds to a distinct subsystem in power flow analysis.

E.2 Depth-First Search (DFS)

Depth-First Search (DFS) is a fundamental algorithm used to traverse or search through a graph. DFS starts at an arbitrary node and explores as far as possible along each branch before backtracking. DFS is often used to identify connected components in a graph.

Given a graph $G = (I, K)$, the DFS algorithm can be used to explore the entire graph and identify all the nodes that are reachable from a starting node.

The pseudocode for DFS is as follows:

E.2.1 DFS Pseudocode

The DFS algorithm has a time complexity of $O(|I| + |K|)$, where $|I|$ is the number of nodes and $|K|$ is the number of edges in the graph. This makes DFS a highly efficient algorithm for traversing graphs of varying sizes.

Algorithm 1 Depth-First Search (DFS)

Input: Graph $G = (I, K)$
Output: Connected components of G
function DFS(i) {Perform DFS from node i}
  Mark i as visited
  for all neighbors j of i in G **do**
    if j is not visited **then**
      DFS(j) {Recursively explore connected nodes}
    end if
  end for
end function
function FindComponents(G)
  Initialize all nodes in G as unvisited
  for all nodes i in G **do**
    if i is unvisited **then**
      DFS(i) {Call DFS for each unvisited node}
    end if
  end for
end function=0

E.3 Applications in Power Systems

In the context of power flow analysis, DFS is applied to identify subsystems of buses and branches. Once connected components are found, we can ensure that each subsystem (whether AC or DC) has at least one reference node for voltage or angle.

- For AC subsystems, at least one node must have a known voltage magnitude and one node must have a known phase angle.
- For DC subsystems, at least one node must have a known voltage magnitude.

By applying DFS to the power grid graph G, we can separate the grid into connected components and determine the appropriate reference nodes for each subsystem.

E.4 DFS Example on a Power Grid

Consider a simple grid with nodes $\{1, 2, 3, 4\}$ and edges $\{(1, 2), (2, 3), (3, 4)\}$. The DFS algorithm will traverse the graph starting from node 1 and explore all its connected nodes, identifying the entire grid as a single connected component.

The use of DFS is essential in handling both AC and DC subsystems when performing power flow analysis on modern power systems, where each subsystem must satisfy the reference node condition described in Section 4.5.7.